Applications and Industry®

March 1959

Transactions Papers

58-222 Design Considerations for Large Industrial Rectifiers.....Bowar . . . 1

58-920 Temperature Distributions.....Eckert, Hartnett, Irvine, Birkebak . . . 5

58-903 Automatic Gage Controller for Reversing Steel Mill.....Duke, Hulls . . . 10

58-118 Terminal Spacings for High-Altitude Applications.....Duncan, Rectanus . . . 16

58-796 Transfer Functions of Loaded Synchronous Machine.....Hamdi-Sepen . . . 19

58-917 Energy-Conversion Properties of Induction Machines.....Riaz . . . 25

59-249 Communication Systems for Railway Traffic Control.....Sibley . . . 30

59-30 Rapid Heating of Dielectric Materials at 915 Mc.....Feiker, Gittinger . . . 35

59-77 Some Unusual Designs of Electric Resistance Heating.....Hynes . . . 40

58-224 Anode Breaker Testing.....Harris, Scully, Stewart . . . 43

Conference Papers Open for Discussion.....See 3rd cover

NUMBER 41

Published Bimonthly by

AMERICAN INSTITUTE OF ELECTRICAL ENGINEERS

Communication and Electronics—March 1959

58-401	Evaluation of Enamel Magnet Wire	Saums, Pendleton	1
58-1025	Matrix Synthesis of High-Speed Logic	Schubert	4
58-173	Transfer Efficiency in Mag. Amplifiers—II	Pula, Lynn, Ringelman	8
57-1097	Negative-Impedance Voice Repeater Employing Transistors	Howell	11
57-786	Review of Telephone Development	Wallenstein	15
58-1208	Progress in the Field of Insulating Materials	Callinan	22
57-809	Subdivision of Telephone Traffic	Molnar	28
58-814	Pagemaster Receiver and Modulation Equipment	Young	45
58-813	City-Wide Personal Signaling at Allentown-Bethlehem, Pa.	Kraus	52
58-989	Systems Engineering of Personal Radio Signaling Systems	Strack	55
57-1015	Design of Random-Noise Transformers	Vore	59
58-326	Properties of Octafluorocyclobutane, a Dielectric Gas	Blodgett	63
58-117	Magnet Wire for 600 C Temperature Transformers	Wareham	66
58-879	Residual Polarization of $BaTiO_3$ Ceramics	Saito, Yamanaka	70
58-188	Development of Ceramic Hydrogen Thyratrons	Price, Coolidge	76

(*See inside back cover*)

Applications and Industry. Published bimonthly by the American Institute of Electrical Engineers, from 20th and Northampton Streets, Easton, Pa. AIEE Headquarters: 33 West 39th Street, New York 18, N. Y. Address changes must be received at AIEE Headquarters by the first of the month to be effective with the succeeding issue. Copies undelivered because of incorrect address cannot be replaced without charge. Editorial and Advertising offices: 33 West 39th Street, New York 18, N. Y. Nonmember subscription $8.00 per year (plus 50 cents extra for foreign postage payable in advance in New York exchange). Member subscriptions: one subscription at $2.50 per year (balance of $5.00 subscription price to be paid by application of annual dues) to any one of three divisional publications: Communication and Electronics, Applications and Industry, or Power Apparatus and Systems: additional annual subscriptions $5.00 each. Single copies when available $1.50 each. Second-class mail privileges authorized at Easton, Pa. This publication is authorized to be mailed at the special rates of postage prescribed by Section 132.122.

Printed in United States of America

Number of copies of this issue 13,700

Design Considerations for Large Industrial Semiconductor Rectifiers

GERALD J. BOWAR
ASSOCIATE MEMBER AIEE

THE SUCCESS in the use of germanium rectifier cells in low-voltage industrial rectifiers since their introduction in 1952 has created a need for higher voltage rectifiers with comparable advantages in efficiency and low initial and maintenance cost. To obtain higher voltages, germanium cells must be operated in series until such time that higher voltages per single cell are made possible.

This paper covers the development of a germanium rectifier rated 250 volts at 7,778 amp (amperes) d-c per cubicle or section. It uses four cells in series. Eighteen of these sections are connected as shown on the one-line diagram represented by Fig. 1 to supply 140,000 amp at 250 volts d-c or a total kw capacity of 35,000 to operate a chlorine line.

The curves or data included in this paper are substantiated by the results of a full-load test applied to the first production section of this type. Although the experience gained here is for a specific germanium rectifier, the basic design principles should be applicable to other ratings and configurations as well as to silicon.

Design Standards

If semiconductors are to be accepted in the large industrial power field, certain basic requirements should be followed or met so as to uphold the standards set forth by these industries. Some of the main considerations are given in the following:

Mechanical:

1. The unit should be sturdily constructed and rugged in appearance.
2. Component parts should be arranged so that they are readily accessible and easily repaired.
3. Bus bars should be rigidly supported and capable of withstanding the maximum short-circuit stresses that could be encountered.
4. Adequate spacing should be maintained between live parts and casing or ground, particularly between d-c busses where it is unlikely that a circuit breaker will be installed.
5. Nontracking or arc-resistant materials should be used for insulating conductors which are connected to high-energy-level d-c loads. Flame-retardent materials should be given serious consideration, particularly when the voltages go above 300 volts.

Electrical:

1. The unit should be conservatively rated to account for the numerous variables affecting current balance in applying large numbers of series-parallel combinations.
2. Fuses or protective devices for the rectifier elements should be carefully selected and co-ordinated with the main overload protection to provide maximum utilization of the equipment.
3. A sufficient number of reliable auxiliary protective devices should be used to protect the equipment adequately and to keep unnecessary shutdowns to a minimum.
4. Safety requirements should be commensurate with the standards of the industry.

Discussion

Rectifier Cubicle

The approach taken for this design was to have an arrangement as shown in Fig. 2. This is a plan view of one subsection of the rectifier where *R*1 through *R*6 represent the six rectifier elements (nine elements in parallel and stacked in a vertical plane in this instance) in a 3-phase bridge circuit. The rectifier elements are mounted in plug-in-type trays to facilitate making the electrical connections to their respective a-c and d-c busses. The trays were designed so that, when fully engaged in the rectifier subsection, they form a duct confining the cooling air to the cell portion of the tray. A very compact arrangement was thus achieved with the ultimate in convenience for repair and maintenance.

To obtain the current rating of 7,778 amp, four of these subsections are required which make up a complete section as shown in Fig. 3. The end subsection houses the d-c disconnect switches and auxiliary controls. General Electric type *LVD* busway was used on the a-c side extending the full length of the rectifier portion of the section. Electrical connections are made to the vertical a-c risers in each subsection, thus paralleling the four subsections. The d-c busses are collected on either side near the bottom of the cubicle and extended into the d-c switch subsection and then brought up through the switches and out the top for the customer's connections.

In this case a separate blower unit, combined with a chilled-water heat exchanger and filter, was furnished by the customer to supply cooling air to the rectifier elements. The air was forced through a duct build into the floor where it entered the rectifier at the bottom and discharged out the top into the room. The air in the rectifier was confined to the cell area of the germanium trays by ducts extending from the lower tray level to the upper portion of the cubicle base. The base was thus pressurized and formed an integral part of the main air duct.

Fig. 4 shows a section without side panels or trays with the internal assembly nearly completed.

Fig. 5 shows a completed section which was taken while the rectifier was being set up for test.

Germanium Trays

The germanium tray consists of four germanium cells connected in series, a fuse, four parallel resistors, and an individual cell-failure indicator. The two lamps on the front of the tray provide indication when either the fuse opens or when one or more of the four cells fail. The germanium tray and cell are shown in Figs. 6 and 7, respectively.

The four cells, when mounted in the tray, are attached to the insulating side panels which also serve as the series-connection point between the cells. The parallel resistors and cell-failure indicator elements are all mounted in the fuse compartment which lies between the front cover and the first germanium cell.

Protective Devices

Twenty-four 20-microfarad capacitors were installed in the rectifier to improve the commutating duty. One of these is connected across each leg of the bridge in each subsection near the center tray.

The auxiliary protective devices in this rectifier section include:

1. A pressure switch sensing the pressure in the main air duct supplying cooling air

Paper 58-222, recommended by the AIEE Industrial Power Rectifiers Committee and the Semiconductor Metallic Rectifiers Committee of the Communication and Electronics Division and approved by the AIEE Technical Operations Department for presentation at the AIEE Winter General Meeting, New York, N. Y., February 2–7, 1958. Manuscript submitted October 28, 1957; made available for printing July 1, 1958.

Gerald J. Bowar is with the General Electric Company, Philadelphia, Pa.

The author wishes to express his appreciation to A. Schmidt, Jr., N. J. Lipstein, L. W. Burton, F. W. Kelley, G. R. Lezan, and J. P. Wiles for their assistance in the development and analysis of the design described in this paper.

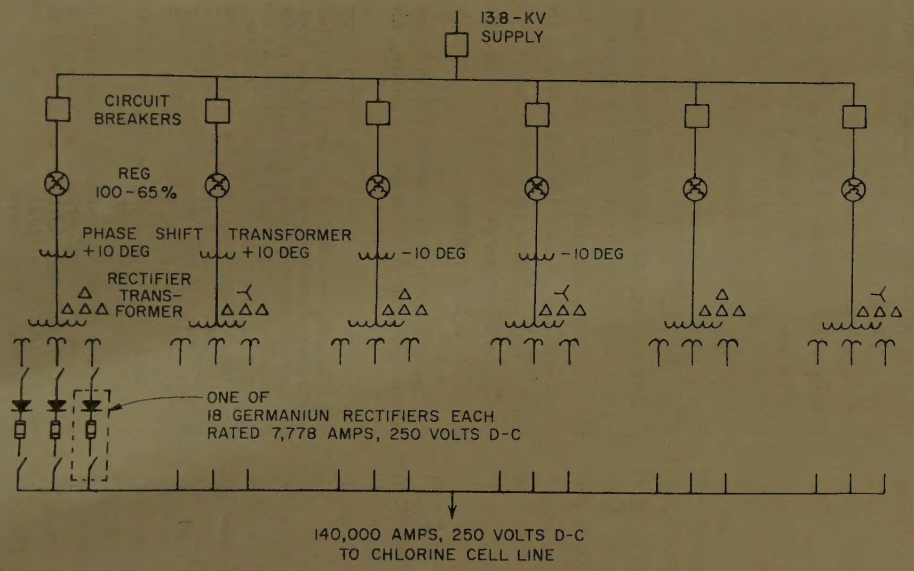

Fig. 1. One-line diagram of germanium power supply

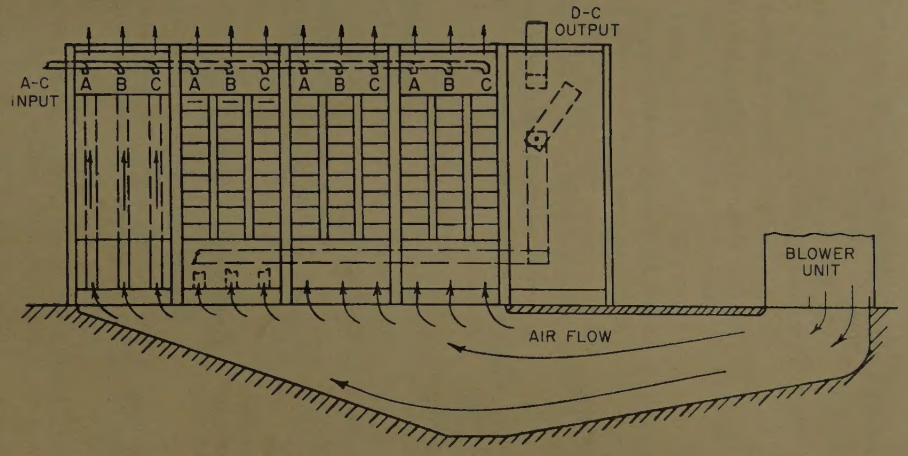

Fig. 3. Elevation view of complete cubicle and air duct in floor

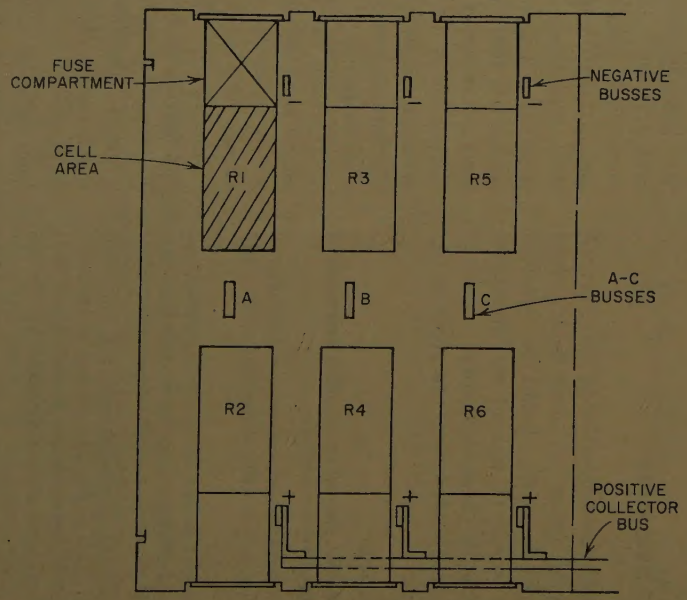

Fig. 2. Plan view of one subsection

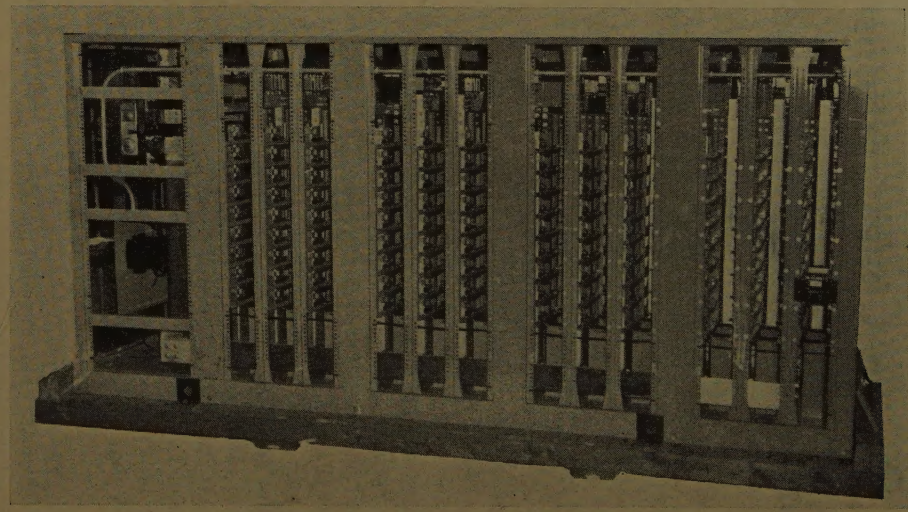

Fig. 4. Rectifier section in final assembly stage

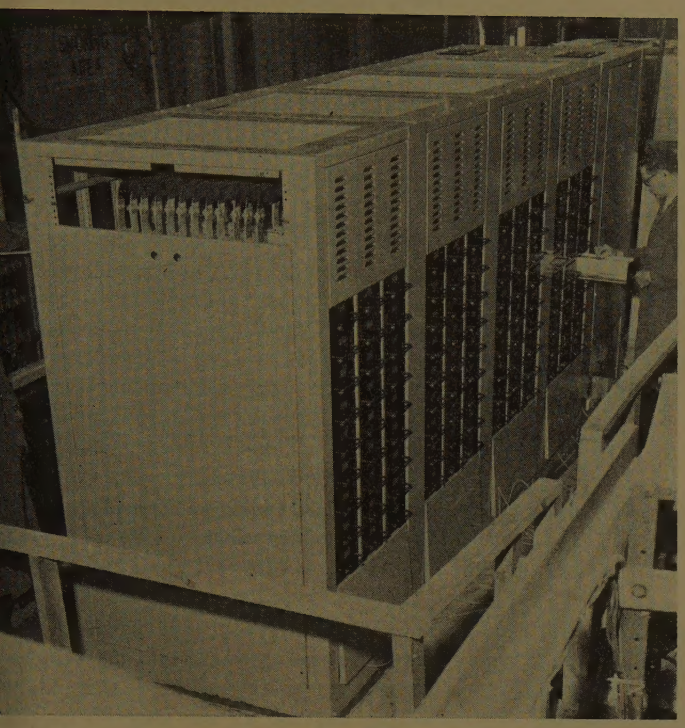

Fig. 5 (left). Rectifier section on load test stand

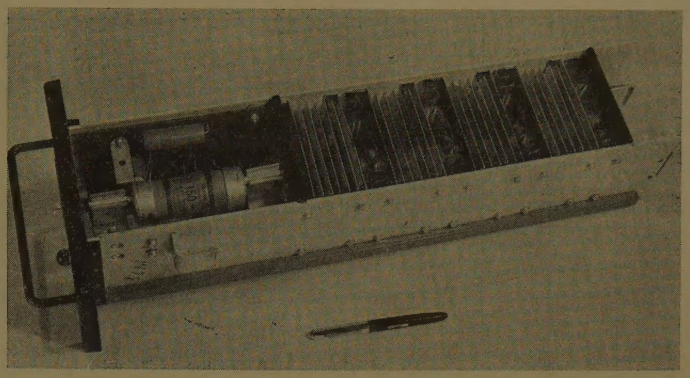

Fig. 6 (above). Positive germanium tray assembly

to the rectifier elements. This device provides a tripping signal for the main breaker if the pressure, and thus the flow, drop below a set value.

2. An overtemperature device consisting of a resistance temperature detector, located in one of the discharge air paths, which is used in conjunction with an overtemperature relay. This device provides overtemperature protection for the germanium cells when operating at rated load and higher than rated ambient or sustained overloads without compensating for or reducing the ambient.

3. A fuse monitor system provides a tripping signal when the third fuse in any one leg of the bridge opens.

4. An individual cell-failure device which provides indication only when one or more of the germanium cells in a tray fails.

Design Problems

After the general physical arrangement and objectives were established, the design problems centered around the germanium tray and the cubicle structure and bussing.

During the initial design, one of the first problems that had to be resolved was the selection of the number of series cells and a means for insuring equal sharing of the inverse voltage. Four cells were selected to be used in series based on previous experience on low-voltage applications, and 250-ohm resistors were used in parallel with each cell to equalize the inverse voltage. This value was selected by compromising between the maximum voltage the series string could withstand (limiting the voltage to 200 volts maximum per cell) and the maximum watts loss that could be tolerated in the equipment. Under the worst conditions the series string of cells can thus withstand 647 volts and the full-load losses represent approximately 0.3% reduction in efficiency. The maximum surge voltage expected across the string of four cells was 600 to 650 volts which was the anticipated recovery voltage of the fuse. A 150-amp current-limiting-type fuse was used in this case. The tests conducted on the complete section indicated that this peak recovery voltage would be well below 600 volts.

Another basic problem was the selection of the number of cells required in parallel. A number of factors contributed to this selection, namely: volume of air flow, ambient air temperature, air temperature rise in the vertical cooling path, and current unbalance between the parallel elements within the cubicle. The most indeterminate factor in the early design stages was the current unbalance expected when assembling such a large number of cells in a single unit. The final selection was a 6-4-36 cell combination or four cells in series with 36 elements or trays in parallel. This corresponds to approximately a 13% derating in current as compared to the normal rating of these cells when applied to smaller rectifiers used for electrochemical service.

The germanium tray design was an intricate problem within itself primarily consisting of the selection of satisfactory clips for plug-in-type use, providing adequate air seals to be provided between the trays along with matching them to the guide rails provided in the rectifier cubicle. Opposite hand units were made to distinguish readily between the positive and negative side. A forward grading system was established for the complete trays and limits assigned for those to be used in parallel in any one leg. For this production test a single-phase half-wave circuit was used. A 100-amp average short-circuit current was applied with the cooling air controlled to hold the average junction temperatures to 65 degrees centigrade and the voltage drop across the output terminals recorded A 60-millivolt spread in these readings was allowed for one tray grade. The total number of tray grades was limited to three for each of the positive- and negative-type trays. Each leg of the rectifier bridge, consisting of 36 trays, was thus permitted to use any one of the three grades.

In determining the basic configuration of busses and rectifier elements within the cubicle, an attempt was made to provide a symmetrical arrangement and thus equalize as nearly as possible the impedance drops through the numerous parallel paths. The resistive drop in the vertical a-c and d-c busses was equalized by making them

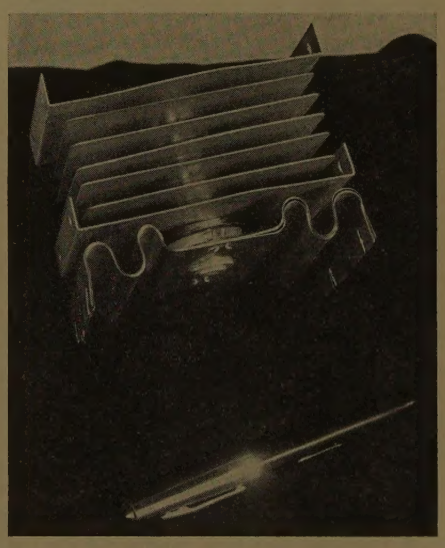

Fig. 7. Germanium cell assembly

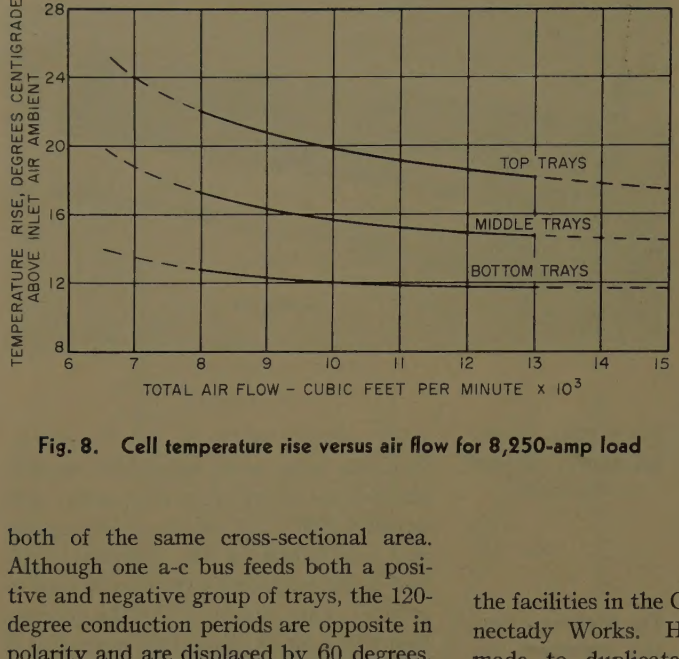

Fig. 8. Cell temperature rise versus air flow for 8,250-amp load

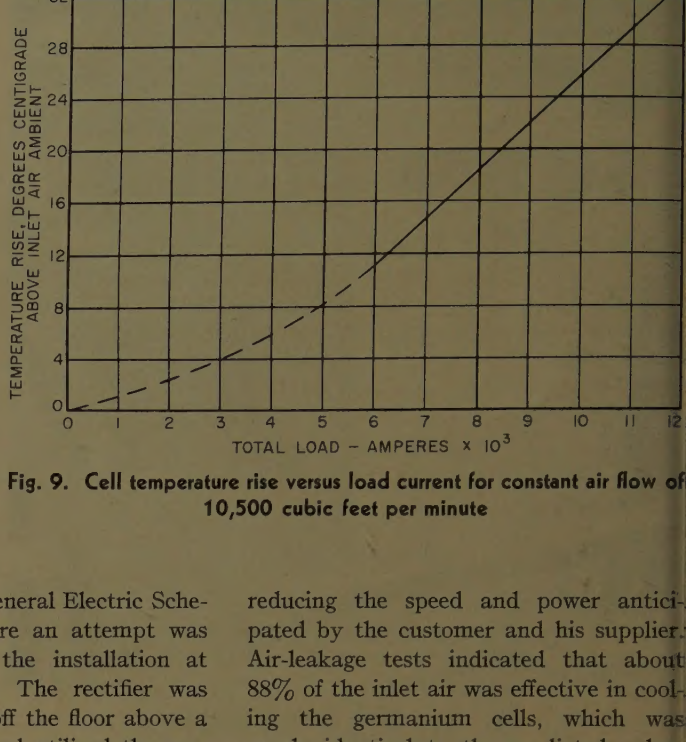

Fig. 9. Cell temperature rise versus load current for constant air flow of 10,500 cubic feet per minute

both of the same cross-sectional area. Although one a-c bus feeds both a positive and negative group of trays, the 120-degree conduction periods are opposite in polarity and are displaced by 60 degrees, so it was assumed that each d-c riser should be of the same cross-sectional area as the a-c riser. A variation in the reactance of the nine parallel paths in one leg connecting these two busses was anticipated, however with the top and bottom trays having a lower reactance and thus carrying more current than the middle trays.

An attempt was also made to balance the impedance drops in the bus bars interconnecting the four rectifier subsections. For the a-c feed, type *LVD* busway was used as previously mentioned. This busway consists of 2-by-$^1/_4$-inch bus bars spaced on 3/4-inch centers and interlaced phase-wise to provide a low-voltage drop. Use of this type of busway reduced the reactive drop present on the a-c side which made it easier to match the d-c busses where there was no reactive drop.

A full-load test conducted on this section revealed the existence of a phase-current unbalance within the cubicle. It became apparent that because of the bus configuration, the commutating reactance between adjacent phases in the four subsections was not the same, with the result that the output current included a circulating component. Inspection of oscillograms indicated that this circulating component originated during commutation and that the currents were steady during the remainder of the conducting period. To correct this condition, small amounts of iron were installed around the vertical a-c busses in varying amounts until a satisfactory balance was achieved.

Full-Load Test

A full-load test was conducted on the first production rectifier section utilizing the facilities in the General Electric Schenectady Works. Here an attempt was made to duplicate the installation at the customer's site. The rectifier was mounted a few feet off the floor above a fabricated air duct and utilized the customer's blower unit as shown in Fig. 5. Electrically, however, the rectifier was connected to a fixed a-c source yielding an open-circuit voltage of nearly 300 volts d-c. The rectifier was loaded through a circuit breaker to some motor-generator sets which pumped power back into the line. Operation under test was thus accomplished by applying full voltage to the section under open-circuit conditions, and then closing the circuit breaker and gradually bringing up the load to the value desired.

Extensive tests were conducted with varying air flows and loads with checks being made on current balance, temperature rise, and general over-all performance. The commutating voltage and current was observed and photographed during which time some experimentation was done with varying capacitances in the circuit. In addition, several fault tests were made by purposely blowing some fuses and taking oscillograms of the currents feeding the fault.

Summary of Test Results

Air Flow

The total air-flow rating for this rectifier section was 10,500 cubic feet per minute at 32 degrees centigrade ambient.

The air-flow distribution through the rectifier trays varied approximately ±3% from the mean in the 24 parallel paths, which was better than expected. The duct itself exhibited a rise in pressure between the blower and rectifier, thereby reducing the speed and power anticipated by the customer and his supplier. Air-leakage tests indicated that about 88% of the inlet air was effective in cooling the germanium cells, which was nearly identical to the predicted value. The air-flow performance thus met or exceeded expectations in all respects.

Current Balance

The total current unbalance expected as a result of these tests is as follows:

1. Current unbalance in parallel trays due to limits of grading ±5.5%.
2. Current unbalance in vertical paths due to cubicle design ±5%.
3. Phase-current unbalance between subsections due to cubicle design ±10%.
4. Subsection current unbalance ±1.5%.

The total unbalance is thus ±22.0%. Allowing for variation in the test results, the total unbalance should be within ±25% which compares favorably to that total unbalance expected in the early design stages.

Temperature Rise

The average temperature rise above the inlet air ambient on several of the germanium cells as measured by thermocouples is plotted against air flow for the top, middle, and bottom row of trays for a load of 8,250 amp on Fig. 8. The temperature differential between the top and bottom trays closely follows the difference in air temperature as expected. The curves are also quite flat, indicating that variations in air flow should not have an appreciable effect on temperature rise.

Fig. 9 shows a plot of temperature rise versus load which is also of interest. This appears to be a linear function when operating above approximately 3/4 load which is exactly what is expected assum

ng constant air density which is essen-ially true for the small differential in emperatures involved.

General Comments

During the 3-week test period, this unit was operating at full load or above for approximately 30 hours. Two cells (864 used in the section) failed during this period, one failure occurring on the initial application of voltage. Both trays with the failed cells were purposely left in the rectifier without any subsequent failures during this test period.

The observations made on the commutating duty indicated that the 20-microfarad capacitors selected were adequate. It was originally thought that individual capacitors across each cell might be needed to improve the commutating duty, but these were found to have no significant effect.

Another test that was tried consisted of removing and reinserting a tray while operating at full load. This was done on several trays with no arcing observed nor any signs of such noted on the contacts upon further examination when the unit was shut down.

One of the final tests was the application of 150% current to one of the four subsections. This load was held for 5 minutes with no ill effects.

Conclusions

The experience gained from this rectifier design shows that considerable emphasis should be placed on attaining a good symmetrical arrangement of components resulting in the best inherent reactance balance in all parallel conducting paths.

These tests have proved that this design of series-parallel combinations of germanium cells is basically sound and it is expected that its performance will meet with good customer acceptance and satisfaction. The tests further prove that design of large blocks of power using semiconductors is only in its infancy. The development of larger cells with greater current-carrying capacity coupled with higher inverse voltages, which are expected with silicon, would further simplify this type of design. These features, combined with the high efficiency of semiconductor elements, make them a natural candidate as the most economical source of d-c power in the future.

The Electrical Analog for Determining Temperature Distribution in Electrical Components

E. R. G. ECKERT
NONMEMBER AIEE

J. P. HARTNETT
NONMEMBER AIEE

T. F. IRVINE
NONMEMBER AIEE

RICHARD BIRKEBAK
NONMEMBER AIEE

SPACE and weight limitations in present-day aircraft necessitate miniaturization of air-borne electric equipment. Such miniaturization generally results in high heat dissipation per unit volume which may lead to local temperatures which exceed the material limitations, causing failure of the component. To avoid such failure, electrical engineers must examine the heat-transfer problem when designing compact electric apparatus. It is the purpose of this paper to present a method of heat-transfer analysis which is relatively simple and straightforward and which utilizes concepts and equipment familiar to electrical engineers. The proposed method is based on the fact that the differential equations describing the flow of heat are identical to those for the flow of electric current; consequently, an electrical analog of the heat-flow problem can be readily constructed and the electrical measurements of current and voltage can be directly translated to the equivalent thermal quantities, heat flow and temperature.

The authors' attention was directed to such cooling problems when they were asked by Jack & Heintz, Inc., Cleveland Ohio, to aid in the determination of the temperature distribution in a high-performance generator coil. The electrical analog was used to solve this particular problem, but it should be emphasized that the method has wide utility.

Nomenclature

e = voltage
E = dimensionless voltage defined by $E = e - e_a / e_w - e_a$
h = heat-transfer coefficient, Btu/hr (British thermal units per hour) square foot, degrees Fahrenheit
i = current flow
i''' = current-density, current per cubic inch
k_t = conductivity of generator coil material
l = electrolytic-tray variable trough length inch
L = maximum dimension of generator coil or analog cross section
n = direction normal to surface
N_q = dimensionless ratio $q'''L^2/k_t(t_w - t_a)$
N_h = dimensionless ratio hL/k_t
q = heat flow, Btu/hr square inch
q''' = internal heat generation, Btu/hr cubic inch
Q = total heat flow, Btu/hr
Q''' = total internal heat generation, Btu/hr
t = temperature, degrees Fahrenheit
T = dimensionless temperature ratio defined by $T = t - t_a / t_w - t_a$
x, y = co-ordinates, inch
X, Y = dimensionless co-ordinates defined as $X = x/L$ and $Y = y/L$

Subscripts

a = air stream
avg = average
e = electrical analog
h = refers to dimensionless parameter in which the heat-transfer coefficient appears
max = maximum
q = refers to dimensionless parameter in which the internal heat generated appears
t = thermal
w = isothermal wall

Analytical Basis for Electrical Analog

The rotor cross section of the Jack & Heintz aircraft generator is shown in Fig. 1 with the generator coil given special designation. An expanded section of the generator coil is given in Fig. 2(A), and the following analysis applies to this

---

Paper 58-920, recommended by the AIEE Air Transportation Committee and approved by the AIEE Technical Operations Department for presentation at the AIEE Summer General Meeting and Air Transportation Conference, Buffalo, N. Y., June 22–27, 1958. Manuscript submitted March 25, 1958; made available for printing August 21, 1958.

E. R. G. Eckert, J. P. Hartnett, T. F. Irvine, and Richard Birkebak are all with the University of Minnesota, Minneapolis, Minn.

The authors acknowledge the assistance of Roland C. Birkebak in the design of the apparatus and the collection and analysis of the experimental data, the work of F. J. Bradac in the construction of the equipment, and the financial support of Jack & Heintz, Inc.

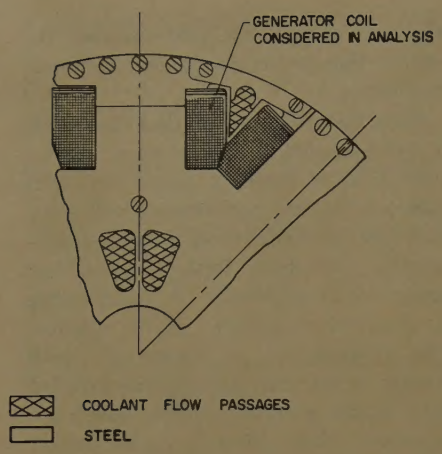

Fig. 1. Rotor cross section

Fig. 2 (right). Sketch of electrolytic analog

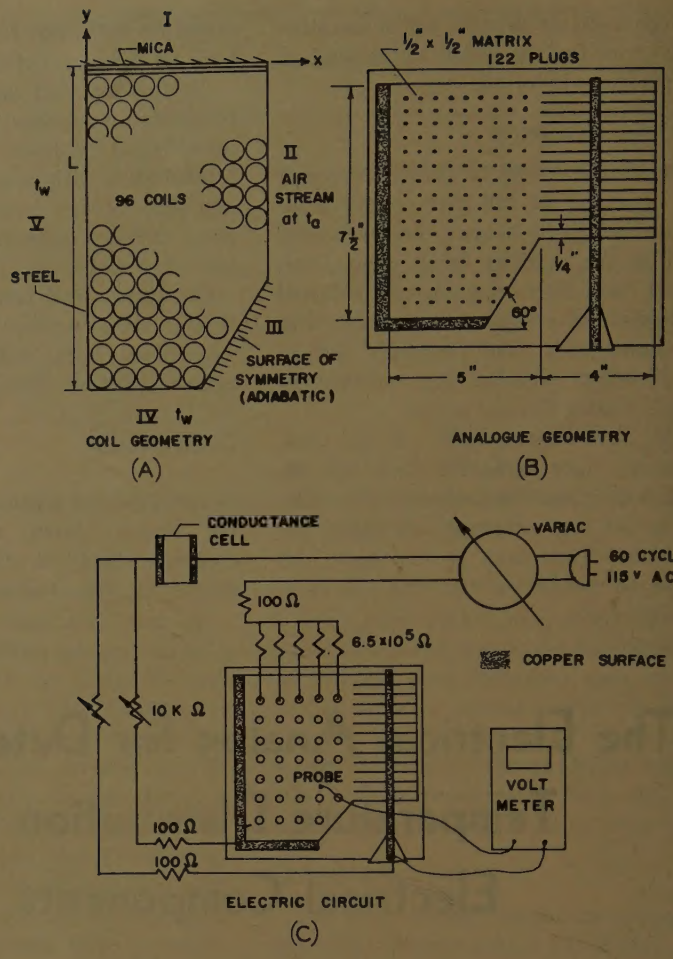

geometry. It is assumed that the following data are specified: 1. the heat-generation rate which may be calculated from electrical losses, 2. the temperature of the cooling air, which may be determined by direct measurement, 3. the heat-transfer coefficient for the coolant gas flow over the coil surface which may be estimated from established relations for convection heat transfer if the mass flow rate and the physical properties of the coolant gas are specified, 4. the temperature within the steel material immediately adjacent to the coil (assumed to be constant in the present problem), which may be determined by direct measurement. Starting with this information, the average and maximum temperatures occurring within the coil will now be determined. In addition, the fraction of the total heat generated that flows out through the air-cooled surface will be determined.

It is assumed that the heat flow is steady and 2-dimensional with each coil wire acting as a line source of uniform heat generation. The steady-state 2-dimensional heat-conduction equation with internal heat generation is

$$k_t\left(\frac{\partial^2 t}{\partial x^2}+\frac{\partial^2 t}{\partial y^2}\right)+q'''=0 \qquad (1)$$

Equation 1 can be made dimensionless with

$$X=x/L \quad Y=y/L$$

and

$$T=\frac{t-t_a}{t_w-t_a}$$

where t is the local temperature at any position within the coil, t_a is the air temperature, and t_w is the isothermal wall temperature. The length L is chosen as the maximum coil dimension in the cross section shown in Fig. 2(A). Equation 1 then becomes

$$\frac{\partial^2 T}{\partial x^2}+\frac{\partial^2 T}{\partial Y^2}+\frac{q'''L^2}{k_t(t_w-t_a)}=0 \qquad (2)$$

This equation must be solved subject to the boundary conditions which are imposed on the generator coil, Figs. 1 and 2(A). Surface I is in contact with mica insulation, and it is assumed that no heat flows across this surface; the same assumption is made for surface III because of symmetry of the coil geometry. An air stream at temperature t_a flows past surface II and heat transfer by convection occurs. Surfaces IV and V are in contact with the steel surface of the armature and are at a constant temperature. These boundary conditions can be summarized as

Along face I

$$\frac{\partial t}{\partial y}=0$$

or

$$\frac{\partial T}{\partial Y}=0$$

Along face II

$$-k_t\partial t/\partial x=h(t-t_a)$$

or

$$-\frac{\partial T}{\partial X}=\left(\frac{hL}{k_t}\right)T$$

Along face III

$$\partial t/\partial n=0$$

or

$$\partial T/\partial\left(\frac{n}{L}\right)=0$$

Along face IV

$$t=t_w$$

or

$$T=1$$

Along face V

$$t=t_w$$

or

$$T=1$$

Due to the configuration of the generator coil and the complexity of the boundary conditions, solutions to equation 2 are not readily obtainable. However, the dimensionless heat-transfer parameters involved which control the problem can be obtained directly from equation 2 and the boundary conditions. The dependent dimensionless temperature T is seen to

epend on the independent dimensionless alues of the position, heat-generation ate and convective heat-transfer co-fficient:

$$f\left(X, Y, \frac{q'''L^2}{k_t(t_w-t_a)}, \frac{hL}{k_t}\right)$$

The solution to this heat-transfer prob-em can be readily obtained by consider-ng the equivalent electrical problem herein the same geometry is utilized and ne equivalent electrical boundary condi-ons are imposed. The 2-dimensional teady-state equation describing the elec-ric potential in a conducting material aving the shape as shown in Fig. 2(A) nay be written:

$$\left(\frac{\partial^2 e}{\partial x^2}+\frac{\partial^2 e}{\partial y^2}\right)+i'''=0 \qquad (3)$$

Equation 3 can be made dimensionlesss hen the potential parameter $E=(e-e_a)/(e_w-e_a)$ and the dimensionless ngths $X=x/L$ and $Y=y/L$ are intro-uced.

$$\frac{\partial^2 E}{\partial X^2}+\frac{\partial^2 E}{\partial Y^2}+\frac{i'''L^2}{k_e(e_w-e_a)}=0 \qquad (4)$$

The boundary conditions to be im-osed on the electrical analog to the coil eometry shown in Fig. 2(A) are

long face I

$\frac{e}{y}=0$

$E/\partial Y=0$

long face II

$k_e\frac{\partial e}{\partial x}=\left(\frac{k_e}{l}\right)(e-e_a)$

$\frac{\partial E}{\partial X}=\left(\frac{k_e}{l}\right)\frac{L}{k_e}E$

long face III

$=0$

$E/\partial(n/L)=0$

ong face IV

$=e_w$

$=1$

ong face V

$=e_w$

$=1$

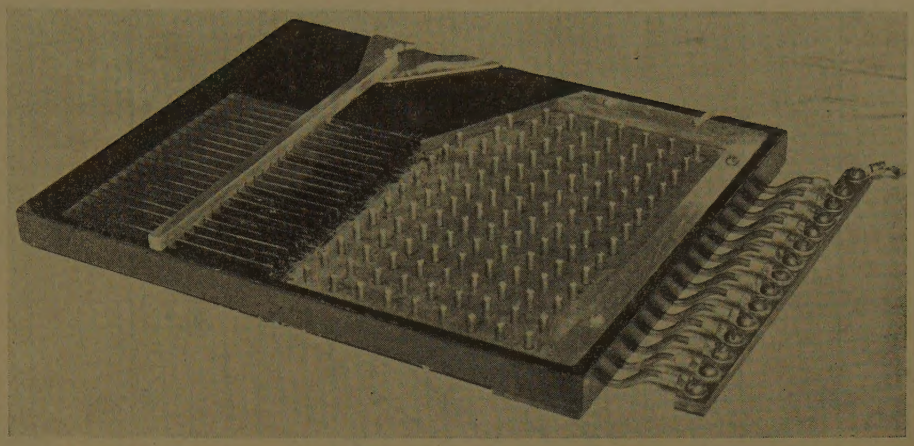

Fig. 3. Actual electrolytic analog

In the electrical analog the thermally insulated surface I and the adiabatic surface III are replaced by electrically insulated boundaries; on surfaces IV and V, a constant-voltage condition is substituted for the isothermal conditions. On surface II the thermal conductance, h, is replaced by the electrical conductance, $k_e/1$, and electric current flows through this conductance to a constant-voltage surface simulating the air stream.

The thermal and electrical equations 2 and 4 are identical, as are their boundary conditions; consequently, a solution to the electrical problem is also a solution to the thermal problem. The following summarizes the analogy.

Independent Parameters:

Thermal

$$\frac{q'''L^2}{k_t(t_w-t_a)}=N_q$$

$$\frac{hL}{k_t}=N_h$$

Electrical

$$\frac{i'''L^2}{k_e(e_w-e_a)}=N_q'$$

$$\frac{(k_e/l)L}{k_e}=\left(\frac{L}{l}\right)=N_h'$$

Dependent Parameters:

Thermal

$$\left(\frac{t-t_a}{t_w-t_a}\right)$$

$$\frac{Q_w}{Q'''}$$

Electrical

$$\left(\frac{e-e_a}{e_w-e_a}\right)$$

$$\frac{I_w}{I'''}$$

The independent electrical parameters, N_q' and N_h', are now varied over the range of interest and the results are directly interpreted in terms of the thermal problem. It may be noted that Q_w/Q''' is also listed with its electrical analog I_w/I''': This quantity is the ratio of the flow of heat (or electric current) through the isothermal faces to the total heat (or current) generated in the coil.

Electrolytic-Tray Analog

The coil geometry was magnified by a factor of 7.5 with the resulting dimensions of the analog given in Fig. 2(B). The electrolytic tray was constructed from a Bakelite material, and the coil geometry milled into the Bakelite plate to a depth of 1/4 inch. Fig. 3 shows an over-all view of the tray. The copper wires of the generator coil which generate heat

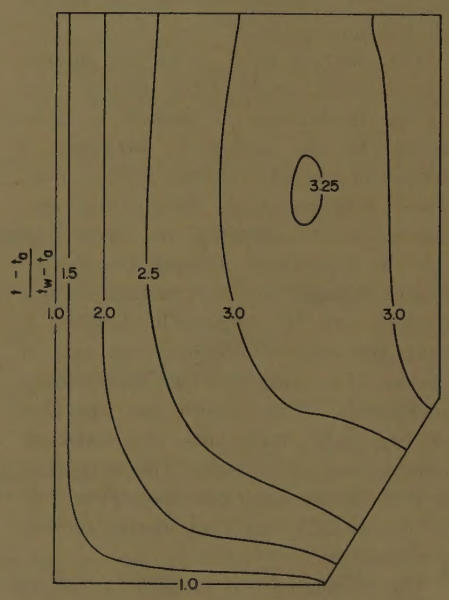

Fig. 4. Isothermal lines for generator coil

$N_q=24$
$N_h=2$

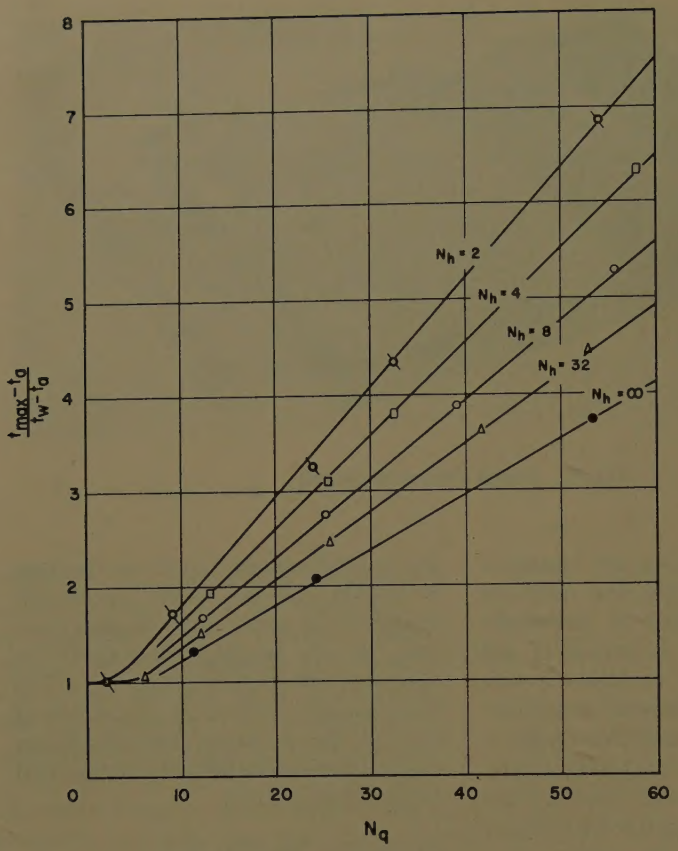

Fig. 5 (above). Maximum core temperature

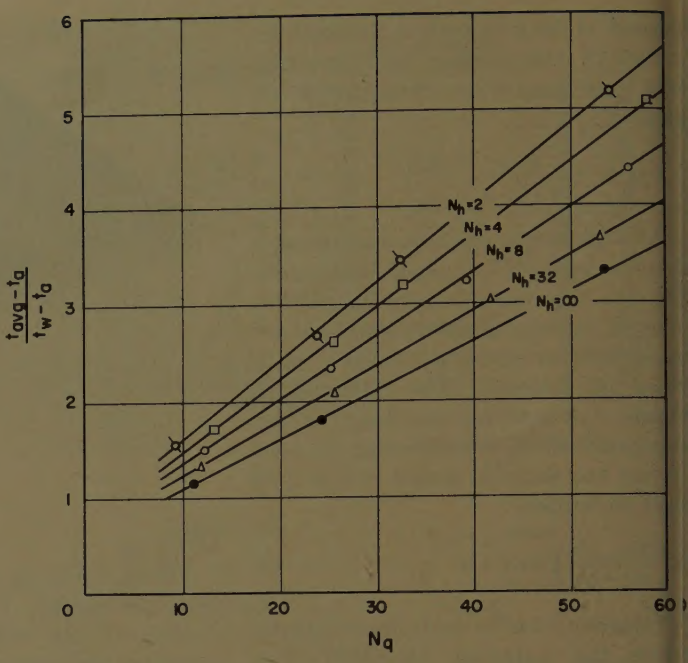

Fig. 6 (above, right). Average core temperature

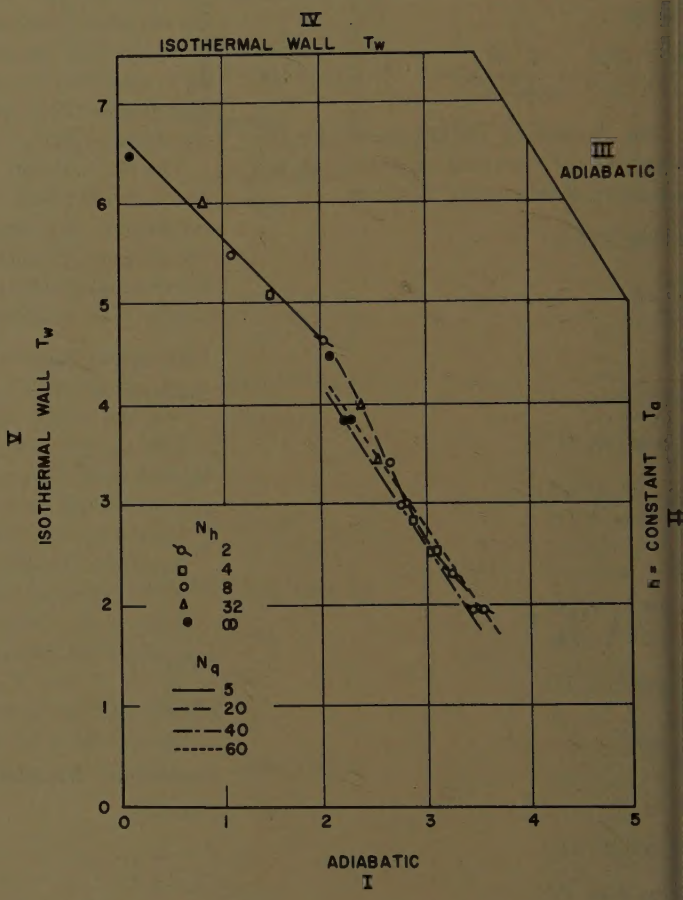

Fig. 7 (right). Position of maximum temperature in coil

uniformly are obtained in the analog by a series of brass plugs shown in Figs. 2 and 3. In order that the current flow through each brass plug be equal, resistors of 6.5 $\times 10^6$ ohms are placed in series with each plug as shown in Fig. 2(C). As a result, the potential drop across the electrolyte is small as compared to the drop across these resistors, and the conditions of uniform heat generation in the coil wires is closely approximated.

The heat transfer from the nonisothermal wall face II of the generator coil to the isothermal air stream is represented in the analog by arranging a series of linear electric resistances. These resistances are incorporated into the analog by extending the electrolytic tray by a number of small troughs arranged normal to the surface. These troughs are of adjustable length, so that the electric conductance can be varied (i.e. varying the heat-transfer coefficient). The copper bar indicated in Fig. 2(B) represents the constant-temperature air stream. The isothermal wall of the generator coil, faces IV and V, is represented by an equipotential surface, a copper bar.

The completed tray is filled to a depth of 1/4 inch with ammonium nitrate, an electrolyte. A conductance cell for measuring the resistivity of the electrolyte was connected directly into the circuit, Fig. 2(C). The dimensions of the cell at the electrolyte surface are 4 by 1 inch and its depth, 1/4 inch. This gives a length to area ratio of 1 inch^{-1} and as a result the resistance measured across the cell gives the specific resistivity ρ_e. (i.e., $\rho_e = 1/k_e$) directly in ohm-inches. The entire electric circuit is shown in Fig. 2(C).

Procedure

The resistivity of the solution was measured at the beginning and at the end of each test to insure that it remained constant. A check was made on the uniformity of current generation at six points in the coil and it was found that

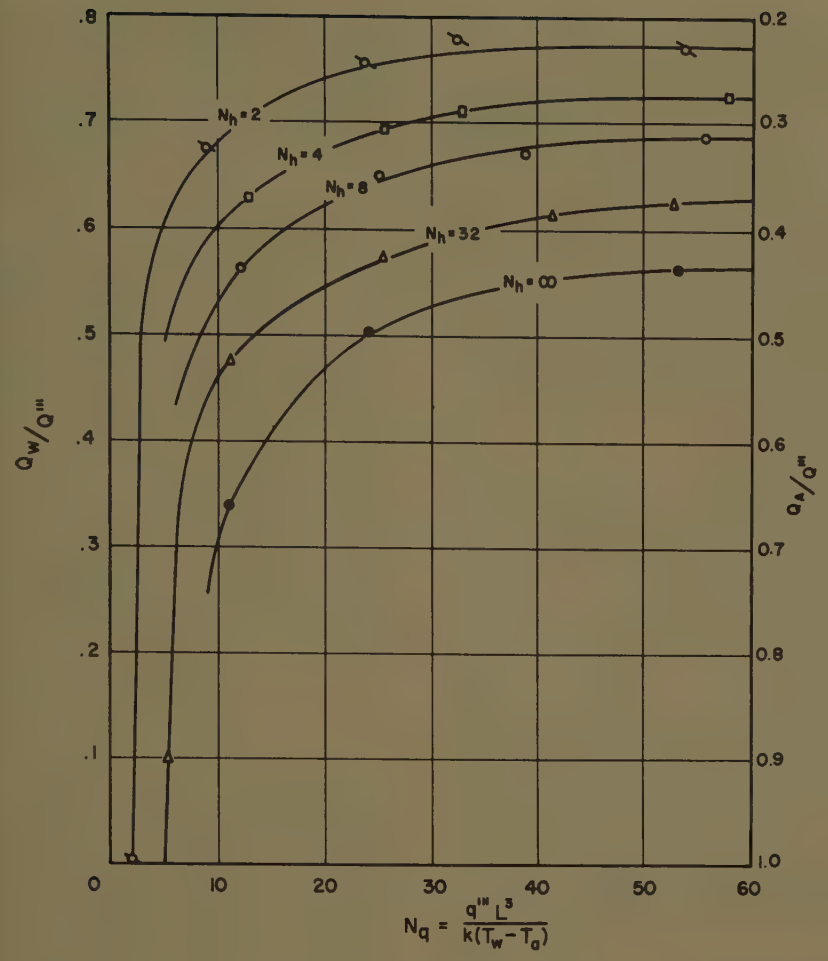

Fig. 8. Heat flow through isothermal wall

this condition was approximated within $\pm 1\%$ if the specific resistivity of the electrolyte was kept less than 60 ohm-inches.

The heat-transfer coefficient represented by the extended tray and the potential difference from the equipotential surface to the equipotential air-stream copper bar were set to desired values. Then the total input current, the current flow to the constant-potential surfaces, and to the air-stream bar were measured. The potential difference from the brass plugs to the air-stream bar were measured with a high-impedance vacuum-tube voltmeter and the equipotential lines throughout the tray were plotted. A typical example is shown in Fig. 4. Sixty-cycle a-c power was used to prevent polarization.

A prescribed value of N_q was obtained either by varying the current or the potential difference, $e_w - e_a$, while a prescribed value of N_h was obtained by moving the copper bar from the coil boundary. The total current flow, the current flow through the isothermal wall, and the potential distribution were then measured.

Results

The range of independent parameters, N_q and N_h, investigated for the generator coil were

$N_q = 5$ to 60

$N_h = 2$ to ∞

The resulting value of the dimensionless maximum core temperature occurring in the generator as a function of the N_q and N_h parameters is shown in Fig. 5. For values of N_q greater than 10, the maximum temperature varies essentially linearly with N_q. A change in the heat-transfer coefficient for small values of N_h is seen to have an appreciable effect on the maximum temperature, while for larger values of N_h, a much smaller change in the maximum temperature is achieved.

Fig 6 shows the variation of the average core temperature defined as

$$\int_0^A t\,dA \Big/ \int_0^A dA$$

as a function of N_q and N_h. Again, as for the maximum core temperature, for values of N_q greater than 10, the average temperature varies linearly with N_q.

Not only are the maximum and average core temperatures desirable for use in the design of the coil, but also the position of the maximum temperature within the coil is of importance. Fig. 7 gives the variation of the position of maximum temperature for various values of N_q and N_h. For a decreasing heat-transfer coefficient on face II the maximum temperature moves away from face V and when N_h is zero (i.e. face II insulated) the maximum obviously occurs at the junction of faces I and II.

The total energy generated in the coil must be transferred out through the surfaces II, IV, and V. The ratio of the heat flow to the isothermal surfaces IV and V to the total energy generated, Q_w/Q''', is shown in Fig. 8. The fraction of the generated energy which flows to the air-cooled wall is given on the right scale as Q_a/Q'''. At low values of the dimensionless heat-generation rate, N_q, the heat-flow distribution is extremely

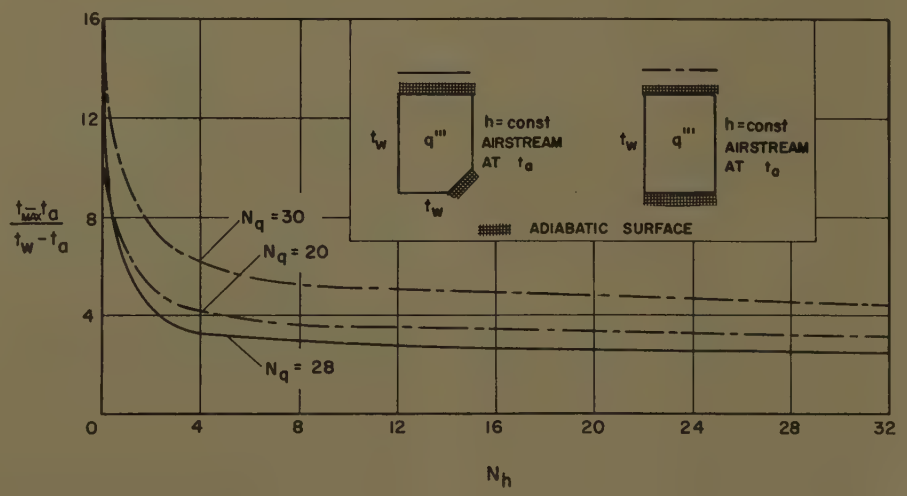

Fig. 9. Heat-transfer results for present coil geometry compared with analytical results for a simpler model

sensitive to slight changes in N_q and N_h. It can be observed that Q_w/Q''' approaches zero for $N_h=2$ at a finite value of N_q. This indicates that at this condition the air stream just carries away all of the energy generated. Turning to large values of heat generation, say N_q greater than 20, the distribution of the heat flow is found to be essentially independent of N_q and dependent only on N_h.

Finally, an analytical approach was used to verify the results obtained from the analog. A finite difference method was used to calculate the temperature distribution in the coil and the results were in good agreement with the analog values. Additionally, the actual geometry was approximated by a simple rectangular geometry as shown in the upper-right-hand corner of Fig. 9. The temperature distribution in this simple geometry may be determined by direct solution of the conduction equation, equation 2, and the resulting dimensionless maximum temperature is shown in the dotted curves on Fig. 9. It is seen that the general shape of the curves and the magnitude of the answers for this simple geometry are in good agreement with the results found for the actual coil geometry. On the basis of these additional analytical checks, it is concluded that the analog results are reliable.

Summary

1. The analogy between the flow of electricity and the flow of heat can be used to advantage to determine by electrical measurements the temperature distributions in electrical components.

2. The method was applied to a particular generator coil to obtain, under a variety of operating conditions, the temperature distribution, the average coil temperature, the location and magnitude of the maximum coil temperature, and the distribution and disposition of the internally generated heat flux.

References

1. Temperature Distribution in Generator Coils, E. R. G. Eckert, J. P. Hartnett, T. F. Irvine, Jr., Roland, Richard Birkebak. *Technical Report*, Heat Transfer Laboratory, University of Minnesota, Minneapolis, Minn., June 1957.

2. Temperature Distribution in Generator Coils, Report No. 2, E. R. G. Eckert, J. P. Hartnett, T. F. Irvine, Jr., Richard Birkebak. *Ibid.*, Oct. 1957.

3. Analogue for Solution of Heat-Conduction Problems, W. R. Simmons. *Preprint 233*, American Institute of Chemical Engineers, New York, N. Y., Dec. 1955.

4. An Electrolytic Analogue Applied to the Solution of a Thermal Conduction Problem, P. E. McNall, Jr., J. E. Janssen. *Paper no. 54-SA-45*, American Society of Mechanical Engineers, New York, N. Y., June 1954.

An Automatic Gage Controller for a 56-Inch Reversing Steel Mill

R. L. DUKE
ASSOCIATE MEMBER AIEE

L. R. HULLS
MEMBER AIEE

THIS PAPER describes an automatic gage-control system which has recently been put into service on a 56-inch 4-high reversing cold mill. Measurement of gage is achieved by suitable addition of signals proportional to the force tending to separate the work rolls and the unloaded separation between the work rolls. Control of gage is by screwdown and strip tension.

The theoretical basis of this type of gage measurement is considered in this paper and particular reference is made to various practical limitations to the ultimate accuracy. The complete control scheme is described and the paper concludes with a brief report on the results which have been obtained from the installation.

Measurement of Gage

The usual method of measuring strip gage is by using either a flying micrometer in physical contact with the strip, or a noncontact radiation or X-ray gage. There is a very serious objection to using these techniques for an automatic gage-control system, which arises from the physical impossibility of locating the measuring device at the roll bite (i.e. the area where the mill work rolls are in contact with the strip being rolled). If a measurement of gage is not made at the roll bite, there is a transport time or delay time between the time a gage change occurs and the time when the change is detected by the measuring device. The magnitude of the transport delay is dependent entirely upon the distance between the roll bite and the measuring gage, and the speed of the strip. At high mill speeds, therefore, this transport delay will be comparatively small and it is unlikely that the performance of an automatic controller would be seriously compromised. At low mill speeds, however, the transport delay will increase and it will eventually result in serious instability problems with the added restriction that it becomes impossible for the controller to maintain gage right up to the end of the strip.

This state of affairs is particularly unfortunate because the characteristics of the rolling process are such that it is a comparatively simple matter to control gage once the mill has attained its proper rolling speed, and it becomes difficult to do so during acceleration and deceleration, a period when the transport delay will have its most serious effect.

From a consideration of the previous remarks it will be concluded that in an automatic gage-control scheme, regardless of the type of rolling mill to which it is applied, the basic requirement for achieving the best possible performance is a means of measuring gage at the roll bite.

This requirement may be met by using the properties of the rolling mill itself, as a means of measuring output gage. If the mill is regarded as an elastic member obeying Hookes law, and it is assumed that there is no elastic recovery of the material being rolled after it leaves the roll bite, then output gage h_2 is defined by the mill equation as follows:

$$h_2 = F/m + S_0$$

where

h_2 = output gage, inches
F = roll force, defined as the force in tons tending to separate the work rolls
m = elastic coefficient of the mill, tons per inch
S_0 = the separation of the work in inches when F is equal to zero and is controlled by the mill screws

The equation shows that a signal proportional to output gage may readily be

Paper 58-903, recommended by the AIEE Metal Industry Committee and approved by the AIEE Technical Operations Department for presentation at the AIEE Fall General Meeting, Pittsburgh, Pa., October 26–31, 1958. Manuscript submitted April 9, 1958; made available for printing August 27, 1958.

R. L. Duke and L. R. Hulls are with the Canadian Westinghouse Company, Ltd., Hamilton, Ont., Canada.

The authors acknowledge the engineering assistance of R. B. Sims, Davy and United Engineering Company, Ltd., Sheffield, England.

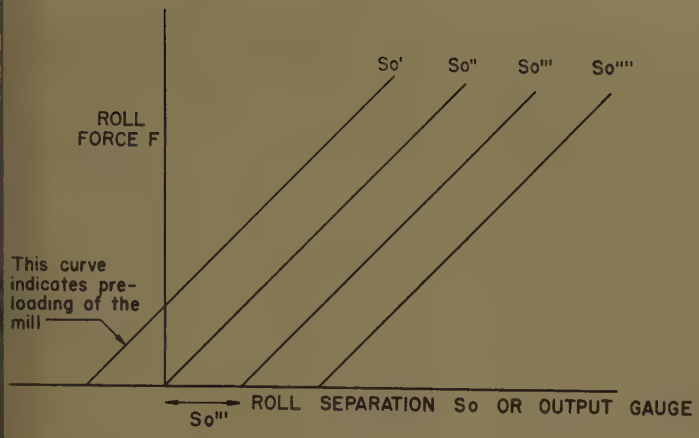

Fig. 1. Mill elastic equation

obtained by the addition of signals proportional to roll force, F, and roll separation, S_0.

The mill equation represents a family of parallel straight lines of slope m with each line corresponding to a value of S_0. Fig. 1 shows a set of these lines obtained by plotting roll force F against h_2.

Control of Gage

Having described the basic principle underlying this technique of measurement it is necessary to relate this to the rolling process, to determine which factors affect the output gage, and to consider the means available for regulating the output gage. For a given setting of the mill screwdowns the output gage will depend upon the following important factors: the ingoing gage, the physical properties of the strip, the front and back tensions, the coefficient of friction between the work rolls and the strip, and the diameter of the work rolls. All these variables may be described on the roll-force h_2 plot by a family of curves known as the plastic curves for the material being rolled. The equations to these curves are very complex and the mathematical derivation involves a somewhat lengthy analysis.[1] However, for the purpose of comprehending the behavior of the mill a simple graphical description of these curves will suffice.

Since both the mill equation and the plastic equation determine output gage for any given value of roll force, they may be regarded as two simultaneous equations. The value of output gage which satisfies both equations will be the gage rolled by the mill.

In Fig. 2, the straight line A is the equation for the mill for a given setting of the screwdown mechanism. The curve B is the plastic equation curve for the material being rolled. It will be seen that the two curves intersect at a point corresponding to output gage h_2. This is simply a graphical method of solving the two simultaneous equations. Now let it be supposed that the properties of the incoming strip change so that there is now a new plastic equation curve C, which intersects the mill line at a point corresponding to the heavier gage h_2'. In other words, a change in the incoming strip has caused the output gage to increase. To correct for this change, the screws may be screwed down so that there is now a new mill line D parallel to the original line but displaced from it so that it now cuts the plastic curve C at a point corresponding to the original output gage h_2. It will be noted that in order to maintain this same gage the roll force has been increased from F to F'. This graphical picture thus provides an illustration of the simple way in which output gage may be controlled by movement of the mill screws. Under normal rolling conditions, therefore, adjustment of screw position provides a very convenient method of controlling gage. From a regulating system point of view it must be remembered that movement of the screws involves the acceleration of reasonably high inertias and hence there is a definite limit to the speed of response on an automatic system using screwdown control only.

When the material is thin the plastic equation curve can become parallel to the roll force axis and at very high values of roll force the curve may even bend toward the region of heavier gage, and consequently the screws will lose their effectiveness as a means of control. Under extreme conditions, not normally encountered in practice, it is possible to reach a point where turning the screws to increase the roll force will actually increase the output gage.

Fig. 3 shows a family of plastic curves for four different values of back tension, together with a mill equation line. It will readily be seen that there are four values of output gage corresponding to each value of tension. Tension, therefore, provides an alternative means of controlling output gage.

The general shape of the plastic curves is such that tension is comparatively ineffective for the control of the heavier gages. Fortunately, tension provides effective control for thin-gage material, a condition under which satisfactory screwdown control may not be possible.

In a single-stand mill where steel is unwound from an entry reel, passed between the mill work rolls, and coiled up on a delivery reel, tension may be very rapidly controlled by regulation of the armature current in the reel-drive machines. Hence tension provides a very fast method of gage control for the thinner gages. Although in a single-stand mill there is no difficulty in regulating front and back tension, this is not the case in the multistand tandem mill where the front and back tension for a given stand will depend upon the conditions in all the the other stands. Consequently, the practice of automatic control in the tandem mill is a much more complex problem, although the physical phenomena associated with the mill equation and the

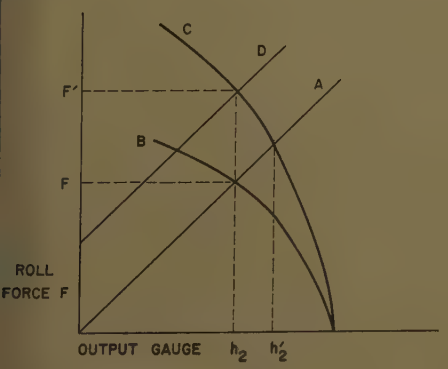

Fig. 2 (left). Determination of output gage from simultaneous solution of mill plastic and elastic equation

Fig. 3 (right). Effect of changes in tension on output gage

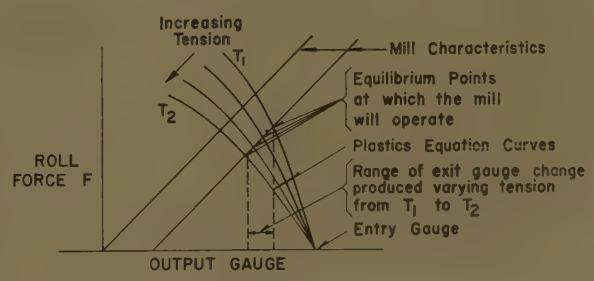

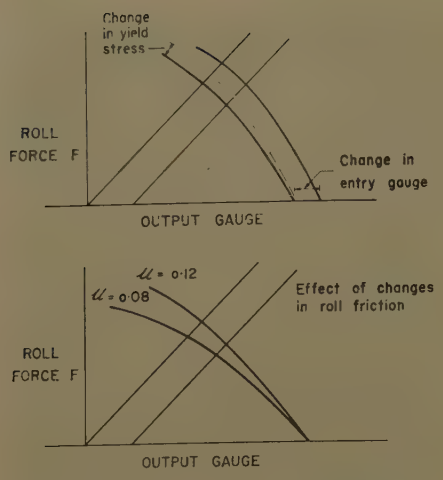

Fig. 4. Effect of changes in roll friction, entry gage, and yield stress on output gage

plastic equation are valid whether the roll bite under consideration be that of a single stand or one of a number of tandem stands.

The principal factors which are going to cause the output gage to change and call for corrective action from the automatic control system are changes in input gage, roll bite friction, and yield stress. Fig. 4 shows a set of plastic curves for changes in these variables. It shows that changes in roll bite friction have considerable effect, and since friction reduces with increasing mill speed it is this fact which introduces the well-known speed effect of output gage reducing during acceleration of the mill.

Description of System

In the 56-inch single-stand reversing cold mill to which the gage-control system has been fitted, position synchros are driven directly from the gear wheels which turn the splined end of the mill screws. This provides a minimum of backlash between the screw and the measuring synchros. A synchro transmitter is driven by one screw and a differential synchro is connected to the other. The receiver synchro is positioned by a small servomotor. The servomotor is driven by an amplifier which is connected in a self-balancing circuit so that the receiver rotor is automatically moved to a position corresponding to the mean position of the two mill screws. A potentiometer driven by the same servomotor provides an electric signal which is accurately proportional to the mean screw position. This device gives a measure of S_0 and the potentiometer has consequently been referred to as the S_0 potentiometer.

An electronic signal proportional to roll force F is obtained by summing the output from the load-cell resistance strain-gage bridges, in a mixing transformer.

The electric summing amplifier and follow-up servomotor, Fig. 5, receive the various input signals, sums them in accordance with the mill equation, and provides a resultant correcting signal which is fed into the payoff reel-tension regulator and the variable-voltage screwdown motor regulator.

The electronic summing amplifier feeds a follow-up servomotor or self-balancing potentiometer circuit, driving a 400-cycle-per-second linear synchro, whose output is fed back into the summing amplifier. Since the servomotor shaft will always turn unless the input signal is zero, the output signal from the linear synchro will always be equal to the sum of the signal inputs to the summing amplifier.

The principal signals which are fed into the summing amplifier are the roll force signal F/m, the roll position S_0, and a set gage-reference signal, which is obtained from a set of decade resistances accurately calibrated in steps of 0.0001 inch. The sum of the signals as given by the output from the linear synchro on the shaft of the follow-up servomotor mill will be equal to the error- or gage-deviation signal (i.e., the difference between the gage reference and the actual gage being rolled). When the reference and rolled gage are in agreement the error is zero and the shaft of the servomotor driving the linear synchro will come to rest at a position corresponding to zero output from the summing amplifier. It is evident that a pointer may be fixed to the servomotor shaft and calibrated to read in thousandths of an inch deviation from the set gage. This servo, driven from the summing amplifier, may therefore be referred to as the gage-deviation servo.

The signal from the linear synchro on the gage-deviation servomotor is rectified in a phase-sensitive detector and amplified in two electronic d-c power amplifiers which feed the screwdown and tension-regulator magnetic amplifiers.

Under automatic control both tension and screwdown are used to control gage. For small gage corrections on thin gages, tension correction assumes the dominant role since the high speed of response enables corrective action to be taken before the slower screwdown regulator has time to operate.

The screwdown control constitutes a position-regulating system and it will, therefore, always tend to reduce the gage deviation to zero, and under these circumstances the tension will always revert to the value set manually by the operator.

To reduce wear by avoiding excessive operation of the screws, particularly during the initial passes, an adjustable dead-band is provided in the screwdown loop.

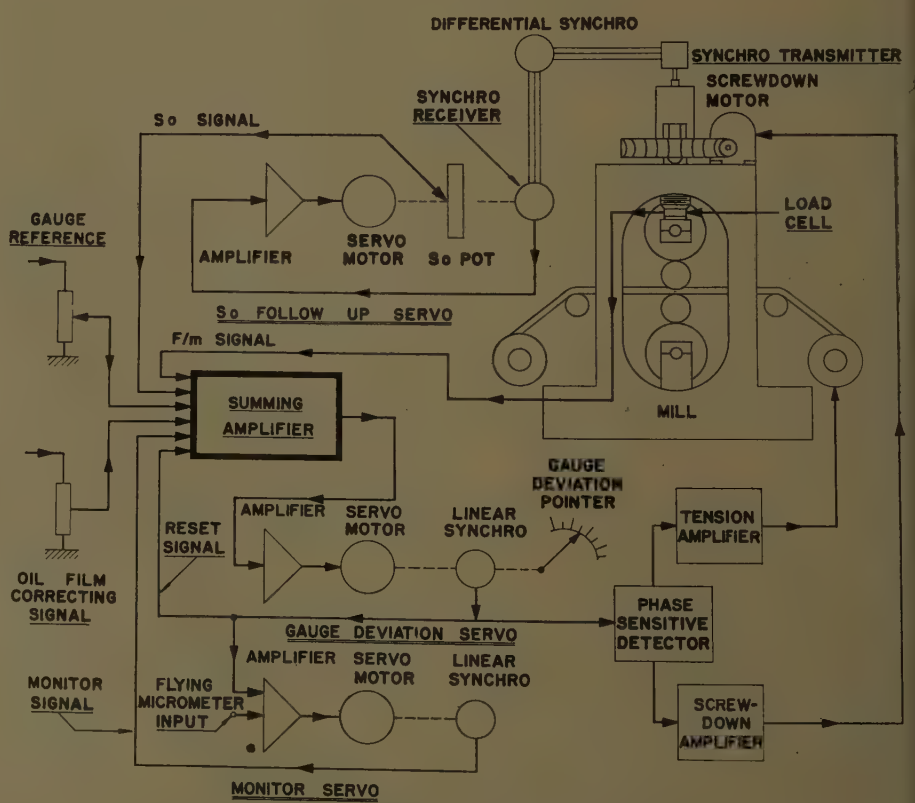

Fig. 5. Block diagram of automatic gage-control system

Any one of four dead-band settings can be selected with a switch calibrated for 0.001, 0.0005, 0.0003 inch, and zero. The gage controller will only operate the screws if the gage deviation exceeds the selected dead-band.

The gain of the screwdown control was adjusted so that a gage deviation of 0.001 inch would drive the screws at their maximum rated speed of 0.515 inch per minute.

Since continuous operation of the tension control presents no wear or maintenance problems there is no deadband in the tension loop.

The gage controller was found to perform satisfactorily using only the unwinding tension for gage-control purposes. When rolling tin-plate gage (i.e., less than 0.015 inch thick) an increase in back tension of approximately 100 pounds per inch width of strip will effect a reduction in output gage of 0.001 inch.

The range of tension control is limited to avoid the possibility of excessive tension, or slack strip. The average tension may be selected by the operator to control strip shape and the gage controller will not cause the pay-off tension to change from this selected value by more than ±5%.

For large corrections the tension amplifier will saturate in its efforts to exceed the permissible 10% band. Under these conditions only the screwdown system is capable of taking the necessary corrective action. On the thicker gages screwdown control is always predominant since under these circumstances tension has little effect upon gage.

It is this feature of dual operation of both tension and screwdown control which is responsible for the successful application of this technique to gage control when rolling tin-plate gages. Attempts to maintain performance by screwdown control alone leads to excessive screw operations resulting from the ineffective efforts of the rather slow screwdown regulator to perform the duties which can so easily be carried out by tension control.

Satisfactory operation of the gage controller does necessitate a certain standard of performance from the screwdown and tension regulators. However, there is no substantial modification necessary to make the system function with the type of equipment normally encountered on a modern rolling mill.

The gage controller also included a monitor system which was found to be necessary in order to overcome some of the inaccuracies which are detailed in the following section.

Factors Affecting the Accuracy of Rolled Gage

In common with all automatic control systems the accuracy limitations imposed upon the controlled variable will depend upon the response of the system and the type of disturbance to which it is subjected. Furthermore, the ultimate accuracy can be no better than the accuracy to which the controlled variable is measured.

In order to achieve satisfactory control of rolled gage, careful consideration must be given to the factors affecting accuracy and compensating devices must be built into the system where necessary.

Temperature Effects

Thermal expansion and contraction of the mill housings, backup rolls, and work rolls will result in a change in the roll opening, S_0, which is not detected by the synchros driven by the screwdown mechanism. The S_0 signal will, therefore, be in error and the gage, as computed from the mill equation, will be incorrect.

This error may be overcome by using a conventional gage-measuring instrument to monitor the automatic gage controller. In the case of the 56-inch mill, the electric deviation signal from a flying micrometer is compared with the signal from the gage-deviation servo and then the difference between the two signals is fed to an integrating servo. The output from the servo then is fed directly to the summing amplifier. The integrator satisfies the necessary requirement for remembering the magnitude of the correcting signal when the monitor gage is not in operation.

Temperature changes in the massive mill housings and rolls take place comparatively slowly and, therefore, there is no necessity for a fast-response monitor. The advantages gained by the elimination of the transport delay are still obtainable when a conventional measuring gage is used to monitor the system slowly.

Change in Oil Film Thickness in the Backup Roll Bearing[2]

Changes in the thickness of the oil film in the backup roll bearings, also result in a change in roll opening which is not detected by the measuring synchros. The thickness of the oil film varies as a function of mill speed but it does not change appreciably with mill load.

When gage measurement is achieved by the technique previously described it is a comparatively simple matter to determine the magnitude of the change in oil film thickness with mill speed.

To do this the mill is run without strip between the rolls, pressure is applied to the rolls, and the speed is varied without changing the position of the screws. At various values of mill speed the decade dials which supply the gage-reference signal are adjusted to reduce the apparent gage deviation to zero. Under these conditions the differences between successive readings on the decade dials give a direct measure of the changes in oil film thickness. Fig. 6 shows the results obtained by running such a test on the mill. It will be noted that the thickness of the oil film increases with speed and the overall result will be a tendency for the gage to reduce with increasing mill speed.

In practice it was found necessary to compensate for the oil film changes by generating a correcting signal, which varies with speed as shown by the dotted line in Fig. 6, and feeding this signal to the summing amplifier.

It is not desirable to rely on the monitor gage to correct for oil film errors as this would necessitate a comparatively fast response monitor which would reintroduce the problem of a transport delay.

Roll Eccentricity

Eccentric rolls will have the effect of introducing a cyclic error into the S_0 signal. The severity of the error due to this cause will be dependent upon the magnitude of the roll eccentricity and the response time of the automatic controller. In practice, normal roll-grinding procedures produce rolls with a sufficiently small eccentricity to enable satisfactory performance to be obtained without an unduly slow controller response.

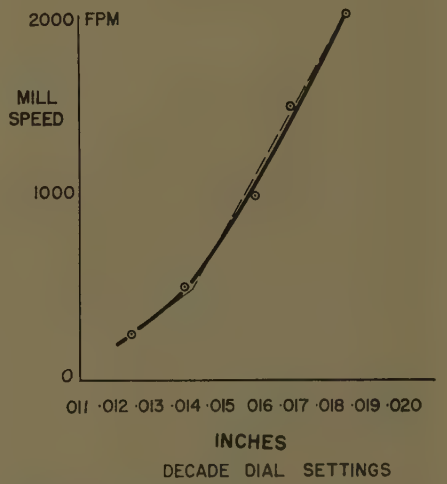

Fig. 6. Result of tests to determine variation of oil film thickness in backup roll bearings with speed for 16½-inch and 53- by 56-inch reversing cold mill

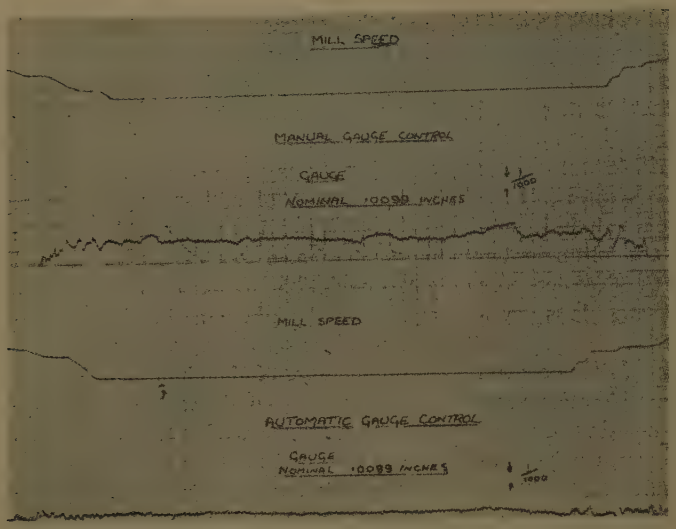

Fig 7. Comparative mill performance on manual and automatic gage control

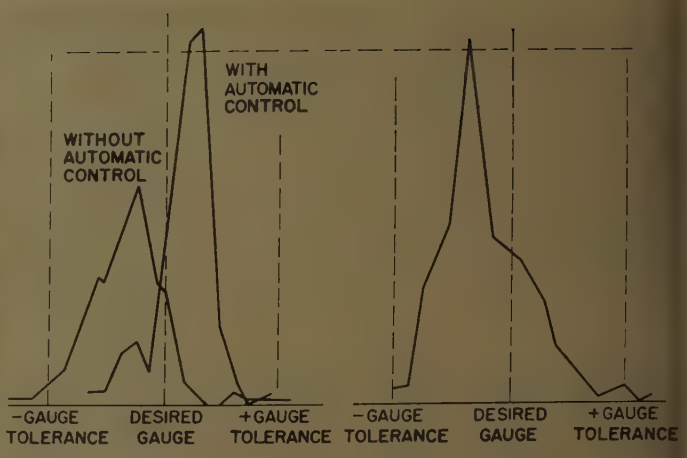

Fig. 8. Gage distribution for tinplate

A—From a single-stand reversing cold mill
B—From a 5-stand tandem cold mill

Speed Effect

It has long been recognized that a rolling mill has an inherent tendency to change gage with speed, the thickness of the strip being rolled decreasing as speed increases, and conversely. It is generally accepted that this effect is due to changes in conditions in the roll bite and changes in the oil film thickness in the roll bearings.

The changes in the roll bite are attributed to changes in friction with speed and they will not result in an error in the gage measurement. However, since these changes will require corrective action to be taken by the automatic controller they constitute a system disturbance which will be introduced every time there is a speed change. Hence even with automatic control there will be a tendency for gage to change during acceleration and deceleration, although the effect will be considerably reduced in comparison with the speed effect without automatic control.

Apparent Changes in Mill Stiffness

In practice it was found that the stress–strain curve of the mill was not linear at low loads and high loads and it was necessary to introduce a further correcting signal which varies with mill load.

The precise reason for this nonlinearity is not clear and it could result from either nonlinearities in the load cells or changes in the mill stiffness coefficient.

Operating Controls

The roller's controls and the method of operation were co-ordinated with existing mill practice on manual control. This insured ready acceptance by the mill crews as the gage control was an addition to, rather than a modification of, established procedure.

Two control desks are used on the mill, one opposite each reel, with much of the control equipment duplicated on each desk. The head roller alternates between desks with each mill reversal so that he is always operating from the delivery side.

Extensions were added to each desk, with the following instruments and control equipment for automatic gage control:

1. Gage setting dials.
2. Gage automatic; manual pushbuttons with indicating lights.
3. Gage-deviation indicator.
4. Mill-load indicators (front and back screws).
5. Monitor selector, which may be either a flying micrometer or X-ray gage. Only the flying micrometer has been used on the 56-inch mill.
6. Gate selector, one desk only.
7. Load-limit selector, one desk only. This sets the value of the mill load for which the automatic controller will lock out and return the mill to manual control.
8. Zero pushbutton to reset S_0 potentiometer.

Operating Sequence

The mill is loaded from a coil box through a leveller and across a hinged table over the reel. The operator may set up the required gage on the delivery desk and on the monitor gage prior to latching the strip into the winding reel. If the gage controller is switched to automatic it will control gage as soon as the mill rolls start turning and the monitor system will be automatically switched on as soon as the strip speed exceeds 150 feet per minute.

During a pass the gage controller and monitor gage may be set up for the next pass on the entry side of the mill and the system automatically switches to the new settings when the mill is reversed.

Before starting the mill it is recom-

Fig. 9. 16½-inch and 53- by 56-inch, 3,000 - foot - per - minute single-stand reversing cold strip mill with automatic gage control

Fig. 10. Load cell mounted between mill screw and backup roll chock

nended that the operator preset the mill screws to eliminate the rolling of off-gage strip while the automatic controller sets the screws after the mill is running.

The operator is able to resume manual control of the mill at any time.

The only setup procedure required is to reset the S_0 potentiometer after a roll change. To do this the operator brings the mill rolls together at some definite pressure, between 600,000 and 700,000 pounds per screw. Then, by pushing the zero pushbutton, the S_0 potentiometer is unclutched from the synchro and reset by the servomotor.

Performance and Results

The gage control was installed and placed in service in April 1957 operating on screwdowns only. Tension control was incorporated approximately one month later. Fig. 7 shows comparative performance on the mill on manual and automatic gage control.

The distribution curves shown in Fig. 8 indicate that the gage produced on the reversing mill is comparable to that produced on a tandem cold-strip mill. Large-scale sampling tests indicate that 98% of the product is rolled to a gage tolerance better than 0.0004 inch.

Appendix. Mill Installation Data

The gage controller was installed on a 56-inch-wide 3,000-foot-per-minute 4-high single-stand reversing cold mill at Hamilton, Ont., Canada. The mill was designed to roll up to 50-inch-wide strip gages 0.050 inch to 0.006 inch, and up to 36-inch-wide silicon electrical grades.

The mill is driven by a geared twin-motor drive rated 4,340 horsepower, 650 volts, 217/542 rpm, with provision to drive through the 53-inch backup rolls or alternatively through the 16½-inch work rolls. Each reel is driven by a tandem drive rated 2,170 horsepower, 650 volts, 244/732 rpm, with a disconnecting clutch between armatures. The reel-operating tension range is 6,000 to 30,000 pounds with 2-motor drives and 3,000 to 15,000 pounds with single-motor drives.

All mill-regulating systems, reel-tension regulators, mill-generator regulators, mill-motor field regulators, and screwdown regulators utilize 400-cycle magnetic amplifiers. The mill was installed in May 1956 and is shown in Fig. 9. Fig. 10 shows the load cells used for automatic gage control, located between the screw and chock.

The screwdowns are adjustable-voltage drives with a 75-horsepower frame-612 mill motor and a 75-kw 250/500-volt generator on each screw.

References

1. The Rolling of Metals, Vol. 1 (book), L. R. Underwood. John Wiley & Sons, Inc., New York, N. Y., 1953, p. 216.

2. Speed Dependent Variables in Cold Strip Rolling, R. B. Sims. *Journal*, Iron and Steel Institute, London, England, vol. 172, Dec. 1952, pp. 285–95.

Discussion

R. M. Sills (General Electric Company, Schenectady, N. Y.): We agree with the authors' use of a combination of screwdowns and tension for the mill described. In fact, we feel that both reversing and tandem cold-reduction steel mills require a combination of screwdowns and tension to achieve fully automatic control of strip thickness, for similar reasons, although on tandem mills the two systems should be on separate stands. Recent experience in the steel industry indicates wider acceptance of this approach.

We also agree that the gagemeter is a significant contribution to gage control through elimination of transport-time delay. However, it is clear from examination of the thickness-deviation charts that eliminating transport time does not completely eliminate thickness deviations. That is, there are still transient deviations which the control has not eliminated.

From information given in the paper we estimate that the screwdown system has a velocity error coefficient of about 1.7. That is, 0.001-inch error produces 0.0086-inch-per-second screw motion. If there is a 5-to-1 attenuation between screw motion and thickness change, a screw speed of 0.0086 inch per second will produce 0.0017-inch-per-second thickness change, so the velocity error coefficient would be 0.0017/0.001 = 1.7. Thus, crossover frequency will be 1.7 radians per second, and response time (to a small step change) would be close to 2 seconds.

In view of the fact that the screwdown regulators use 400-cycle magnetic amplifiers, we would expect that a regulator with better response could be obtained. We feel that fast response is desirable during the early passes to reduce inherent thickness variations as soon as possible. Is the response limited by motor heating or by stability considerations? If it is stability, what is the source of the troublesome phase shift? That is, is it gear backlash, gagemeter time constants, or the screwdown controls?

In this connection, we note that the gagemeter requires the operation of two servomotors, which tend either to make it slow or to complicate it with high-performance servomotor systems. We suggest that better performance could be obtained by eliminating these servomotors through a change in design.

No mention was made of the gain of the tension system. Can the authors give any figures for this? A relatively high gain and fast response through tension would tend to offset slow response of the screwdowns, particularly on the later passes. The screwdown system would then serve primarily as an automatic positioning control for the screwdowns, to keep tension within range. The authors have implied that this is true.

The paper points out that roll eccentricity will introduce a cyclic error into the S_0 signal. It does not point out that this error will be opposite in direction to the true thickness deviation, and that inherently the control will act to accentuate the thickness error rather than reduce it. Also, we are not sure that all operating people would agree that their normal roll-grinding practices would be satisfactory.

Since it is possible to measure total eccentricity by running the mill and gagemeter with no strip, we wonder whether the authors will indicate the magnitude of eccentricity which results from "normal roll-grinding practice."

The paper mentions four dead bands between 0.001 inch and zero, and indicates that these are used to reduce wear on the screwdowns. Do the authors consider that the excessive motion of the screwdowns was due to variations in entering thickness or to the effects of roll eccentricity? Were there any other factors, such as backlash, motor heating, or stability, that would necessitate the use of a dead band? Can any figures be given as to actual dead band used under various conditions?

In this connection we would like to point out that, although adjustable-voltage screwdowns were used, we see no reason why constant-potential screwdowns would not work almost as well if a dead band is used in either case and control by tension is considered to be a vernier. The screwdown control is basically a position servomotor in which screw position is a function of the integral of gage error. Thus, if a sampling control were used, with ON time proportional to error, nearly equivalent results could be obtained with constant-potential screwdown control.

R. L. Duke and L. R. Hulls: With reference to Mr. Sills' comments, the velocity constant available from the screwdown system would be approximately 2 and is limited by the generator field time constant which is the largest delay in the system. The actual gains existing in practice are very difficult to define because the transfer function of the mill is dependent upon the material being rolled and the particular characteristics of the pass. In this connection, the paper listed in reference 1 attempts to analyze the nature of the mill transfer function. In general, the system gains are set up to provide the best over-all operation for the rolling schedule, although there is no doubt that improved performance could be obtained if the system gains were adjusted both in accordance with rolling speed and the characteristics of the particular pass.

As Mr. Sills suggests, the fast response of the tension control does much to offset the sluggish screwdown operation. Here again the actual gain of the tension regulator cannot be readily specified since it involves the variable gain transfer function of the mill itself.

At low rolling speeds the speed of response of the regulator systems is limited by the eccentricity ripple (average value of about 0.004 inch peak to peak) and it is desirable that the regulator system should not be fast enough to follow the ripple. In the case of a theoretical infinitely fast response system the gage control would put into the strip an eccentricity pattern whose magnitude would be exactly equal to the magnitude of the roll eccentricity. Without any gage control the mill would tend to attenuate the ripple thus producing less ripple in the strip than would be the case if the afore-mentioned theoretical system was used.

At present an experimental eccentricity eliminator is being built and it is hoped that this device will enable the regulator system to be speeded up and result in considerable improvement in performance, particularly for the lower rolling speeds with eccentric rolls.

As far as dead-band settings are concerned, the band is narrowed as the strip becomes thinner. Operation of the screwdowns tends to become excessive on the heavier gages where the tension control is not very effective and in this case the presence of a dead band prevents excessive screw operation with the attendant heating of the screwdown motors. The actual setting of the dead band is under the control of the operators and the particular setting will be chosen which best will suit the rolling conditions. We would agree that there is no reason why good results could not be expected from an ON-OFF type of control operating with constant-potential screwdown control.

It is difficult to eliminate the servomotors from the gagemeter equipment as the system involves accuracies of the order of 1 part in 10,000 which are difficult to obtain without the aid of self-balancing potentiometer circuits and their associated servomotors. An attempt has been made to design an equipment using precision summing amplifiers in place of the servomotors. However, this system was abandoned in favor of the greater accuracy available from servomotors.

REFERENCE

1. A ROLLING MILL ANALOG FOR THE STUDY OF NONLINEAR PROBLEMS ASSOCIATED WITH GAGE CONTROL, L. R. Hulls, K. R. Canfor. *AIEE CP 57-685* (available on request).

Terminal Spacings for High-Altitude and Ultrahigh-Temperature Electronic Transformer Applications

G. I. DUNCAN
ASSOCIATE MEMBER AIEE

W. A. RECTANUS
AFFILIATE MEMBER AIEE

FUTURE ELECTRONIC equipment mounted aboard high-speed military aircraft and guided missiles will have to withstand high altitudes, ultrahigh temperatures, and radiation. Present goals as established by the U. S. Air Force for electronic power transformers are 100,000 feet altitude, 500 C (degrees centigrade) ambient temperature, and intense nuclear radiation. With terminal spacings normally designed for air dielectric strengths at altitudes up to approximately 50,000 feet and temperatures up to 125 C, additional information is needed on breakdown voltages under these new conditions.

The work described in this paper was part of Air Force Contract no. *AF33(616)-3623* for developing temperature- and radiation-tolerant electronic power transformers. It began with a literature search to obtain data on terminal spacing required at high altitudes. While several sources of information were found,[1–5] the data reported were not readily adaptable to the particular design problems. In general, these data were concerned with electrode configurations, electric field conditions, gap lengths, and pressure ranges outside the area of interest.

The objective of this work then became the experimental determination of the voltage-spacing characteristics for the terminals of electronic transformers operating in altitudes up to 100,000 feet and in temperatures up to 500 C. Effects of radiation were not included in this investigation.

The theories pertaining to gaseous breakdown are fully discussed in the works of Loeb[6] and Cobine.[7] At the instant of breakdown, two different types of discharge were observed over the altitude range covered. Up to approximately 70,000 feet the discharge was by sparking; above that altitude it was a glow-type discharge. Evidence of breakdown was also observed on the instruments located in the test circuit. The techniques used for the measurement of voltage were taken from AIEE Standard no. 4.[8]

Data were obtained on the voltage breakdown of needle and sphere electrodes, as well as ceramic-type hermetic terminals as a function of spacing and air density. The tests on needles and spheres were made for 1/4-inch to 4-inch spacings at sea level and at other pressures corresponding to altitudes up to 150,000 feet.

While the needle gap is not an approved method for making voltage measure-

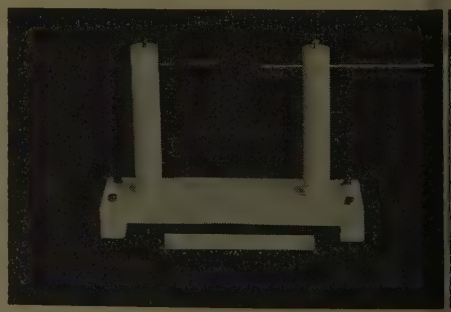

Fig. 1. Needle electrode assembly

Paper 58-118, recommended by the AIEE Air Transportation Committee and the Electrical Insulation Committee of the Communication and Electronics Division, and approved by the AIEE Technical Operations Department for presentation at the AIEE Winter General Meeting, New York, N. Y., February 2–7, 1958. Manuscript submitted October 14, 1957; made available for printing September 12, 1958.

G. I. DUNCAN and W. A. RECTANUS are with the General Electric Company, Fort Wayne, Ind.

The authors wish to acknowledge the help and guidance of G. E. Walter, H. B. Harms, and M. Halleck, as well as the assistance of Howard Ulrich and Gene Galloway in accumulating test data.

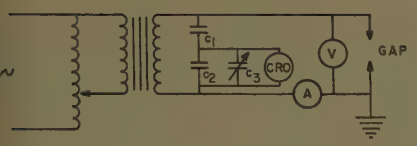

Fig. 2. Schematic wiring diagram

—Ammeter (Polyranger)
—Electrostatic voltmeter (Rawson)
RO—Cathode-ray oscilloscope (Tektronix)
$_1$=2.2 micromicrofarads
$_2$=100 micromicrofarads
$_3$=Variable air dielectric capacitor

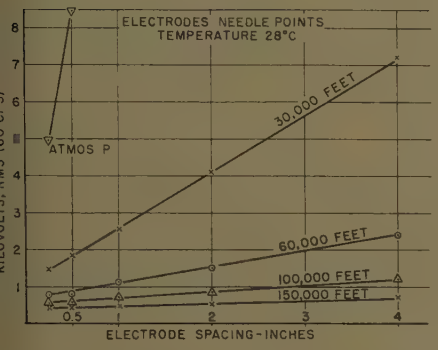

ig. 3. Dielectric strength of air as a function f needle electrode spacing and altitude

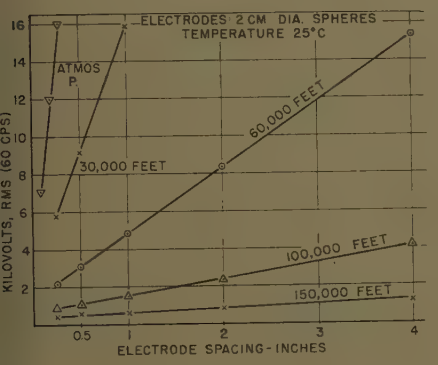

ig. 4. Dielectric strength of air as a function f a 2-centimeter-diameter sphere electrode spacing and altitude

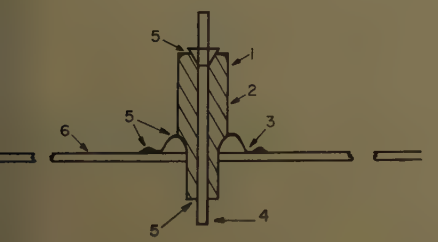

ig. 5. High-temperature hermetic terminal

1—Alumina ceramic insulation
2—Alumina glaze insulation
3—Nickel-iron alloy gasket
4—Nickel-iron alloy conductor
5—Silver solder seals
6—18-8 type 308 stainless steel

ments in dielectric tests, it is however, a condition encountered when connections are made to transformer terminals. The breakdown voltage on needle electrodes is typical of the erratic results obtained with such connections. The sphere gap method of voltage measurement is a method approved in AIEE Standard no. *4* and represents the best or ideal conditions encountered in spacing terminals with the two sets of data, where the designer has a choice between the worst and best possible conditions. Obviously the data on available terminals narrow the choice.

Needle Point Electrodes

The 60-cycle voltage breakdown of air between needle electrodes at fixed spacings of 1/4 inch, 1/2 inch, 1 inch, 2 inches, and 4 inches was measured in a standard altitude chamber at station level pressure, and at air pressures corresponding to 30,000 feet, 60,000 feet, 100,000 feet, and 150,000 feet altitude. The measurements were made at normal room ambient temperature with the needle electrodes mounted in a ceramic insulator as shown in Fig. 1. Gap lengths were fixed by precision measuring blocks. A new pair of needle electrodes was used for each test condition. Data were determined as the average of three readings at each condition. Needles were 14 gage with a 1/32-inch point radius and 14 degrees total taper. The schematic diagram of the test setup is shown in Fig. 2.

The test results are plotted as a function of altitude and gap length in Fig. 3. They can be summarized as follows: For the range of spacings investigated, the breakdown voltage is a linear function of electrode spacing for any given air density or altitude setting. The slopes of the breakdown versus spacing curves decrease as altitude is increased. At 150,000 feet, the difference in breakdown voltage from a 1-inch to a 4-inch electrode spacing is but 200 volts. For a 1-inch electrode spacing, the breakdown voltage decreases from 2,600 volts at 30,000 feet to 500 volts at 150,000 feet.

Sphere Electrodes

The 60-cycle voltage breakdown of air between standard 2-centimeter-diameter sphere electrodes at 1/4-inch, 1/2-inch, 1-inch, 2-inch, and 4-inch gap lengths was measured in an altitude chamber at station level pressure and at pressures corresponding to 30,000 feet, 60,000 feet, 100,000 feet, and 150,000 feet altitude. The measurements were made at a normal room ambient temperature, and the gap lengths were fixed by precision measuring blocks. Data were an average of three readings for each test condition. The test circuit was the same as shown in Fig. 2.

Table I. Hermetic-Type Terminals

Terminal	Flashover, Kv*	Outside Diameter, Inches	Terminal to Ground Distance, Inches
A	5.0	0.250	0.375
B	8.0	0.375	0.625
C	16.5	0.750	1.125
D	6.5	0.300	0.375
E	9.0	0.530	0.625
F	17.0	0.530	1.250

*Per MIL-T-27A specification. Values are average based on 60 cycles rms at sea level and 50% relative humidity.

The test results are given in Fig. 4. They are similar to those experienced with the needle point electrodes except that the slopes of the individual breakdown versus spacing curves for a particular altitude are steeper and are displaced upward. For example, for a 1-inch electrode spacing as altitude increased from 30,000 to 150,000 feet, the breakdown voltage decreased from 16,000 volts to 600 volts. As the electrode spacing is increased from 1 inch to 4 inches at 150,000 feet, the breakdown voltage increases from 600 to 1,300 volts.

Hermetic Terminals

Tests were made on six different hermetic-type terminals as shown in Table I. The general type of terminal used is shown in Fig. 5. These terminals were selected because of their good electrical properties at elevated temperatures. For testing purposes, ten of each of the terminals were mounted in steel cases. The breakdown voltage of the terminals was measured at station level, and at other air pressure corresponding to 30,000 feet, 60,000 feet, 100,000 feet, and 150,000 feet altitude. The measurements were made at

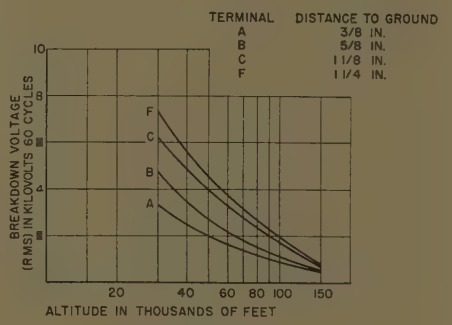

Fig. 6. Breakdown voltage of hermetic terminals as a function of altitude

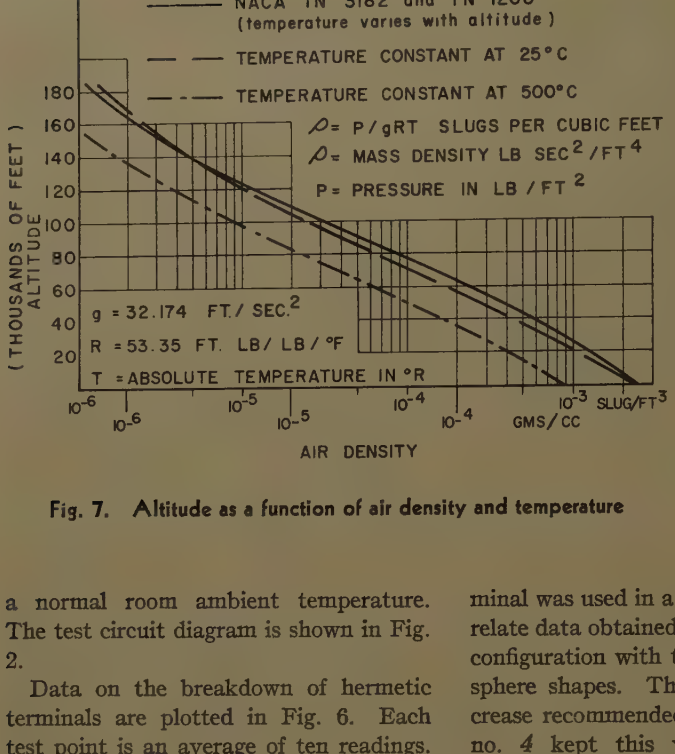

Fig. 7. Altitude as a function of air density and temperature

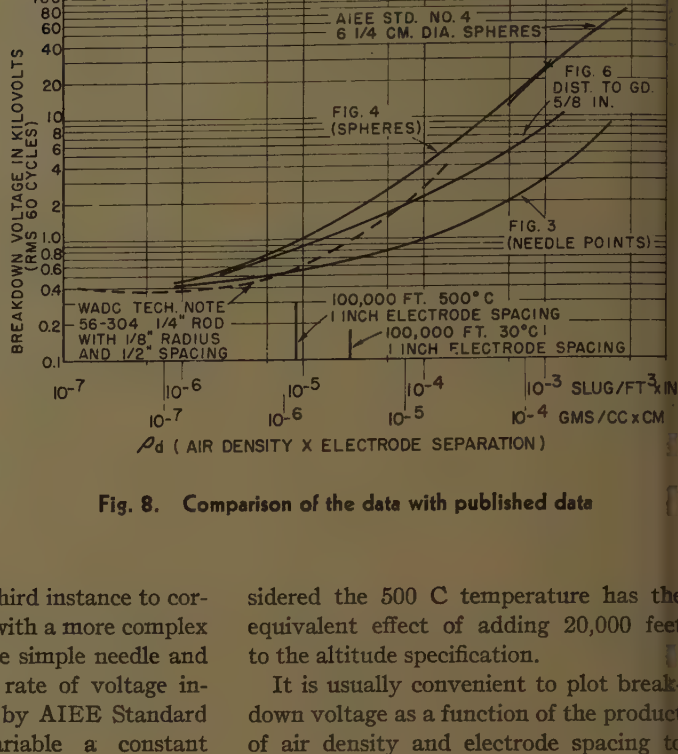

Fig. 8. Comparison of the data with published data

a normal room ambient temperature. The test circuit diagram is shown in Fig. 2.

Data on the breakdown of hermetic terminals are plotted in Fig. 6. Each test point is an average of ten readings. In the presentation of these data, the distance to ground is used as the variable parameter, with the largest spacing being $1\frac{1}{4}$ inch. The data are consistent with the sphere and needle point electrode data in that a linear relationship exists between breakdown voltage and spacing for a given altitude setting. A terminal with a $1\frac{1}{4}$-inch distance to ground experiences a reduction in breakdown voltage from 14,500 to 1,900 volts as the altitude is increased from station level to 100,000 feet.

Correlation of Data and Significance of Results

The dielectric breakdown strength of air is dependent[7,9] upon its density, the electrode spacing, the electrode material, the electrode configuration, the frequency of the voltage, and the rate of increase of the voltage. For an electric device that has a 100,000-foot altitude and 500 C temperature specification, air density becomes a major variable for the designer to consider in establishing the necessary distance between terminals, and between terminals and ground. If a metallic terminal is used and a single frequency is specified for the device, the remaining two variables that must be seriously considered are electrode configuration and rate of increase of the voltage. This investigation used needle points and sphere configurations that are believed typical of the worst and the best possible situations that can be encountered in transformer applications. A particular type of terminal was used in a third instance to correlate data obtained with a more complex configuration with the simple needle and sphere shapes. The rate of voltage increase recommended by AIEE Standard no. 4 kept this variable a constant throughout the investigation.

The density of the standard atmosphere as recommended by the National Aeronautics and Space Administration (formerly National Advisory Committee for Aeronautics[9,10]) is plotted as the solid line in Fig. 7 up to an altitude of 180,000 feet. It takes into account the variations in temperature of the atmosphere. If a constant temperature of 25 C were maintained, the density-altitude relationship would be that represented by the long dashed line. Then, if the temperature were increased to 500 C, the curve with the short dashes would be obtained. These serve to give a qualitative indication of the effect altitude has on air density and to show that a 500 C temperature can, also, significantly affect air density. Throughout the range of variables considered the 500 C temperature has the equivalent effect of adding 20,000 feet to the altitude specification.

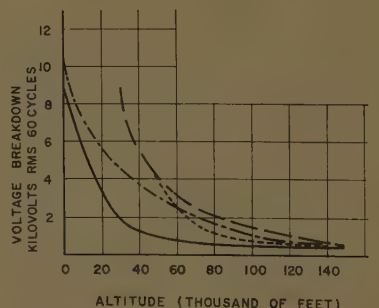

Fig. 9. Comparison of dissimilar electrode configurations of fixed spacings

1/2-inch needles
1/2-inch cylinders
5/8-inch terminals
1/2-inch spheres

It is usually convenient to plot breakdown voltage as a function of the product of air density and electrode spacing to compare and obtain greater utility from gaseous breakdown data. The use of these co-ordinates is based on Paschen's Law[6,7] which states that for a uniform field the voltage just before the discharge of the gap is a function of the product of the pressure and gap length. Accuracy is assured only by the use of data obtained with electrodes that produce a uniform dielectric field. Presentation in this manner is, therefore, a comparison tool and should not be used for design purposes.

With this in mind, the data from four sources are compared in Fig. 8. Besides indicating consistency of data obtained in this investigation with other published data, the range of the density-gap length variable with which we are concerned for transformer applications up to 150,000 feet is a decade or two from the minimum breakdown voltage condition obtainable with a uniform field. The needle and sphere data bracket both the 5/8-inch hermetic terminal data obtained in this investigation and the data for rods with 1/2-inch separation taken from the literature.[11] Cobine establishes the value of the potential difference at which minimum breakdown occurs with his data published[7] on flat-plate electrodes.

Rigorous comparisons and correlations should be made only with data taken for specific spacings and densities. Fig. 9 contains data from this investigation for sphere, needle, and terminal configurations and from the literature for 1/2-inch cylinders. A 1/2-inch gap for simple electrode shapes and a 5/8-inch termina

were selected for analysis. The cylinder data take an intermediate position between the needle and sphere data. Above 150,000 feet and even somewhat below, electrode shape has little effect on the breakdown voltage. For the 1/2-inch-electrode spacing used, this voltage is approximately 500 volts.

Analysis of the data also shows that spacing is not highly significant above 150,000 feet. At 4 inches, for example, the comparable voltage values range from 700 volts for needle electrodes to 1,200 volts for sphere electrodes. Extrapolation of the data indicates that this latter value would become 700 volts at approximately 170,000 feet.

Conclusions

The data reported in this paper should form a basis for the designer to establish safe voltage breakdown distances between terminals and between terminals and ground for transformer applications that require 100,000 feet altitude and 500 C temperature ratings. The data show that terminal spacings under these conditions must be severely derated from their normal ambient values.

Air dielectric strength data were obtained for the simple electrode shapes such as needle points and spheres and correlated with those taken on a specific terminal type representative of more complex shapes. It was found that: 1. the terminal dielectric system behaves more nearly as sphere electrodes above 70,000 feet and somewhat less ideally below that altitude; 2. electrode separation and electrode shape become less significant as altitudes of 150,000 feet and higher are approached; and 3. the nature of the discharge at breakdown for the electrode shapes evaluated changed from a spark to a glow at approximately 70,000 feet altitude at room temperature.

References

1. Investigation of Porcelain Insulators at High Altitudes, C. V. Fields, C. L. Cadwell. *AIEE Transactions*, vol. 65, Oct. 1946, pp. 656–60.

2. Application of Ideal Gas Theory to the Gaseous Expansion from an Electric Spark, R. B. Edmonson, H. L. Olson, E. L. Gayhart. *Journal of Applied Physics*, New York, N. Y., vol. 25, Aug. 1954.

3. Effect of Altitude on Electric Breakdown and Flashover of Aircraft Insulation, L. J. Berberich, G. L. Moses, A. M. Stiles, C. G. Veinott. *AIEE Transactions*, vol. 63, 1944, pp. 345–54.

4. Space Charge Formation and the Townsend Mechanism of Spark Breakdown in Gases, R. W. Crowe, J. K. Bragg, V. G. Thomas. *Physical Review*, New York, N. Y., vol. 96, no. 1, Oct. 1, 1954.

5. A Small High-Voltage Bushing Design for High Altitudes, F. J. Vogel, H. A. Hart. *AIEE Transactions*, vol. 68, pt. I, 1949, pp. 761–64.

6. Basic Processes of Gaseous Electronics (book), L. B. Loeb. University of California Press, Berkeley, Calif., 1955.

7. Gaseous Conductors (book), J. D. Cobine. McGraw-Hill Book Company, Inc., New York, N. Y., 1941.

8. Measurement of Voltage in Dielectric Tests. *AIEE Standard no. 4*, Sept. 1953.

9. ICAO Standard Atmosphere. *NACA TN 3182*, National Advisory Committee for Aeronautics, Washington, D. C., 1956.

10. NACA Tentative Upper Atmosphere. *NACA TN 1200*, National Advisory Committee for Aeronautics, 1956.

11. Voltage Breakdown at Low Gas Pressures (High Altitudes), J. W. Ballard, C. B. Geesner. *WADC Technical Note 56-304*, Wright Air Development Center, Dayton, Ohio, July 1956.

Transfer Functions of Loaded Synchronous Machine

D. HAMDI-SEPEN
ASSOCIATE MEMBER AIEE

THE GENERAL STUDY of the transient performance of the synchronous machine is based on Park's[1,2] theory. Various authors have presented useful methods for the study of this subject, and a complete bibliography is contained in reference 3. Problems related to the transient operation of the synchronous machine have been treated as well, aiming at the representation of the synchronous machine for analog studies.[10,11]

Any change in the operating conditions of the synchronous machine causes corresponding changes in electrical quantities. In the case of sudden short-circuiting of an unloaded synchronous machine the current decreases steadily from a maximum to its steady-state value. The variation of the armature current is admittedly related to an apparently variable reactance. Although the value of this reactance is continuously changing,[7] for practical purposes it is taken to be equal to a definite value according to the problem considered. For example, in stability problems the synchronous machine is represented by the transient reactance, just as it is represented by the synchronous reactance in steady-state operation problems.

The transient performance of the synchronous machine can be analyzed directly with the aid of circuit equations, without reference to a variable reactance. Although the theoretical results obtained are readily applicable to other problems, this paper will be concerned with variations of the excitation conditions only, assuming constant torque acting on the shaft of the machine, the speed of rotation corresponding to the nominal frequency. It will be further assumed that the variation of the excitation voltage is relatively small, such as 10% to 20% of its initial value. This limitation is necessary for the approximation admitted in the evaluation of certain terms.

The general case of the transients in the synchronous machine, involving further consideration of torque equations relating to angular position of the rotor, is not within the scope of this paper. In the experimental results reported here, the power-angle variation is deduced from oscillographic records.

In order to arrive at rather simple expressions the amortisseur has not been considered. This affects only slightly the results obtained as response to step variations of the excitation voltage and, in the study of the behavior of the voltage-regulating system given as an example, sufficient approximation is obtained.

The general case of the salient pole machine will be treated. It has been found

Paper 58-796, recommended by the AIEE Feedback Control Systems and approved by the AIEE Technical Operations Department for presentation at the AIEE Summer General Meeting and Air Transportation Conference, Buffalo, N. Y., June 22–27, 1958 and re-presented at the AIEE Winter General Meeting, New York, N. Y., February 1–6, 1959. Manuscript submitted June 5, 1957; made available for printing December 15, 1958.

D. Hamdi-Sepen is with the Technical University of Istanbul, Istanbul, Turkey.

The author wishes to acknowledge the use of the facilities of the Department of Electrical Engineering, Massachusetts Institute of Technology, Cambridge, Mass., and the suggestions of Profs. A. E. Fitzgerald and K. L. Wildes; also those of Dr. E. Mishkin, now with the Polytechnic Institute of Brooklyn, Brooklyn, N. Y. Thanks are also due to G. Belfils, Technical Manager of Société ALSTHOM, Paris, France, for the opportunity of working in the research laboratories of this company at Belfort, France, where the experimental results with amplidyne exciter were obtained; and to his staff for its help. The other experimental results were obtained in the laboratories of the Technical University of Istanbul, Istanbul, Turkey.

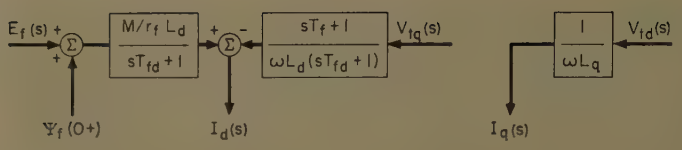

Fig. 1 (above). Block diagram of the synchronous machine

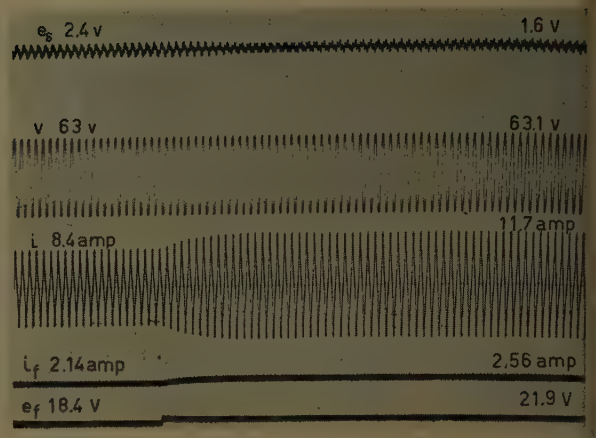

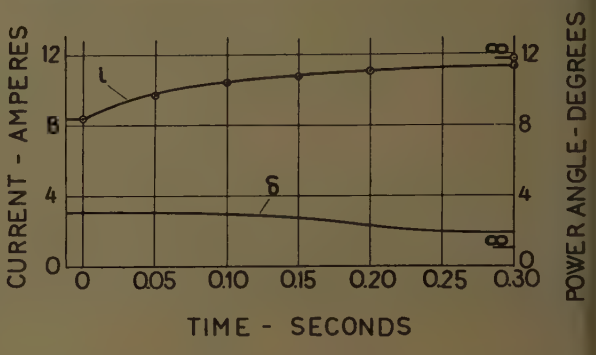

Fig. 2 (right). Results for entirely reactive load with $\phi = 90$ degrees lag

that in round-rotor machines saliency can be of the same order of importance as saturation.[12,13]

Theoretical Considerations

During the operation of the synchronous machine under given terminal conditions the operating conditions of the machine can be changed by the variation of: 1. the voltage applied to the field terminals, and 2. the torque acting on the shaft of the synchronous machine.

In response to the variation of these quantities, two others are changed. They are: 1. the armature current, both in amplitude and phase, and 2. the power angle.

Consider a synchronous machine operating as an alternator connected directly to an infinite bus. If the power of the considered machine is negligible as compared to the power of the system, and if no reactance exists between the terminals of the synchronous machine and the infinite bus, the changing of the excitation of the synchronous machine can change the current delivered but not the voltage at the terminals. Thus the voltage of a loaded machine is not a directly regulated quantity. In case an impedance is connected between the machine terminals and the infinite bus, the voltage at the terminals of the machine will change with the current.

When the synchronous machine is delivering power with current lagging or leading the terminal voltage, any change in the voltage applied to the field circuit terminals will alter both current and power-angle values. A similar changing of current and power angle will occur if the torque acting on the shaft of the synchronous machine is changed, with constant excitation.

Thus in studying the transient performance of the synchronous machine, the voltage applied to the field terminals and the torque acting on the shaft of the machine may be regarded as input functions, while the current and the power angle are output quantities, as considered in feedback control technique.

Impedance Loaded Machine

In a synchronous machine delivering power to an impedance load, with constant torque acting on the shaft, any increase in the voltage applied to the field terminals will increase the armature current. Consequently the RI^2 (resistance impedance) losses in the resistance of the load will increase, with constant driving torque the speed of rotation will decrease, and the system will be operating at a frequency lower than the nominal.

This question will not be considered further in this paper. The case of a pure reactance load or an impedance with negligible resistance is a particular case of the more general problem of the performance of the synchronous machine connected to an infinite bus through an external reactance, in which the voltage of the infinite bus is considered equal to zero.

Synchronous Machine Connected to Infinite Bus

The values of the components of the armature current as given by equations 20 and 23 in Appendix I are related with the condition

$$v_q^2 + v_d^2 = v^2 \qquad (1)$$

With constant torque acting on the shaft of the machine, any change in the value of e_f will cause the variation of v_q; v_d and consequently i_q will also be changed, the power angle being

$$\delta = \tan^{-1}\frac{v_d}{v_q} \qquad (2)$$

The various terms in equation 21 will be considered. The d-component of the current is dependent upon the following:

1. The voltage $E_f(s)$ applied to the field terminals. If this voltage is varied in the form of a step function to a constant value $\bar{E}_f$, this term is $(\bar{E}_f/s)K_1G_f(s)$ and evaluated as a function of time. If the variation of e_f can not be represented as a simple Laplace transform to be introduced in equation 21 it is possible to replace its variation in a step-by-step calculation by elementary step functions replacing the actual variation of e_f.

2. The voltage v_q in general is not a known function of time, and is dependent upon δ; the evaluation of the term $V_q(s)K_2G_2(s)$ is possible just in the form of Duhamel's integral in a step-by-step calculation. If the machine is entirely reactive loaded, neglecting the armature resistance v_d would be zero, and v_q constant and equal to v; this term will be $(\bar{V}/s)K_2G_2(s)$ and evaluated. This can still be approximately admitted in operation with lagging power-factor angle about 40 to 30 degrees, for example, according to machine characteristics. The variation of δ and consequently of v_q remains small so that the hypothesis of its constancy is not much in error.

3. The term $\psi_f(0+)K_1G_1(s)$ represents the initial conditions.

As no amortisseur winding in q-axis is considered, neglecting the armature transients, the q-component of the current is directly

$$i_q = v_d/\omega(L_q + L_x) \qquad (3)$$

In equations 21 and 23 using $V_q = 0$ and $V_d = 0$ one obtains the expressions of the current components in the case of the reactance-loaded machine considered in the preceding paragraph.

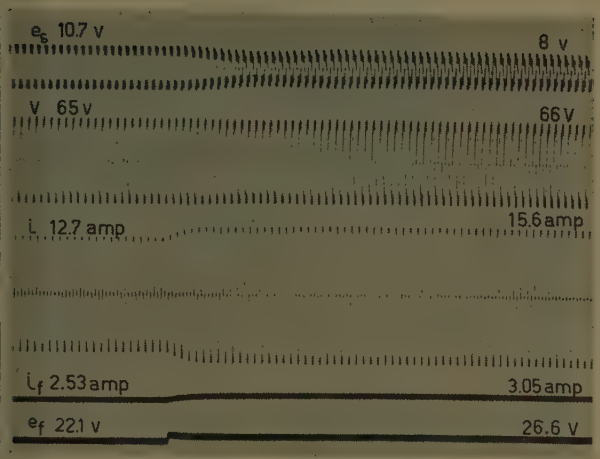

Fig. 3. Results for operation
A (left)—ϕ=47.5 degrees lag
B (right)—ϕ=47 degrees lead

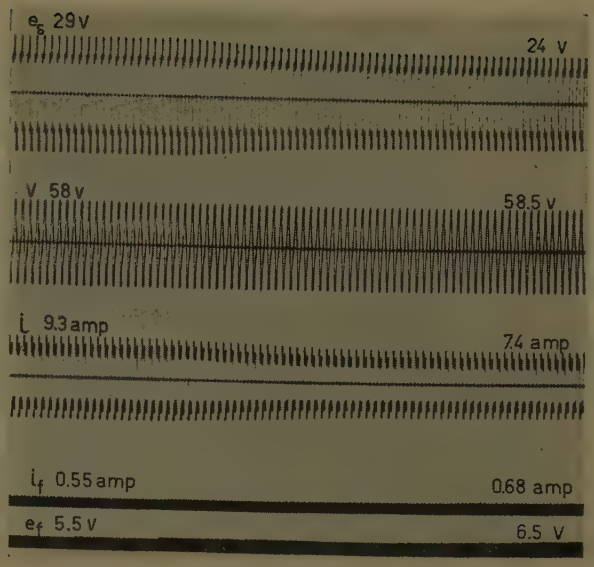

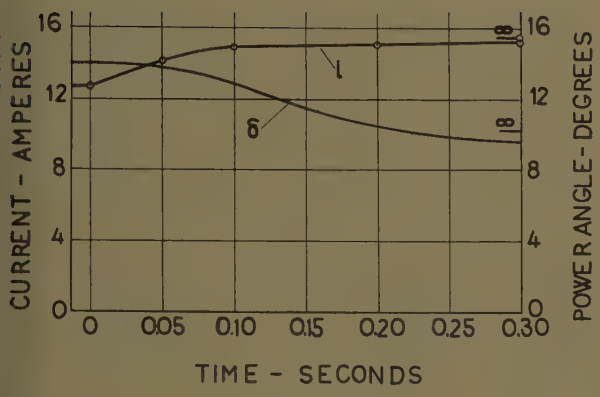

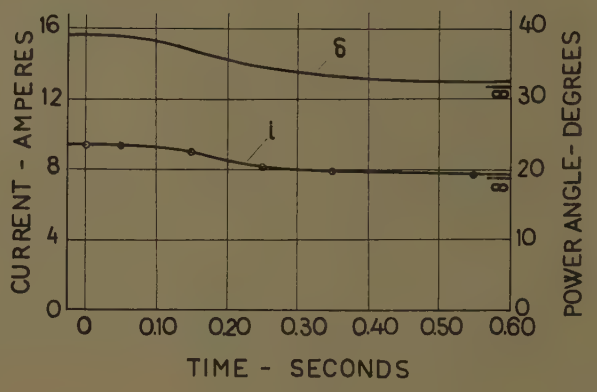

Transfer Functions of Loaded Synchronous Machine

Equations 18(A) and 23 are the basic equations determining the transient operation of the synchronous machine and can be represented in the form of block diagrams as in Fig. 1. $E_f(s)$, $V_{tq}(s)$, and $V_{td}(s)$ are input functions, while $\psi_f(0+)$ represents the initial conditions. $I_d(s)$ and $I_q(s)$ are the output quantities.

The block diagram as given in Fig. 1 can be introduced as representing the synchronous machine in any closed-loop system such as the example treated in Appendix II.

Experimental Results

The accompanying oscillograms have been obtained on a 7-kva 110–190-volt 1,500-rpm 50-cycle 3-phase machine. The unsaturated value of X_d is 8.5 ohms and the transient reactance X_d' is 1.7 ohms. We neglect the armature resistance which is 0.279 ohm. M is 0.284 henry; L_f is found equal to 5.59 henrys. r_f is 8.57 ohms, but is larger for currents about 0.5 amp (ampere). Its value is calculated from e_f and i_f as measured. T_f is equal to 0.65 second, and T_{fd}= 0.131 second. The machine was directly connected to the infinite bus.

Tests have been made with terminal voltage about 0.5 per unit, in unsaturated conditions, for quantities related to the d-axis. It is known that the case is different for quantities related to the q-axis.[14]

The variation of the power angle during transients is obtained with the aid of the following arrangement: An auxiliary alternator is mounted on the shaft of the main synchronous machine, with the same number of poles with movable stator. The power angle δ is calculated from phasorial difference voltage $e\delta$ between the voltage of this auxiliary alternator and a voltage taken over a resistor connected between phase and neutral of the infinite bus. These two voltages are regulated to have the same amplitude, and the stator of the auxiliary alternator is rotated so that the phasorial difference between these two voltages is zero when the synchronous machine connected to the infinite bus is running at no load. The stator of the auxiliary alternator remains in this position. During tests these voltages were regulated to 44 volts.

With the foregoing values of the constants, the solution of equations 20 and 23 for the transient current components are

$$i_d = \bar{E}_f\ 0.87\left(1-\epsilon^{-\frac{t}{T_{fd}}}\right) - V_q\left(0.118+0.472\,\epsilon^{-\frac{t}{T_{fd}}}\right)+\psi_f(0+)\ 6.68\,\epsilon^{-\frac{t}{T_{fd}}}$$

$$i_q = V_d/\omega L_q \qquad (4)$$

In case V_q is variable such as $V_q(t)$, the term containing this voltage component is evaluated in form of Duhamel's integral in a step-by-step calculation.

The value of L_q to be introduced in the last equation is deduced from δ as measured. The saturation effect on this reactance is rather important in this machine.

In Fig. 2 are given the results obtained during operation with entirely reactive load. The initial conditions were $v_t=v=$ 63 volts, $i_d=i=8.4$ amp, $i_f=2.14$ amp, $e_f=18.4$ volts; e_f was suddenly increased to 21.9 volts. The figures on the curves $e\delta$, v, and i in the oscillograms are rms values.

The curves of Fig. 2 give the armature current from oscillogram with calculated points, and the power angle calculated from $e\delta$ as recorded. The errors between calculated and measured values are less than about 3%, partly because of the

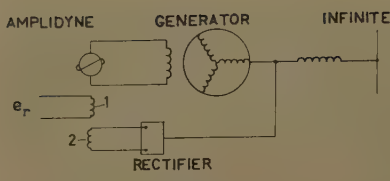

Fig. 4. Voltage-regulating system with amplidyne exciter

reading of the oscillograms which cannot be as precise as the reading of an instrument. The small variation of δ has no effect on the value of the current.

In Fig. 3(A) are given the results obtained during operation with lagging power-factor angle $\phi=47.5$ degrees, in response to a sudden increase of e_f from 22.1 volts to 26.6 volts. The initial conditions were $v=65$ volts, $i=12.7$ amp, $i_f=2.53$ amp.

From the curves of Fig. 3(A) it will be seen that nearly the entire variation of the current has occurred before any relatively important variation of the power angle. Subsequently, the further variation of the power angle has no effect on the value of the current. The variation of the armature current is dependent practically upon the variation of its d-component. The value of ϕ at the end of the transients is 62.5 degrees lag. The i_q component of the current used in the calculation is deduced from δ as recorded.

The case is entirely different for operation with leading power-factor angle, as seen in Fig. 3(B). The machine was operating with $\phi=47$ degrees lead, when the voltage at the field terminals was increased from 5.5 volts to 6.5 volts, and the initial conditions were $v=58$ volts, $i=9.3$ amp, and $i_f=0.55$ amp.

The variation of the armature current is entirely dependent upon the variation of its quadrature component and related to the power angle as seen from the curves of Fig. 3(B), though the variation of δ remains related to the variation of ψ_d. Steady-state value of ϕ is 42 degrees lead.

The performance of the voltage regulating system given in Fig. 4 and considered in Appendix II has been tested on a 15-kva 220-volt 39.5-amp 1,500-rpm 50-cycle 3-phase machine. In Fig. 5 the block diagram of the system is given.

For saturated conditions, L_d is 0.0184 henry and M is 0.182 henry. The ratio of field-leakage flux to total field flux is given by manufacturer as 10.5%. Assuming armature leakage of same order, we admit L_{fd}/L_f equal to 0.21; introducing this value in L_{fd} as defined in the Nomenclature with the foregoing values of L_d and M, L_f is found equal to 3.42 henrys. The other constants are

$L_1=L_2=0.91$ henry
$r_1=12.7$ ohms
$r_2=550$ ohms
$r_Q=3$ ohms
$T_{12}=0.073$ second
$T_Q=0.09$ second
$L_x=0.00574$ henry
$L_{fdx}=1.37$ henrys
$r_f=27.7$ ohms
$T_f=0.124$ second
$T_{fdx}=0.0494$ second

With the rectifier used k is 1.35. K as defined in Appendix II is 1,860 and $E_{fo}=74$ volts. The amplidyne was a 2-pole machine with 125 turns per pole for control fields 1 and 2 (Fig. 4).

With the foregoing values of the constants from equation 32 the incremental variation of the effective value of the armature current is in amp

$$\Delta i=\Delta\bar{E}_r[4.88-1.52\epsilon^{-30t}-6.9\epsilon^{-7.65t}\sin(11.8t+29°)] \quad (5)$$

The synchronous machine operating with entirely reactive load, the reference voltage e_r was increased suddenly from 6.9 volts to 7.5 volts.

The initial conditions were $e_f=93$ volts, $i_f=3.35$ amp, $i=i_d=2.4$ amp, $v_t=210$ volts, and $v=202.5$ volts.

The oscillogram in Fig. 6 gives the terminal voltage and the armature current, shown in curve *a;* curve *b* is calculated with equation 5. The steady-state values after the transients were $e_f=107$ volts, $i_f=3.85$ amp, $i=5.4$ amp, $v_t=220$ volts, $v=203$ volts.

The difference between curves *a* and *b* is due to the time lag introduced by effects not considered in this analysis, in the variation of the terminal voltage of the synchronous machine actually increasing

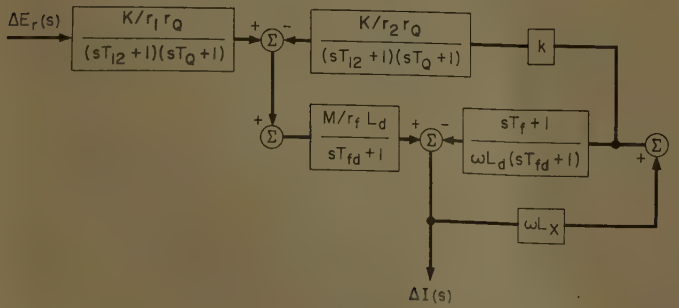

Fig. 5. Block diagram of voltage-regulating system of Fig. 4

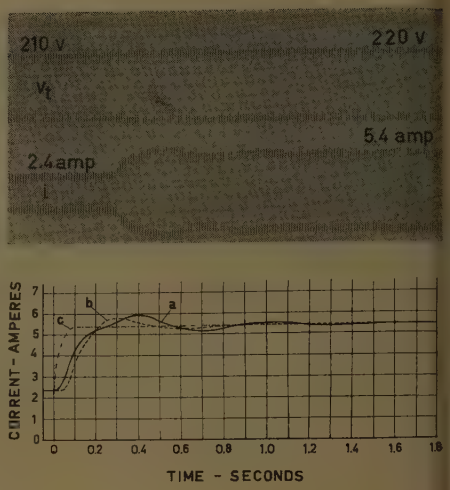

Fig. 6. Terminal voltage and armature current of generator as response to an increase of the reference voltage applied to the control field of amplidyne exciter

a—Armature current from oscillogram
b—Calculated current
c—Calculated current neglecting amplidyne transients

the net control ampere-turns of the amplidyne. Curve *c* is calculated neglecting amplidyne transients, that is, taking $T_{12}=0$, $T_Q=0$.

Conclusions

The expressions of the transient current components have been derived from circuit equations.

The d-component of the transient current is dependent upon the voltage applied to the field terminals and the terminal voltage component corresponding to the resultant flux component along d-axis.

For operation with an entirely reactive load this voltage component is equal to the terminal voltage and is constant for a machine connected to infinite bus. The current in this case depends only upon the excitation voltage.

When the synchronous machine is operating with relatively large lagging power-factor angle so that v_q can be regarded as constant, these conclusions are still valid and the variation of the armature current is dependent practically upon the variation of its component along direct axis.

In case the machine is operating with leading power-factor angle, the variation of both components of the terminal voltage must be taken into account. The armature current variation is almost entirely dependent upon the variation of its quadrature axis component related to the power angle, whose variation however is also dependent upon the variation of the component of the resultant flux along d-

axis. This case is not within the scope of this paper.

An example of use of the transfer functions as derived has been given in the performance calculation of a voltage-regulating closed-loop system with amplidyne exciter, including the consideration of the saturation effects in the amplidyne.

Nomenclature

v = voltage at the infinite bus
v_q, v_d = components of v along q- and d-axis
v_t = terminal voltage of the synchronous machine
v_{tq}, v_{td} = components of v_t along q- and d-axis
i = armature current
i_d, i_q = components of i along d- and q-axis
ϕ = power-factor angle
δ = power angle
ω = speed, electrical radians per second
L_d, L_q = self-inductances per phase
M = mutual inductance between phase and field windings
r = armature resistance
ωL_x = external reactance
e_f = voltage applied to field terminals, also terminal voltage of amplidyne exciter
i_f = field current
L_f, r_f = self-inductance and resistance of field winding
ψ_d, ψ_q = flux linkage components along d- and q-axis
ψ_f = field-winding flux linkage
e_r = reference voltage applied to the terminals of the control field winding of amplidyne
i_1 = current in this winding
L_1, r_1 = self-inductance and resistance of this control field winding
k = ratio of the direct voltage from rectifier to the effective value of the alternating voltage applied
i_2 = current in the field winding of the amplidyne at which the feedback voltage is applied
L_2, r_2 = self-inductance and resistance of this winding
K_E = ratio of the electromotive force induced in quadrature axis circuit of the amplidyne to the effective ampere-turns of control circuits; in case these circuits have the same number of turns, K_E will be in volts per net amp; sum of currents i_1 and i_2
e_Q, i_Q = electromotive force induced and current in short-circuited quadrature axis circuit of amplidyne
L_Q, r_Q = self-inductance and resistance of this circuit
K_{dQ} = ratio of output voltage of the amplidyne to current in short-circuited quadrature axis circuit
K = factor as defined in Appendix II

The various time constants and corresponding inductances are defined as follows:

$$T_f = L_f/r_f$$

$$T_{fd} = \left(L_f - \frac{1.5M^2}{L_d}\right)/r_f$$

$$T_{fdx} = \left(L_f - \frac{1.5M^2}{L_d+L_x}\right)/r_f$$

$$T_{12} = L_1(r_1+r_2)/r_1r_2$$

$$T_Q = L_Q/r_Q$$

$$L_{df}(s) = L_d - \frac{1.5M^2s}{L_fs+r_f}$$

e_δ = voltage equal to the phasorial difference between the voltage of the infinite bus and the voltage of the same amplitude of an auxiliary alternator as defined in this paper

$F(s)$ and $X(s)$ are Laplace transforms of $f(t)$ and $x(t)$, the equations defining the relationship being

$$F(s) \underline{\Delta} \mathcal{L} f(t)$$

$$X(s) \underline{\Delta} \mathcal{L} x(t)$$

$f(0+)$, $x(0+)$ are initial values of $f(t)$ and $x(t)$
$\Delta x(t)$ is an incremental variation of $x(t)$, that is $\Delta x(t) = x(t) - x(0+)$
$\Delta X(s)$ is the Laplace transform of $x(t)$
$\bar{X}$ is a constant value of the variable x

Appendix I. Derivation of Transfer Functions of Loaded Synchronous Machine

The equations of Park in their differential form are for the armature winding with $d\theta/dt$ speed of rotation

$$v_{tq} = \frac{d\psi q}{dt} + \psi d\frac{d\theta}{dt} - ri_q \tag{6}$$

$$v_{td} = \frac{d\psi d}{dt} - \psi q\frac{d\theta}{dt} - ri_d \tag{7}$$

and for the field winding

$$e_f = \frac{d\psi f}{dt} + r_f i_f \tag{8}$$

In this connection, for a 3-phase machine without amortisseur winding,

$$\psi_d = Mi_f - L_d i_d \tag{9}$$

$$\psi_q = -L_q i_q \tag{10}$$

$$\psi_f = L_f i_f - 1.5Mi_d \tag{11}$$

Neglecting the armature transients and resistance, in case of no saturation, and assuming constant speed of rotation corresponding to the nominal frequency, the application of Laplace transformation to the foregoing equations gives

$$V_{tq}(s) = \omega\Psi_d(s) \tag{12}$$

$$V_{td}(s) = -\omega\Psi_q(s) \tag{13}$$

$$E_f(s) = s\Psi_f(s) - \psi_f(0+) + r_f I_f(s) \tag{14}$$

$$\Psi_d(s) = MI_f(s) - L_d I_d(s) \tag{15}$$

$$\Psi_q(s) = -L_q I_q(s) \tag{16}$$

$$\Psi_f(s) = L_f I_f(s) - 1.5MI_d(s) \tag{17}$$

From the foregoing equations one obtains

$$\left(L_d - \frac{1.5M^2s}{L_fs+r_f}\right) I_d(s) = \frac{M}{L_fs+r_f}[E_f(s)+\psi_f(0+)] - \frac{V_{tq}(s)}{\omega} \tag{18}$$

and

$$I_d(s) = [E_f(s)+\psi_f(0+)]\frac{M}{r_fL_d(sT_{fd}+1)} - \frac{V_{tq}(s)}{\omega}\frac{sT_f+1}{L_d(sT_{fd}+1)} \tag{18A}$$

In case the machine is connected to an infinite bus through an external reactance ωL_x,

$$V_{tq}(s) = V_q(s) + \omega L_x I_d(s) \tag{19}$$

From equations 18 and 19

$$I_d(s) = [E_f(s)+\psi_f(0+)] \times \frac{M}{r_f(L_d+L_x)(sT_{fdx}+1)} - \frac{V_q(s)}{\omega}\frac{sT_f+1}{(L_d+L_x)(sT_{fdx}+1)} \tag{20}$$

This equation can be written

$$I_d(s) = E_f(s)K_1G_1(s) - V_q(s)K_2G_2(s) + \psi_f(0+)K_1G_1(s) \tag{21}$$

with

$$K_1G_1(s) = \frac{M}{r_f(L_d+L_x)(sT_{fdx}+1)} \tag{22}$$

$$K_2G_2(s) = \frac{sT_f+1}{\omega(L_d+L_x)(sT_{fdx}+1)} \tag{22A}$$

If the incremental variations of the variables are considered equation 21 takes the form

$$\Delta I_d(s) = \Delta E_f(s)K_1G_1(s) - \Delta V_q(s)K_2G_2(s) \tag{22B}$$

The quadrature component of the current is

$$I_q(s) = \frac{V_d(s)}{\omega(L_q+L_x)} \tag{23}$$

Saturation Effects

The foregoing results have been obtained for an unsaturated machine. The saturation effects in a synchronous machine can be taken into account, as shown in a previous paper,[14] for quantities related to d-axis by dividing the synchronous reactance by a properly defined factor. If the machine is operating with entirely reactive load no other influence need be considered. Thus L_d will be divided by the saturation factor determined by initial values of voltage and currents. The saturated value of L_d can also be directly deduced from these values. The mutual inductance M would be divided by the saturation factor corresponding to the q-component of the terminal voltage on the no-load characteristic. In a case of an entirely reactive load this component of the voltage is equal to the terminal voltage.

Neglecting the variation of the leakage reactance due to saturation,[15] the saturated value of L_f can be deduced from expressions of leakage reactance such as the transient

reactance. In the case treated as an example in this paper the ratio of field leakage to field flux was known. The saturated value of L_f was deduced from the value of L_{fd} as defined in the Nomenclature.

Appendix II. Calculating the Performance of Voltage-Regulating System with Amplidyne Exciter

The voltage-regulating system considered is given in Fig. 4. The reference voltage e_r is applied to the control field circuit (1) of the amplidyne. The feedback voltage is applied to the second control field (2). This direct voltage is k,v_t, v_t being the effective value of the terminal voltage connected to the rectifier. The synchronous machine is represented by transfer functions as derived in Appendix I.

Amplidyne performance treatments have been presented by various authors.[16-18] In the following the saturation effects in the amplidyne will be taken into account.

With the incremental variations of the variables, the Laplace transform equation for circuit 1 is

$$\Delta E_r(s)=(L_1s+r_1)\Delta I_1(s)-Ms\Delta I_2(s) \qquad (24)$$

and for circuit 2

$$k\Delta V_t(s)=(L_2s+r_2)\Delta I_2(s)-Ms\Delta I_1(s) \qquad (25)$$

From these equations, neglecting the leakage flux between circuits 1 and 2, with L_1 equal L_2, one obtains with T_{12} as defined in the Nomenclature

$$\Delta I_1(s)-\Delta I_2(s)=\Delta E_r(s)\frac{1}{r_1(sT_{12}+1)}-k\Delta V_t(s)\frac{1}{r_2(sT_{12}+1)} \qquad (26)$$

Under unsaturated conditions

$$e_Q=K_E(i_1-i_2) \qquad (27)$$

and for the current

$$\Delta I_Q(s)=\frac{\Delta E_Q(s)}{r_Q(sT_Q+1)} \qquad (28)$$

The amplidyne terminal voltage incremental variation which is also the variation of the voltage applied to the field terminals of the synchronous machine will be, in case of no saturation,

$$\Delta E_f(s)=K_{dQ}\Delta I_Q(s)=\Delta E_r(s)JN(s)/r_1-k\Delta V_t(s)JN(s)/r_2 \qquad (29)$$

with

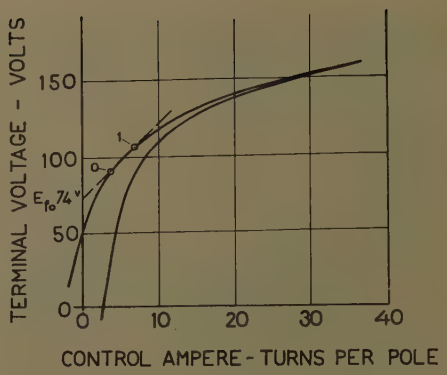

Fig. 7. Load characteristic of the amplidyne

$$JN(s)=\frac{K_EK_{dQ}}{r_Q(sT_{12}+1)(sT_Q+1)} \qquad (30)$$

Replacing this value of $\Delta E_f(s)$ in equation 22B with v_q constant and taking into consideration that

$$\Delta V_{tq}=\omega L_x\Delta i_d \qquad (31)$$

the effective value of $\Delta I_d(s)$ which, in a case of an entirely reactive load as considered here, is equal to the incremental variation of the effective value of the armature current will be

$$\Delta I(s)=\Delta E_r(s)\times\frac{\frac{K_EK_{dQ}M}{r_1r_fr_Q\sqrt{2}}}{(L_d+L_x)(sT_{12}+1)(sT_Q+1)(sT_{fdx}+1)+\frac{K_EK_{dQ}k\omega L_xM\sqrt{3}}{r_2r_fr_Q\sqrt{2}}} \qquad (32)$$

Saturation Effects

As generally the amplidyne is operating under saturated conditions, the foregoing results need to be modified in order to take into account the saturation effects.

In deriving equation 29 it has been assumed that the amplidyne load characteristic giving the terminal voltage as a function of the resultant ampere-turns of the control circuits was a straight line through the origin.

The actual load characteristic of the amplidyne used in the experimental studies reported in this paper is given in Fig. 7. The point (0) corresponds to the initial conditions, while (1) is the steady-state operating point.

The linear correlation factor between e_f and the resultant control ampere-turns will be taken into account by a new constant factor K instead of K_EK_{dQ}, this time along the straight line through points (0) and (1), and a constant value E_{fo} must be introduced.

The terminal voltage of the amplidyne is

$$e_f=E_{fo}+K(i_1-i_2)/r_Q \qquad (33)$$

defining the factor K which will replace K_EK_{dQ} in equation 32, in the case of saturation of the amplidyne.

References

1. Two-Reaction Theory of Synchronous Machines, Generalized Method of Analysis—Part I, R. H. Park. *AIEE Transactions*, vol. 48, July 1929, pp. 716–30.

2. Two-Reaction Theory of Synchronous Machines—II, R. H. Park. *Ibid.*, vol. 52, June 1933, pp. 352–55.

3. Synchronous Machines (book), C. Concordia. John Wiley & Sons, Inc., New York, N. Y., 1951.

4. Power System Stability (book), S. B. Crary. John Wiley & Sons, Inc., 1947.

5. Voltage Variation of Suddenly Loaded Generators, H. C. Anderson. *General Electric Review*, Schenectady, N. Y., vol. 48, Aug. 1945, pp. 25–33.

6. Electrical Transmission and Distribution Reference Book. Westinghouse Electric Corporation, Pittsburgh, Pa., 1950.

7. The Operational Impedance of the Synchronous Machine, M. L. Waring, S. B. Crary. *General Electric Review*, vol. 35, Nov. 1932.

8. The Effects of Generator Voltage Regulators on Stability and Line Charging Capacity, F. S. Rothe. *Report no. 321*, CIGRE, Paris, France, 1954.

9. Effect of a Modern Amplidyne Voltage Regulator on Underexcited Operation of Large Turbine Generators, W. G. Heffron, R. A. Phillips. *AIEE Transactions*, vol. 71, pt. III, Aug. 1952, pp. 692–97.

10. Fundamental Equations for Analogue Studies of Synchronous Machines, D. B. Breedon, R. W. Ferguson. *Ibid.*, vol. 75, pt. III, June 1956, pp. 297–306.

11. Analogue Computer Representations of Synchronous Generators in Voltage Regulation Studies, M. Riaz. *Ibid.*, Dec., pp. 1178–84.

12. Some Measurements on the Excitation and Load-Angle Characteristics of Large Alternators, J. W. Byrne, D. Carroll. *Report no. 310*, CIGRE, 1956.

13. The Diagnosis of Steam Turbine Alternator Performance by Stroboscopic Method, E. B. Powell. *Report no. 101*, CIGRE, 1956.

14. Saturation Effects in Synchronous Machines, Djabir Hamdi-Sepen. *AIEE Transactions*, vol. 73, pt. III-B, Dec. 1954, pp. 1349–53.

15. A New Approach to the Calculation of Synchronous Machine Reactances—Part II, M. E. Talaat. *Ibid.*, vol. 75, pt. III, June 1956, pp. 317–27.

16. Metadyne Statics (book), J. M. Pestarini. John Wiley & Sons, Inc., 1952.

17. Fundamentals of the Amplidyne Generator, J. L. Bower. *AIEE Transactions*, vol. 64, 1945, pp. 873–80.

18. Transient Analysis of the Metadyne Generator, M. Riaz. *Ibid.*, vol. 72, pt. III, Feb. 1953, pp. 52–62.

Energy-Conversion Properties of Induction Machines in Variable-Speed Constant-Frequency Generating Systems

M. RIAZ
MEMBER AIEE

IN A LIST of more than 380 technical problems affecting the defense of the United States prepared by the National Inventors Council (Office of Technical Services, U. S. Department of Commerce) appears the following item under the general heading of Power Supplies: *741. AC Generators*—Constant frequency, variable speed AC Generators." This is but one indication of the importance attached today to the problem of constant-frequency a-c generation, particularly with regard to air-borne applications. In recent years, many solutions to this problem have been proposed, developed and, in some instances, specific constant-frequency generating systems have been actually utilized in aircraft and guided missiles.

Two basic approaches have been considered: The initial approach had to do with the development of constant-speed drives capable of converting the variable speed of a propeller or turbine prime mover to a constant-speed output shaft which drives an a-c generator. This system is presently employed in many types of aircraft, the control of the constant-speed drives being normally effected on a differential principle by hydraulic means, although pneumatic and mechanical drives have also been suggested. All these systems suffer from a complexity and reliability standpoint, resulting from the close manufacturing tolerances necessary to achieve the desired control at the speeds involved, and from the auxiliary equipment required to supply oil, high-pressure air, and the like.

Despite the relative success of some of these systems, attention has also been given to the possibility of developing all-electric constant-speed drives. The all-electric constant-speed drive assumes the configuration of a variable-speed generator connected to a motor suitably controlled to run at constant speed. One particular arrangement, initially proposed by Pestarini,[1] using d-c metadynes for the generator and motor, offers some interesting possibilities, notwithstanding its large weight and size and the complexities associated with commutators. Another recently suggested arrangement[2] uses a variable-frequency a-c generator to supply the stator excitation of an induction motor, the rotor of which is excited by the difference between the unregulated stator frequency and a standard frequency derived from a relatively low power source. The motor then runs at a constant speed in synchronism with the standard controlled frequency and drives a conventional a-c generator. A basic feature of an all-electric drive is the possible utilization of the variable-speed generated power, whether d-c or a-c, to supply certain types of electrical loads in addition to the constant-speed motor load.

All constant-speed drive systems essentially introduce an extra piece of equipment placed between an input varying speed shaft and the a-c generator. An alternate approach to the problem of constant-frequency generation is to derive this constant-frequency output directly from the variable-speed rotating shaft. Several systems have been suggested along this line of which two kinds can be distinguished; one involves new types of constant-frequency alternators, and the other involves rectification of variable-frequency a-c power followed by its inversion to constant frequency. This inverter-type system is now coming to the fore as a consequence of the recent development of semiconductor devices capable of operating at high power levels. Furthermore, it provides an interesting method of generating constant frequency for those aircraft or missile systems in which the prime source of power is not in the nature of a shaft speed but in the form of direct current.

The majority of the suggested constant-frequency variable-speed a-c generators employs some form of induction machine in conjunction with auxiliary a-c or commutator machines which may, in some cases, form an integral part of the induction machine.[3]

It is with these induction-machine systems arranged to produce constant-frequency generation that this paper is mainly concerned. The object is to determine the basic physical limitations and advantages inherently present in the design of such systems. The approach adopted in this study is based upon consideration of the energy-conversion properties of induction machines.

Electromechanical Energy Conversion in the Induction Machine

Although the theory of the induction motor is now undoubtedly well established and may be found in almost any textbook on rotating electric machines,[4] it is desirable to describe briefly the fundamental characteristics of an induction machine. This review will serve to illustrate the nomenclature and conventions adopted in the analysis. To emphasize the electromechanical energy-conversion aspect, the induction machine as shown in Fig. 1 will be viewed from its three terminal parts through which power is either delivered or received, depending on the particular mode of operation. The relationships between the terminal quantities are given by the performance equations of the induction machine. For steady-state polyphase operation, these equations may be written on a per-phase basis as:

$$V_s=(R_s+jX_s)I_s+jaX_mI_r \quad (1)$$

$$V_r=jsaX_mI_s+(R_r+jsX_r)I_r \quad (2)$$

$$T_e=\frac{paX_m}{\omega_s}\,\mathcal{R}e[jI_s{}^*I_r] \quad (3)$$

where

V_s, V_r = stator and rotor terminal voltage phasors
I_s, I_r = stator and rotor current phasors
R_s, R_r = stator and rotor resistances
a = equivalent rotor-to-stator turns ratio
s = slip = $(\omega_s-p\omega_m)/\omega_s$
ω_s = stator electrical angular frequency
ω_m = rotor angular speed
p = number of pairs of poles
X_s, X_r = stator and rotor self-reactances at stator frequency
X_m = component of stator self-reactance due to mutual flux (mutual reactance referred to the stator)
T_e = electromagnetic torque developed, taken to be positive when acting on the rotor in the direction of its rotation

Paper 58-917, recommended by the AIEE Air Transportation Committee and approved by the AIEE Technical Operations Department for presentation at the AIEE Summer General Meeting and Air Transportation Conference, Buffalo, N. Y., June 22–27, 1958. Manuscript submitted March 21, 1958; made available for printing July 2, 1958.

M. Riaz is with the University of Minnesota, Minneapolis, Minn.

This study was conducted at the Massachusetts Institute of Technology and was supported in part by Wright Air Development Center under Contract *AF 33(616) 3984*.

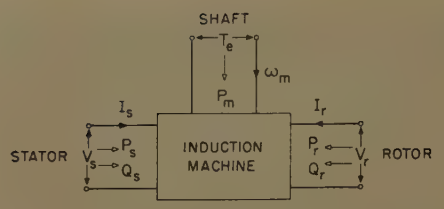

Fig. 1. Block diagram of the induction machine as viewed from its terminals

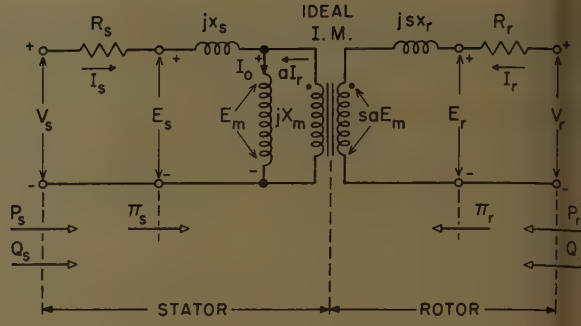

Fig. 2. Electrical equivalent circuit of the induction machine

x_s = stator leakage reactance = $X_s - X_m$
x_r = rotor leakage reactance = $X_r - a^2X_m$

It is often convenient for numerical calculations to express the performance of an induction machine in terms of an equivalent circuit. The particular form of the equivalent circuit illustrated in Fig. 2 may be derived directly form equations 1 and 2 using the concept of an ideal induction machine having a voltage ratio of $as/1$ and a current ratio of $1/a$. This equivalent circuit made up of two subnetworks is convenient because it separately exhibits each of the stator and rotor circuits and so conforms with the terminal representation given in Fig. 1. The polarities and directions of the voltages, currents, and powers are indicated in Fig. 2. Power will be taken to be positive when delivered to the induction machine. In order to stress the power conversion characteristics of the induction machine, the stator and rotor resistances are assumed to form part of the external circuits connected to the machine and attention is focused on the electrical terminals defined by the voltages E_s and E_r in Fig. 2. The per-phase power expressions are defined as

$$\Pi_s = P_s - |I_s|^2 R_s = \Re e[I_s^* E_s] = |I_s||E_s| \cos\theta_s \quad (4)$$

$$\Pi_r = P_r - |I_r|^2 R_r = \Re e[I_r^* E_r] = |I_r||E_r| \cos\theta_r \quad (5)$$

$$Q_s = \Im m[I_s^* E_s] = |I_s||E_s| \sin\theta_s \quad (6)$$

$$Q_r = \Im m[I_r^* E_r] = |I_r||E_r| \sin\theta_r \quad (7)$$

$$P_m = -T_e\omega_m = -T_e(1-s)\frac{\omega_s}{p} \quad (8)$$

where P and Π indicate real or active power and Q denotes reactive power.

Carrying out the operations implicit in the foregoing definitions through the use of equations 1, 2, and 3 yields

$$\Pi_s = aX_m \Re e[jI_s^* I_r] \quad (9)$$

$$\Pi_r = saX_m \Re e[jI_s I_r^*] = -s\Pi_s \quad (10)$$

$$P_m = -(1-s)\frac{\omega_s}{p} \times \frac{paX_m}{\omega_s} \Re e[jI_s^* I_r] = -(1-s)\Pi_s \quad (11)$$

The addition of these three equations gives

$$\Pi_s + \Pi_r + P_m = 0 \quad (12)$$

which is an expression of the principle of conservation of power.

The relation between stator and rotor reactive powers assumes the form

$$Q_s + \frac{Q_r}{s} = Q_0 \quad (13)$$

where

$Q_0 = |I_s|^2 x_s + |I_r|^2 x_r + |I_0|^2 X_m$
= sum of reactive powers needed to establish leakage and magnetizing flux

This also expresses a conservation principle in terms of reactive powers.

Equations 10, 11, and 13 are of fundamental significance in characterizing the steady-state properties of the induction machine. The electrical properties may therefore be summarized by considering the four basic transformations performed by this electromechanical energy converter:

1. A frequency transformation between stator and rotor given by

$$\omega_r = s\omega_s \quad (14)$$

where s is the slip.

2. A transformation of stator to rotor voltages given by the ratio 1 to as.

3. A transformation of the stator and rotor active powers determined by slip only as expressed by equation 10.

4. A transformation of reactive powers as given by equation 13.

Characteristics of Induction Machines

The characteristics that govern any particular mode of operation of the induction machine can be derived as special cases of the general analysis presented in the previous section. The examination of what happens to the power flow leads to distinguishing six basic types of operation. These six types are illustrated in Fig. 3; their distinctive features are solely determined by the value of the slip and the direction of energy conversion. A brief discussion of each of these possible configurations follows next.

CASE A: $s<0$; $T_e>0$

This case corresponds to that of an induction motor operating above synchronous speed when, in addition to the

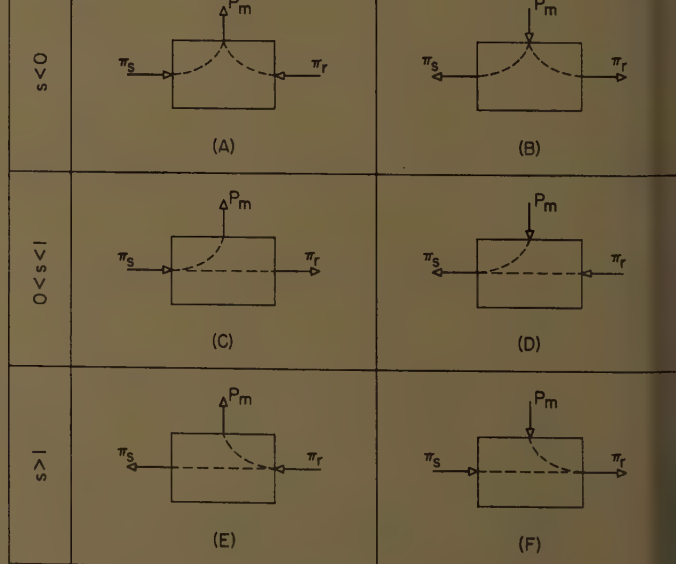

Fig. 3. Power transfer in induction machines

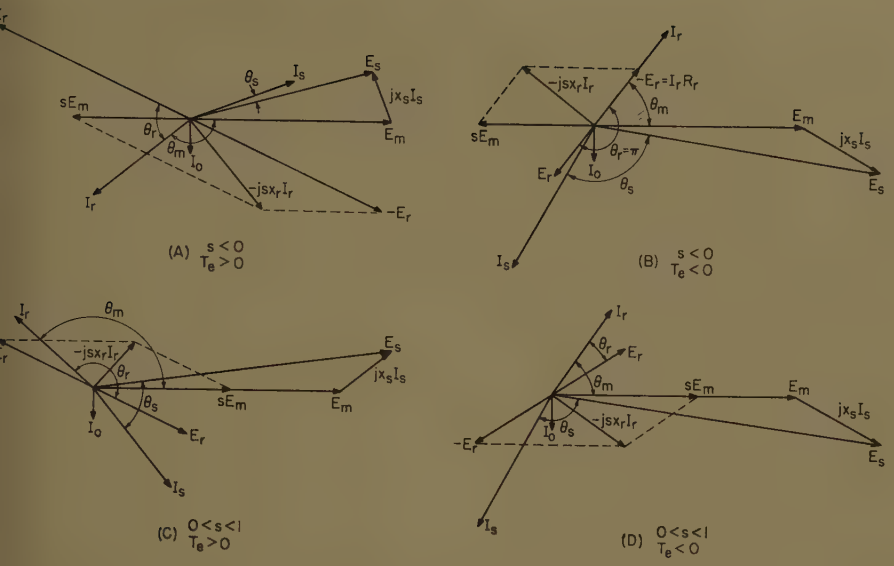

g. 4. **Phasor diagrams corresponding to the different modes of operation of an induction machine**

ower supplied to the stator, slip-fre-uency power is fed to the rotor. For a xed slip frequency, the motor speed is early independent of load. By shifting ie phase of the injected rotor voltages, ie power factor at which the motor op-ates can be controlled. This can be en from the relation.

$$\theta_s = \tan^{-1}\frac{Q_s}{\Pi_s} = \tan^{-1}\frac{Q_0 - (Q_r/s)}{-\Pi_r/s}$$

which $s<0$. For instance, leading-ower-factor operation results when Q_r is egative and greater than $|sQ_0|$. This ondition of operation is described by the iasor diagram of Fig. 4(A).

ASE B: $s<0$; $T_e<0$

This is the case of the mechanically iven induction generator which delivers ctive power to external loads connected the stator and rotor. Included in this ower are the I^2R losses in both stator and otor. The lagging reactive power de-ands ($Q>0$) of the loads as well as the active power Q_0 of the machine must be pplied by suitable external circuits hich usually assume the form of capaci-rs or overexcited synchronous gene-tors conected in parallel to the induction nerator.

The conventional induction generator s a short-circuited rotor ($\Pi_r = I_r^2 R_r$). It characterized by a load and power fac-r operation that is completely deter-ined by the value of slip. If op-ated in parallel with synchronous ma-ines, the induction generator has its ltage and frequency fixed by these ma-ines. If used in an isolated system, the duction generator can provide its own citation when a suitable capacitor bank connected across its terminals, thereby establishing a resonant circuit condition. The phasor diagram governing this situation is shown in Fig. 4(B). Only the active component of stator current $I_s \cos\theta_s$ (neglecting stator resistance effects) can be supplied by the generator to a load while the lagging reactive component of stator current has to be furnished by external capacitors or synchronous machines. A factor expressing the efficiency of power conversion in the induction generator may be defined as

$$\eta_g = \frac{\text{stator power output}}{\text{mechanical power input}} = \frac{-\Pi_s}{P_m} = \frac{-\Pi_s}{-(1-s)\Pi_s} = \frac{1}{1-s} \quad (s<0)$$

The limitation of the ordinary induction generator to operate at a fixed slip for a constant frequency and fixed load may be overcome by injecting suitable voltages in the rotor circuit.

CASE C: $0<s<1$; $T_e>0$

This is the case of the induction motor operating below synchronous speed. In general, the rotor slip-frequency power may supply, in addition to the rotor $I_r^2R_r$ losses, some external active or passive circuits which are so adjusted as to control speed and power factor. The phasor diagram for this mode of operation is given in Fig. 4(C).

The ordinary induction motor has a short-circuited rotor ($E_r = -I_r R_r$). Its power conversion efficiency is defined as

$$\eta_m = \frac{\text{mechanical power output}}{\text{stator power input (neglecting stator losses)}} = \frac{-P_m}{\Pi_s} = 1 - s \quad (s>0)$$

The power factor angle is

$$\theta_s = \tan^{-1}\frac{Q_s}{\Pi_s} = \tan^{-1}\frac{sQ_0}{-\Pi_r} = \tan^{-1}\frac{sQ_0}{I_r^2 R_r} \quad (s>0)$$

CASE E: $s>1$; $T_e>0$

This also defines a motor operation completely equivalent to Case C, with the role of stator and rotor interchanged. Assuming the same sequence of polyphase excitation, the motor in Case E is excited through its rotor and turns in the opposite direction to the motor operating as in Case C with stator excitation. Because of this reversal of rotation, the slip being customarily defined with respect to the stator becomes greater than unity. Clearly the slip with respect to the rotor is $1/s$.

CASE D: $0<s<1$; $T_e<0$

Here, input power is delivered mechanically to the shaft and electrically to the rotor while the stator supplies electric power to an external load. The phasor diagram representing these conditions is given in Fig. 4(D). This generator operation is characterized by an energy balance in which s-per-unit power is delivered electrically to the rotor circuit and $1-s$ per unit is supplied mechanically to the shaft to produce one-per-unit stator output power. Power amplification is therefore achieved as determined by the ratio

$$A = \frac{\text{electric power output}}{\text{electric power input}} = \frac{-\Pi_s}{\Pi_r} = \frac{1}{s}$$

which is also the frequency-transformation ratio of the induction machine (equation 14).

CASE F: $s>1$; $T_e<0$

This case also refers to a generator operation similar to Case E but with the roles of stator and rotor interchanged. Because the rotor must now be driven in a a direction opposite to that of Case E, it therefore rotates in opposite direction to the rotating field of the stator, thereby establishing a slip s greater than unity.

The resulting power amplification is defined by the ratio

$$A = \frac{-\Pi_r}{\Pi_s} = s$$

Induction-Machine Systems for Constant-Frequency Generation

A variable-speed constant-frequency generating system using induction machines can be viewed from an energy-conversion standpoint as constituting essen-

tially the inverse of a variable-speed a-c motor system. Wheras the problem of speed control of a-c motors has been studied from the earliest days of a-c power systems, it is only recently that engineers are becoming interested in the use of induction machines for generation, especially in air-borne-type applications.

One general and basic method for controlling the speed of an a-c motor consists of inserting voltages of the appropriate frequency, magnitude, and phase in the rotor circuits of the motor. The principle underlying this method of induction machine operation has been discussed under Cases A and C in the previous section. It has led to the invention of numerous configurations known by such names as Kramer, Leblanc, Scherbius systems which have been applied successfully to large polyphase induction motor installations as encountered, for example, in rolling mills and wind-tunnel drives. These systems make use of auxiliary commutator-type machines which act as frequency changers to supply or recover the rotor slip-frequency power without incurring excessive ohmic losses. The Schrage brush-shift motor is another example of a machine system in which frequency changer and main motor are combined in one frame.

All these induction-motor systems can be operated in an inverse manner to supply constant-frequency power when driven from a variable-speed source. However, when considering their use for air-borne applications, the fundamental laws relating to the flow of power in the induction machine should be borne in mind as discussed under Cases B and E or F. Operation above and below synchronous speed can be realized; however, the larger the speed variations (or slip), the larger the size required for the auxiliary apparatus. Furthermore, the use of auxiliary commutator machines may present severe problems in the kind of operations and environments encountered in air vehicles. To eliminate these problems, consideration should be given to the development of new static frequency-conversion equipment employing high-power switching transistors and magnetic cores which could be used in conjunction with induction machines to produce constant-frequency generation.

A different arrangement for providing rotor slip-frequency power to an induction machine without recourse to commutator or rectifier-type apparatus makes use of another induction machine. The configuration built in a single frame may be designated as a double-induction-machine system.[5] This generating system, consisting of two series-connected, mechanically coupled rotors, may be regarded as the counterpart of the self-synchronous system comprising two uncoupled induction motors with interconnected rotor circuits. This machine system running above synchronous speed ($s<0$) is equivalent to an induction generator with variable stator-to-rotor coupling. Whereas an ordinary single-induction generator with fixed load and constant frequency must operate at a fixed slip, the double-induction generator can function with variable slips. However, since there is no way of recovering the slip-frequency rotor power without introducing some rectifier-type device, the efficiency of the double-induction generator is still directly governed by the value of slip exactly as in the case of the ordinary induction machine. Hence when large speed variations are encountered as in many air-borne systems, the efficiency of the induction generator is unavoidably low. Another basic disadvantage is that it is cannot supply lagging reactive power which must then be furnished by suitable capacitors or synchronous machines connected in parallel. The power transfer characteristics of the double-induction generator may be explained by using the block diagrams of Fig. 3. At low values of slip, the system corresponds to the combination of two blocks described by Fig. 3(B) in which both rotors supply as outputs Π_r, their total copper losses. For large slip values, the situation is that of a cascaded arrangement of Figs. 3(A) and 3(B) in which the rotor of one machine supplies power to the other rotor in addition to the total rotor copper losses. The result is that this machine will now operate as a motor above synchronous speed. There is still an over-all generator action, but the efficiency is low.

The characteristics of the double-induction generator are analyzed in some detail in the Appendix.

Conclusions

The simplicity and flexibility exhibited by the induction machine in providing electromechanical energy conversion make it attractive for use in constant-frequency a-c power generating systems. As a drive motor, the machine can be controlled to run at constant speed from a variable-frequency source; as an exciter with integral rotating rectifiers, its rotor power can be used to furnish the field excitation of a conventional alternator driven at constant-speed;[6] as a main generator, it can be combined with suitable auxiliary induction or commutator machines to produce constant-frequency a-c power when driven from a variable-speed source.

However, in considering these machine arrangements for air-borne electric systems, the electromechanical energy-conversion aspects must clearly be kept in mind. From this standpoint, the induction machine is seen to be a generalized electromechanical converter absorbing (or delivering) electric power in its input (or output) stator member, converting (or receiving) the fraction $(1-s)$ of this power as mechanical power, and transforming (or absorbing) the fraction s as electric power in its output (or input) rotor member with a corresponding change of frequency. These power-flow relations establish inherent physical limitations to the design of induction-machine systems as they constitute the governing factors which determine the magnitudes of the efficiencies and the sizes of the auxiliary equipment required, such as capacitors, commutators, or induction machines. By themselves, induction machines are basically inefficient when running at large slips. This characteristic is common to any device in which slip occurs between an input and an output member. To improve the efficiency of the induction-machine system, some form of controllable rectifiers must be used to recover or supply the slip-frequency power. Although this action is conventionally performed by commutator-type machines, switching transistors and magnetic cores offer interesting new possibilities for accomplishing the task.

In addition to these fundamental aspects of energy conversion in induction-machine systems, other problems must also be recognized and studied in order to determine the suitability of these systems for constant-frequency variable-speed electric-power generation. Confining attention to purely electrical matters, the following related considerations are of particular importance in air-borne-type applications.

1. The parallel operation of generating systems.
2. The regulation of frequency, voltage and load division.
3. The transient performance and stability of the generating system.
4. The harmonic content of the output generated voltages.

The satisfactory solution of such problems will undoubtedly contribute to the successful development of constant-frequency variable-speed a-c generators. The generating system employing the induction-machine principle appears to be one possible form of realization which, though

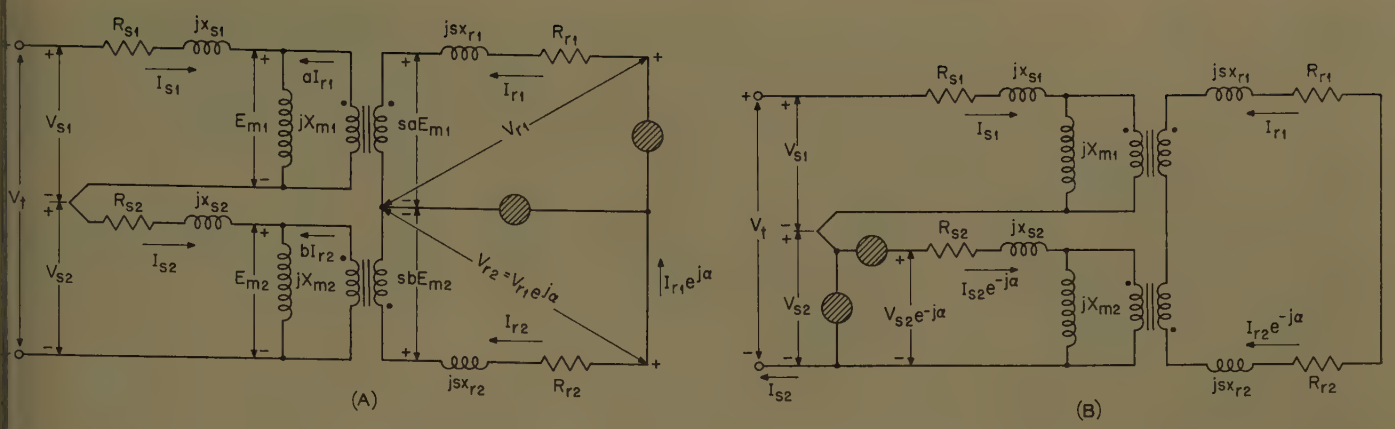

Fig. 5. Equivalent circuit of double induction machine (stator connected in series)

A—Phase shifter in rotor
B—Phase shifter in stator

eset by inherent physical limitations, nay still prove to possess definite ad-antages in some air-borne electric sys-ems.

Appendix. Analysis of the Double-Induction Generator

The double-induction generator consists f two mechanically coupled induction nachines with their stators connected in eries (or in parallel with the possible inter-osition of a variable ratio transformer) and neir rotors in series. An appropriate regu-ator including a capacitor excitation system s assumed present in the stator circuits to ontrol terminal voltage and frequency. A hase shift between rotor impressed voltages s introduced by displacing the rotor wind-ngs relative to each other while maintaining ne stator windings in phase. This phase hift can also be obtained by a stator dis-lacement with the rotors in phase or by a ombination of both stator and rotor dis-lacements. These displacements can be nade either mechanically or electrically by neans of additional windings, usually of the o-called saturating type.

The steady-state equations of the double-nduction generator are first written assum-ng that the two induction machines are not onnected either mechanically or electri-ally. These equations therefore assume ne form given in equations 1 and 2 and are est expressed using matrix notation as

$$[V] = [Z] \times [I]$$

r

$$\begin{bmatrix} V_{s1} \\ V_{r1} \\ V_{s2} \\ V_{r2} \end{bmatrix} = \begin{bmatrix} R_{s1}+jX_{s1} & jaX_{m1} & & \\ jas_1X_{m1} & R_{r1}+js_1X_{r1} & & \\ & & R_{s2}+jX_{s2} & jbX_{m2} \\ & & jbs_2X_{m2} & R_{r2}+js_2X_{r2} \end{bmatrix} \times \begin{bmatrix} I_{s1} \\ I_{r1} \\ I_{s2} \\ I_{r2} \end{bmatrix} \quad (15)$$

he turns ratios are denoted by a for ma-ine 1 and by b for machine 2.

The next step in the analysis is to deter-ine the constraints established by con-ecting the two induction machines to form ne given system configuration. These onstraints reduce to equating the slips in ne two machines and to writing the follow-ing relation between the old variables (un-primed) and the new variables (primed):

$$[I] = [C] \times [I']$$

or

$$\begin{bmatrix} I_{s1} \\ I_{r1} \\ I_{s2} \\ I_{r2} \end{bmatrix} = \begin{bmatrix} 1 & 0 \\ 0 & 1 \\ 1 & 0 \\ 0 & -e^{j\alpha} \end{bmatrix} \times \begin{bmatrix} I_s \\ I_r \end{bmatrix} \quad (16)$$

The constraint matrix $[C]$ is established on the assumption that the stators are in phase and connected in series while the series-connected rotors have a phase shift of α. The impedance matrix $[Z']$ describing the actual system is then obtained from the equation

$$[Z'] = [C_t^*] \times [Z] \times [C]$$

where C_t^* means the conjugate transpose of C. After carrying out the foregoing matrix operations, the performance equations of the double induction machine are finally written as

$$\begin{bmatrix} V_t \\ 0 \end{bmatrix} = \begin{bmatrix} R_{ss}+jX_{ss} & jaX_{m1}-jbX_{m2}e^{j\alpha} \\ jasX_{m1}-jbsX_{m2}e^{-j\alpha} & R_{rr}+jsX_{rr} \end{bmatrix} \times \begin{bmatrix} I_s \\ I_r \end{bmatrix} \quad (17)$$

where

$$R_{ss} = R_{s1}+R_{s2};\quad X_{ss} = X_{s1}+X_{s2}$$

$$R_{rr} = R_{r1}+R_{r2};\quad X_{rr} = X_{r1}+X_{r2}$$

V_t = terminal voltage = $V_{s1}+V_{s2}$

The electromagnetic torque is given by

$$T_e = \frac{p}{\omega_s} \mathcal{R}e[(jaX_{m1}-jbX_{m2}e^{-j\alpha})I_s^*I_r] \quad (18)$$

It is interesting to note that the equations of the double-induction machine are similar to those of a single-induction machine given in equations 1, 2, and 3. The main effect of the double connection appears in the off-diagonal term representing the stator-rotor mutual coupling. Since this coupling may be varied by changing the turns ratio b/a and the phase shift α, it provides an added degree of flexibility which can be utilized to achieve constant-frequency variable-speed system operation. This is in contrast to the single-induction generator capable of operating at only one value of slip for any given load.

The solutions of equation 17 are

$$\frac{I_s}{V_t} = \frac{R_{rr}+jsX_{rr}}{R_{ss}R_{rr}-s(X_{ss}X_{rr}-X_{mm}^2)+j(R_{rr}X_{ss}+sR_{ss}X_{rr})} \quad (19)$$

and

$$\frac{I_r}{V_t} = \frac{bsX_{m2}\sin\alpha+j(bsX_{m2}\cos\alpha-asX_{m1})}{R_{ss}R_{rr}-s(X_{ss}X_{rr}-X_{mm}^2)+j(R_{rr}X_{ss}+sR_{ss}X_{rr})}$$

where

$$X_{mm}^2 = a^2X_{m1}^2+b^2X_{m2}^2-2ab\cos\alpha X_{m1}X_{m2}$$

The stator power is therefore

$$P_s = \mathcal{R}e[I_s^*V_t] = \frac{V_t^2(R_{ss}R_{rr}^2+sR_{rr}X_{mm}^2+s^2R_{ss}X_{rr}^2)}{[R_{ss}R_{rr}-s(X_{ss}X_{rr}-X_{mm}^2)]^2+(R_{rr}X_{ss}+sR_{ss}X_{rr})^2} \quad (20)$$

and the rotor power is

$$P_r = I_r^2R_r = \frac{V_t^2R_{rr}s^2X_{mm}^2}{[R_{ss}R_{rr}-s(X_{ss}X_{rr}-X_{mm}^2)]^2+(R_{rr}X_{ss}+sR_{ss}X_{rr})^2} \quad (21)$$

It is clear from equation 20 that, if s is negative, the stator power may be negative indicating the delivery of a net power out of the double-induction generator. If stator resistances are neglected, the stator power expression becomes

$$\Pi_s = \frac{V_t^2sR_{rr}X_{mm}^2}{s^2(X_{ss}X_{rr}-X_{mm}^2)^2+X_{ss}^2R_{rr}^2} \quad (22)$$

and the power factor angle

$$\vartheta_s = \tan^{-1}\frac{sX_{rr}}{R_{rr}} - \tan^{-1}\times \frac{R_{rr}}{-s[X_{rr}-(X_{mm}^2/X_{ss})]}$$

Hence by modifying X_{mm} control can be effected on the power output or power factor for changing slips. However, the efficiency of the double-induction generator (neglecting stator losses) is still a direct function of slip since, from equations 21 and 22,

$$\eta = \frac{-\Pi_s}{-\Pi_s + I_r^2 R_r} = \frac{1}{1-s} \quad \begin{matrix}(s<0)\\(R_s=0)\end{matrix} \qquad (23)$$

which is the identical relation satisfied by a single-induction generator.

Another procedure for deriving the performance equations of the double-induction generator can also be developed with the use of the equivalent circuit shown in Fig. 2. By combining two such equivalent circuits so as to satisfy the constraints of interconnection (series stator and rotor circuits), a complete equivalent circuit for the double-induction generator can be obtained as illustrated in Fig. 5. The two circuits shown are completely similar except for the location of the phase shifter. The performance equations can then be obtained from a direct inspection of these equivalent circuits and must check with equation 17.

A very similar analysis can be carried out for the case of a double-induction generator in which the stator windings are connected in parallel instead of the series connection discussed here. The characteristics are substantially the same for both types of connections.

References

1. Engineering Design Study for a Two Unit (Electrical) Constant Speed 85 Horsepower Alternator Drive, J. M. Pestarini. *Technical Report 55-236*, Wright Air Development Center, Dayton, Ohio, June 1955.

2. Aircraft Motor Generator with Secondary Standard Frequency Output, L. J. Johnson, S. E. Rauch. *Transactions*, Professional Group on Component Parts, Institute of Radio Engineers, New York, N. Y., vol. CP-5, no. 1, Mar. 1958, pp. 28–31.

3. Future Aircraft Electrical Systems Predicted (abridgement of Direct Engine-Driven Unconventional Electric Systems), K. Martinez. *Journal*, Society of Automotive Engineers, New York, N. Y., Jan. 1958, pp. 68–70.

4. Electric Machinery: an Integrated Treatment of A-C and D-C Machines (book), A. E. Fitzgerald, Charles Kingsley, Jr. McGraw-Hill Book Company, Inc., New York, N. Y., 1952.

5. Alternating Current Generating Arrangement for Constant Frequency, K. Polasek, K. A. Jonsson. *U. S. Patent no. 2,747,107*, May 22, 1956. Also, *British Patent no. 700,036*, Sept. 18, 1951.

6. Arrangement Allowing the Elimination of Brushes in Electrical Machinery, M. E. Rémy. *Revue Générale de l'Electricité*, Paris, France, vol. 64, no. 3, Mar. 1955, pp. 113–18.

Communication Systems for Railway Traffic Control

H. C. SIBLEY
MEMBER AIEE

CONTROL of railway traffic from a central location requires the transfer of large amounts of information between the central location and many points along the railroad. The number of wayside information points depends on the type of signaling installed, which in turn depends on the type and amount of traffic handled by the railroad. Certainly, effective communication is required with all locations where track switches and controlled signals are situated. Information must also be available from a sufficient number of points to keep the dispatcher informed about the location and progress of all trains.

Additional information of a specialized nature is rapidly becoming a significant part of traffic control. An example of this special information is the signal picked up by hot box detectors. Voltages proportional to the temperature of each journal box are transmitted to the dispatcher's office as freight trains pass remote detector locations at normal speed.

The General Railway Signal Company designs and builds many communication systems for railroad signaling. Three of these systems will be described in this paper.

Centralized Traffic Control

Centralized traffic control (CTC) requires reliable 2-way communication between a control office and a number of wayside locations. A typical application of CTC may extend over 200 miles with 40 or more field locations. The plant at a field location may comprise a track switch and signals at the end of a passing siding or may be a fair sized interlocking, that is, a group of switches and signals such as may be found at a terminal or at a junction, previously controlled by a local operator in a tower. A CTC system enables the dispatcher to operate track switches and signals at any location. It also provides information as to the position of all wayside apparatus and the location of trains.

Control System

The control system is the part of a CTC system which provides communication outbound from the control office to any of the wayside locations. The information input to this system is supplied by levers or pushbuttons operated by the dispatcher to control track switches or signals. These levers or pushbuttons are generally located on a control machine or console, placing an entire division of a railroad virtually at the dispatcher's fingertips. A typical control machine is shown in Fig. 1. The output of the control system positions relays at the field locations.

One type of CTC control is a synchronous system using relays and transmitting a polar code. In this system a control code comprises 15 equal time intervals of direct voltage line energization of either polarity. When the system is at rest the line is held energized with negative polarity. Mechanical oscillators provide the time base for the system.

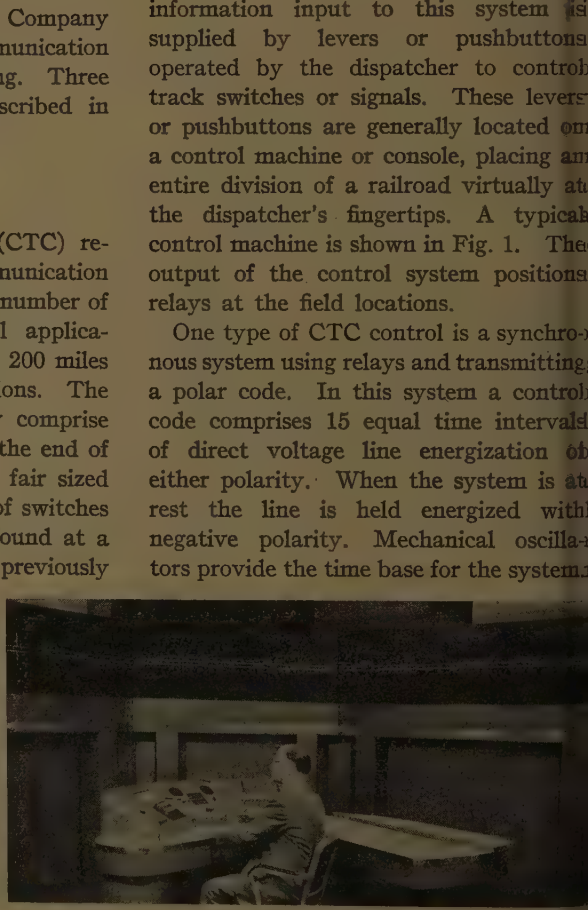

Fig. 1. Typical control machine

Paper 59-249, recommended by the AIEE Land Transportation Committee and approved by the AIEE Technical Operations Department for presentation at the AIEE Winter General Meeting, New York, N. Y., February 1–6, 1959. Manuscript submitted October 23, 1958; made available for printing December 10, 1958.

H. C. Sibley is with General Railway Signal Company, Rochester, N. Y.

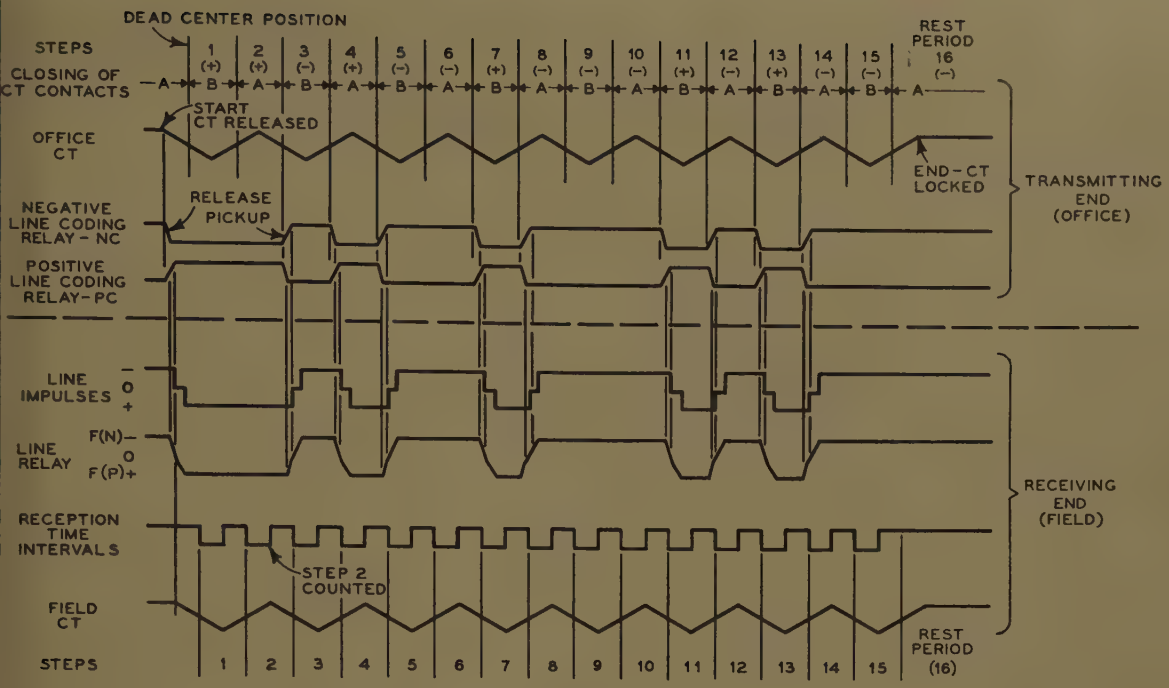

Fig. 2. Sequence of line events, control system

They are mechanically tuned to a frequency of $5\frac{1}{2}$ cycles per second and operate counting relays every half cycle. At the start of a control cycle, the oscillators at the control office and at all field locations are started. A binary counter comprising 4 relays counts the 15 steps of the code and the period of rest. The duration of a control cycle is approximately $1\frac{1}{2}$ seconds.

Fig. 2 shows the sequence of line events of a control cycle. The top two lines are the contact and armature operations of the mechanical oscillator at the control office (designated OFFICE CT). The coding relay operations are shown by the next two lines. The line impulses are the result of the closing of the coding relay contacts.

At the field locations the line relay closes its *P* or *N* contacts, depending on the polarity of line pulses. The mechanical oscillator (FIELD CT) defines the beginning and end of each step in the field. The line labeled RECEPTION TIME INTERVALS shows the portion of each step available for station selection or function control. These intervals are each equal to the duration of a step less the operating time of the counting relays.

Fig. 3 shows, in block form, the components of an office control unit and their functional relationship. The line filter is required to remove the higher harmonics of the code to prevent interference with voice or carrier circuits on the same pair of line wires.

To transmit a control cycle, the dispatcher positions the control levers to set up a route and then presses a start button. One start button is provided for each field location. The appropriate station selection relay is energized to cause the coding relays to generate the proper station selection code. After station selection, the control levers determine the code transmitted for the remainder of the cycle. The oscillator establishes the time of operation of the coding relays. The counting relays serve as a commutator to switch the control of the coding relays among the several control levers and the station selection relay.

Fig. 4 shows a field control unit. The line relay, when it operates for the first time in a control cycle, starts the oscillator. For the remainder of the cycle, the oscillator operates on stored mechanical energy and is not affected by external forces until 15 steps have been counted. Then, the office control unit enters a period of rest, placing continuous energy on the line, and all mechanical oscillators are restored to their latched or rest position. The line relay detects the polarity of line energization.

The function relays are controlled by the line relay and counting relays after the location has been selected by the first part of the control cycle.

The local energy supply for the control system is 28 volts furnished by battery or a rectifier. The line energy for d-c polar operation is a rectifier. The voltage depends on the length and type

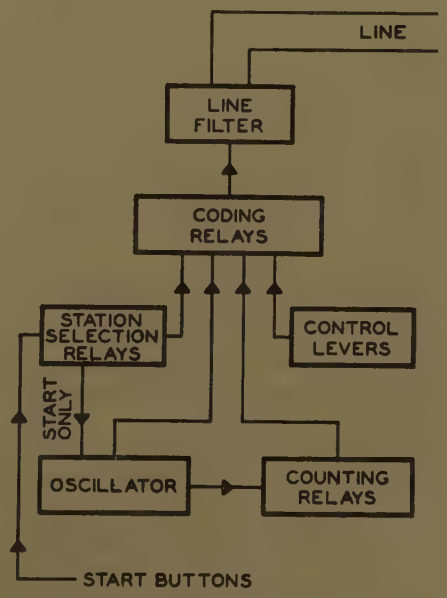

Fig. 3. Office control equipment

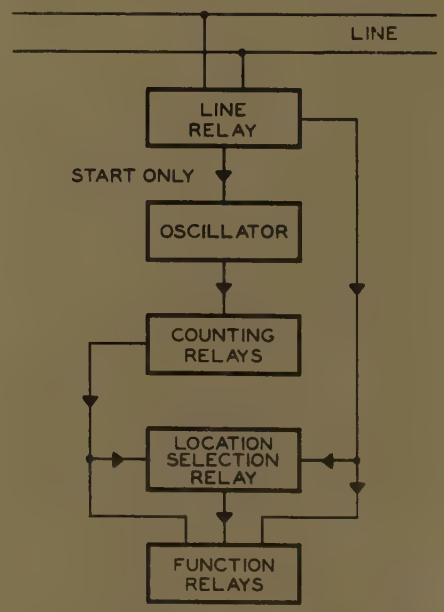

Fig. 4. Field control equipment

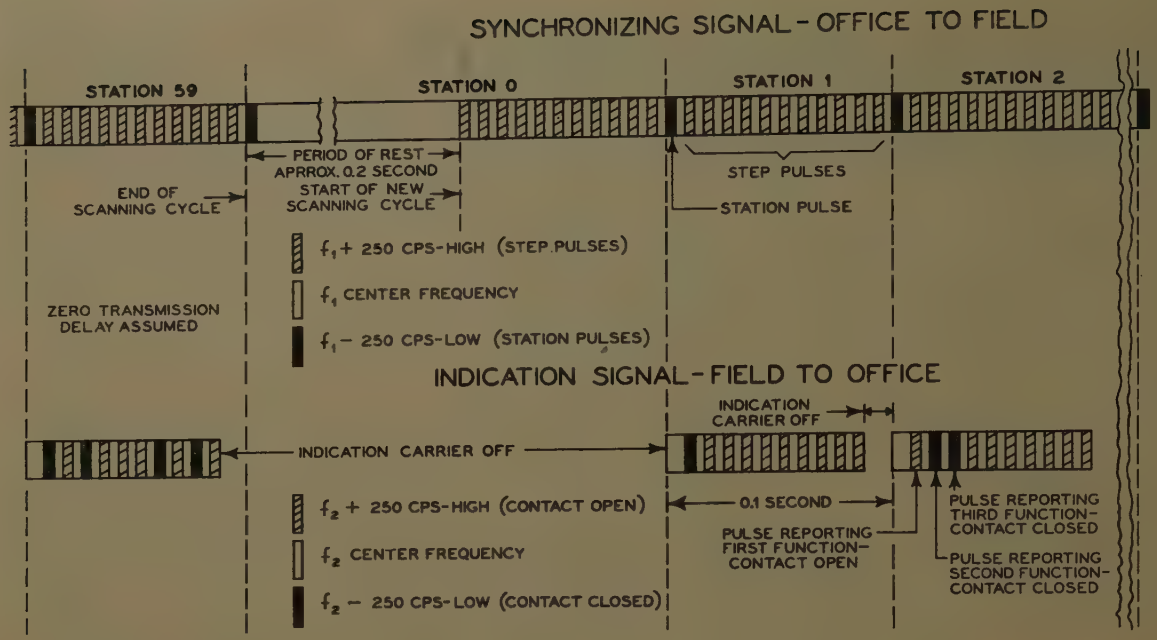

Fig. 5. Line signals, indication system

of line and the number of field locations.

A code repeater is used when the line length and number of field locations exceed the capacity of one line power supply or produce excessive distortion of code pulses. The repeater reshapes the code pulses and keys a line power supply at the repeater location.

A carrier system employing two-way frequency-shift keying is provided when the system is connected to a line already used for a d-c service. The frequency of the carrier transmitter is shifted 100 cycles per second above or below the nominal frequency to provide the carrier equivalent of a polar code.

Indication System

The indication system provides communication inbound from the many field locations to the control office. The input is provided by contacts on signal relays at the field locations and the output is used to position relays at the control office. These relays generally control indication lamps on the dispatcher's panel to show the location of trains and the position of signals and switches.

The indication system used with the control system just described is a continuously scanning, electronic system. The control office continuously calls the roll of all field locations in sequence using a frequency-shift carrier channel. The field locations respond to this roll call on another frequency-shift carrier channel, time sharing this channel. Each field location transmits carrier pulses to the control office to report the position of all functions at that location. The number of pulses transmitted by a field location on each scan is assigned in multiples of ten depending on the amount of wayside apparatus to be reported by that location. Each group of ten pulses is called an indication station. Each pulse represents a two-position field function. If a certain pulse represented a signal, it would be transmitted at one edge of the carrier channel if the signal indicated "stop," or at the other edge if the signal indicated "proceed." In general, an open indication contact results in a pulse of high frequency, that is, center frequency plus 250 cycles per second. A closed indication contact results in a pulse of low frequency, center frequency minus 250 cycles per second. The scanning rate is 100 indications per second. The length of a scan, and therefore the repetition rate, depends upon the number of field stations. A typical installation reports each of 600 field functions every 6 seconds. The line signals for the indication system are shown in Fig. 5.

Fig. 6 is a block diagram of the office indication unit. The synchronizing circuits in the timer establish the scanning rate of the system. The station counter keeps track of the scanning process. The synchronizing signal is sent to the field locations by the carrier transmitter. The carrier receiver separates the pulses from the field according to the direction of frequency shift. The indication circuits in the timer shape these pulses and the step counter counts them. The station counter identifies a group of ten pulses as to origin by its position in the scan. Each group of pulses is routed to its appropriate storage unit. The step counter determines to which stage in a storage unit each pulse is to be sent. The direction of frequency shift determines whether or not the relay connected to the selected stage of the storage unit is to be energized.

Fig. 7 shows the organization of the field indication unit. The carrier receiver feeds the synchronizing signal to the scanner where it is shaped to drive the station counter. Jumpers on the station selector determine at which count the indication unit will transmit its signal to the control office. The indication contacts and step counter work through the diode matrix to form the indication signal.

Cold cathode tubes are used for pulse counting and storage. Considerable energy is saved by using these tubes since they have no heaters. The fact that cold cathode tubes glow during conduction enables the maintainer to make routine checks and locate trouble

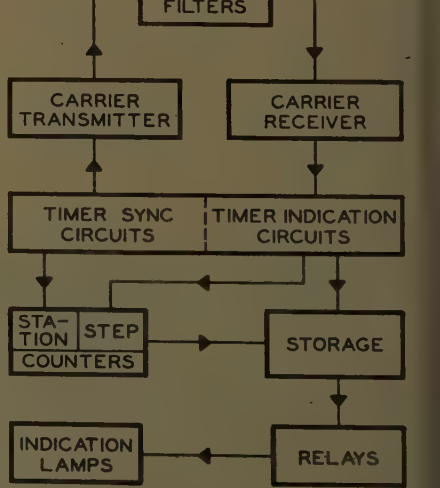

Fig. 6. Office indication equipment

ith no more instrumentation than a oltmeter. Operation of these tubes at ell below rated current has resulted in ng life.

Carrier repeaters of the regenerative ype as well as the simple amplifier type re available when required.

pecial Features of Centralized Traffic Control System

At this point it might be well to men- on the fundamental difference in re- uirements between CTC control and dication systems. Both systems have lectrical contacts as inputs and relays s output devices. The differences are the application.

ONTROL SYSTEM

The control system has inputs originat- g at one geographical location with utputs to be delivered to a multiplicity f locations. Further, the inputs origi- ate in the mind of the dispatcher and an occur no more rapidly than the time quired for him to plan train move- ents and express his wishes by operating ntrol levers or pushbuttons.

The dispatcher executes his plans at he location at a time. The speed re- uired of a control system is that neces- ry to deliver controls to each field cation as quickly as the dispatcher an set them up. The reliability re- uired of a control system is the highest tainable because the apparatus at a eld location is not capable of human dgment and will attempt to execute y control called for. An error in ansmission, if undetected, could set a wrong route or no route at all,

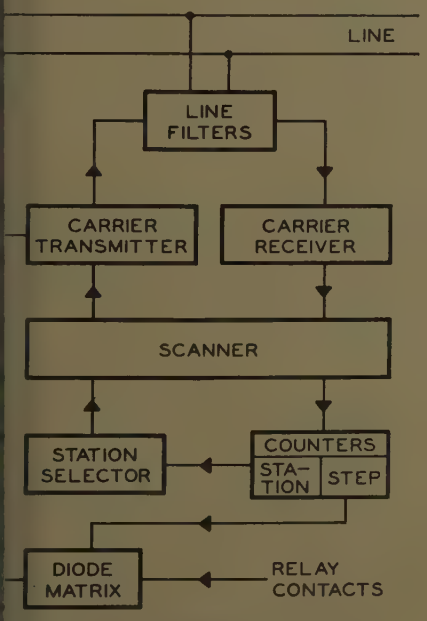

Fig. 7. Field indication equipment

Fig. 8. Diagram of tone system arrangement for one indication

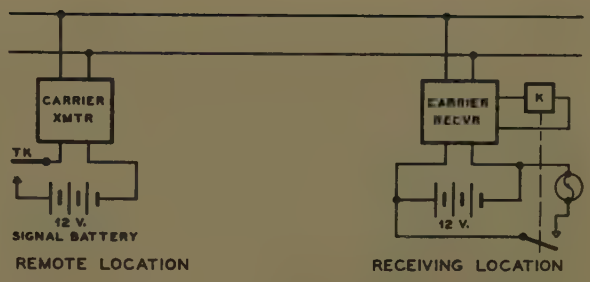

causing train delays. There is no question of safety since all safety circuits are local and no control resulting in an unsafe condition can be executed.

The conditions outlined as to speed and reliability requirements are well met by the relay stepping system previously described. The relays used are designed for extremely long life and reliable contact operation. The control code includes a number of checks reducing the possibility of wrong routes essentially to zero.

INDICATION SYSTEM

The indication system has inputs originating anywhere along a railroad at random times. If there are a dozen trains operating on a division, the information regarding train locations can change frequently in a few seconds as several trains simultaneously cross short track circuits. The electronic scanning system provides the speed and capacity to satisfy these conditions.

MULTISTATION OPERATION

CTC systems differ from conventional communication systems in that they are multistation systems rather than end-to-end. This fact means that every relay or tube added to a field unit is multiplied by 25 or more on any typical installation. It is, therefore, very desirable to keep these units as simple as possible.

Furthermore, since there are so many wayside locations, the line apparatus must be designed to bridge rather than terminate the line and present as little bridging loss as possible.

Since the field locations are unattended, the carrier system must be capable of operating for long periods without adjustment. The carrier receivers are designed to work over a wide range of input signal level. At the time of installation, transmitter output and receiver sensitivity are adjusted for average line conditions. The tolerance in the receiver circuits will allow for variations in line attenuation and tube aging in the carrier units.

Check circuits to prevent a failure in a field location from interfering with the proper operation of the rest of the system are essential. Electronic apparatus common to the entire system, such as the office indication unit and carrier repeaters, are installed in duplicate. A switch on the dispatcher's control machine transfers the operation to the standby equipment in case of trouble.

Block Occupancy Reporting

Railroads having high traffic densities, for example, subways and commuter lines, often require the reporting of train movements over many short track circuits or blocks. A communication system is required which is capable of transmitting many digits of information with only one or two digits originating at any one location. Obviously, this information can be handled by multiconductor cable with d-c or power frequency. To conserve line wire some type of multiplexing is desirable.

A simple tone system is one means of doing the job. Tone transmitters of different frequencies are situated at the various blocks and are keyed when these blocks are occupied. Tone receivers at the dispatcher's office operate relays to energize lamps on a miniature track diagram. Fig. 8 shows this type of system.

An extension of the tone system provides two independent digital indications on one tone channel. The pair of line wires over which the tone system operates carries a direct voltage which is pole-changed 75 times per minute. During the time that the line voltage is of one polarity, each tone channel carries one indication. When the line voltage is switched to the opposite polarity, each tone channel carries a different indication.

The tone transmitters and receivers are transistor operated. The transmitters develop +8 dbm (power in decibels referred to 1 milliwatt) output with 0.020 ampere input at 12 volts. The receivers draw 0.005 ampere with no signal and 0.040 ampere when receiving a signal and operating a relay.

Fig. 9 shows the basic circuit arrangement of the system. Relay CT oscillates continuously applying direct voltage to line wires *LW*1 and *LW*2, alternating

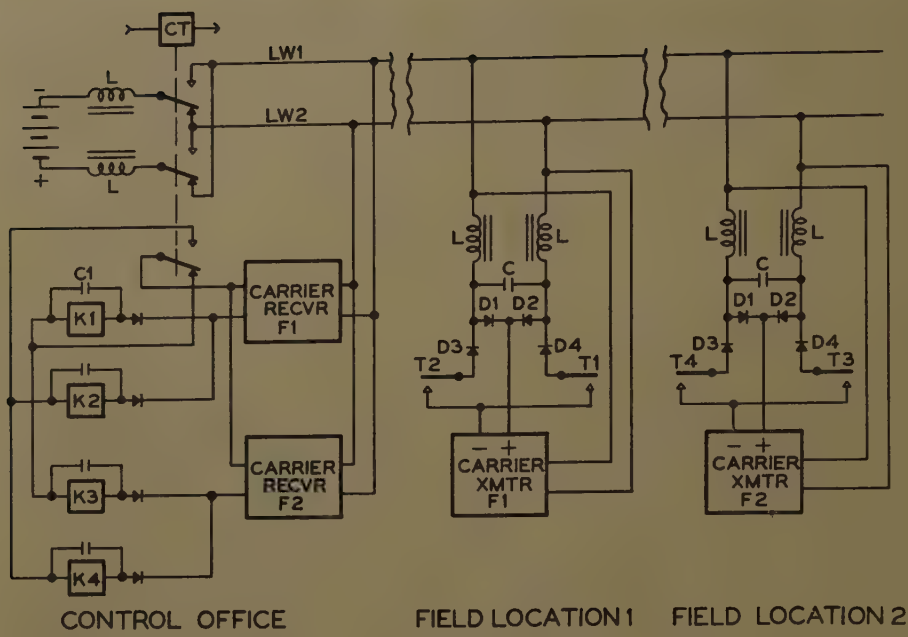

Fig. 9. Diagram of block occupancy reporting system

the polarity each time its contacts change position. A contact of relay CT simultaneously changes the output of carrier receiver *F*1 between relays *K*1 and *K*2 and the output of receiver *F*2 between relays *K*3 and *K*4.

Carrier transmitter *F*1 has its energy input terminals connected to the line through the two relay contacts *T*1 and *T*2, the four diodes and the two inductors marked *L*. The carrier output circuit of the transmitter is connected to the line above the inductors. The purpose of the inductors is to isolate the energy input terminals of the transmitter from the line at carrier frequencies.

The capacitor in parallel with diodes *D*1 and *D*2 removes the peaks from the pole-changed line voltage.

If relay contacts *T*1 and *T*2 at field location 1 are closed, the four diodes form a full-wave bridge rectifier. The path through this bridge from line wire *LW*1 to the minus terminal of the transmitter passes through diode *D*3 and contact *T*2. The path from *LW*2 to minus passes through diode *D*4 and contact *T*1. The return path from the plus terminal of the transmitter to the opposite line wire is through diodes *D*2 and *D*1 respectively. Therefore, contact *T*1 controls the transmitter for one line polarity and *T*2 controls it for the opposite polarity. Further examination of the circuit will show that relay *K*1 is connected to the output of receiver *F*1 at the time that transmitter *F*1 is controlled by contact *T*1. Similarly, relay *K*2 is connected to the same receiver when contact *T*2 is controlling the transmitter.

The capacitors across the relay coils hold the relays energized during alternate swings of relay CT. The inductors *L* at the control office prevent the line battery from loading the line at carrier frequencies.

Several carrier transmitters may be connected to the line at one location using one line coupling unit, the assembly including the inductors, capacitor and part of the diode bridge. The length of line and total number of transmitters which may be used is limited by the voltage and current rating of the line battery or power supply. A recent installation uses 28 carrier transmitters distributed along 11 miles of 14-gage twisted pair in underground duct. Thirty-seven channels are available between 430 and 7,300 cycles per second.

The line circuit and energy input circuit of the transmitters and receivers are designed to be protected by standard railway signal-type lightning arresters (1,000-volt breakdown).

A unique feature of this system is the fact that local energy is not required for the transmitters at the field locations. This arrangement is ideal for a system of this type which often derives inputs from contacts of track relays at locations where a 12-volt battery is not available.

A 12-volt d-c supply is required at the control office to energize the carrier receivers.

Analog Data Transmission

The trend in railroad operation is toward control of longer lengths of territory from one central location. As consolidation of control occurs, hundreds of miles of railroad are operated with no personnel located directly at the wayside. The two systems just described provide a means to control switches and signals and to receive information concerning train movements over these distances. Sometimes it is necessary to relay analog information from the field to the control office. This information may be any signal which is variable over a continuous range such as the level of fuel in storage tanks, the water level of a river at flood stage, or pressures and temperatures in some device.

The analog data system comprises a single-side-band carrier transmitter and receiver with submodulation equipment for frequency-modulated telemetering. The analog data, in the form of voltages, vary the frequency of subcarriers by amounts proportional to the voltages. At the receiving location, the variable frequency subcarriers are converted to voltages identical to the input signals. Subcarrier equipment is available for two or four analog channels. Two digital channels may be provided for additional on/off indications, timing, or marker signals.

An interesting application of this system is in conjunction with a hot-box detector. The hot-box detector is an infrared-sensitive device situated close to the rails. The detector actuates a pen recorder to indicate the relative temperatures of freight car journals as trains pass by at normal speed. An analog data transmission system makes it unnecessary for an attendant to check the record in the field each time a train goes by. The recorders may be located in the dispatcher's office. Where CTC is used, the operator checks each train as it passes remote hot-box detectors and uses the signal system to stop any train which appears to have a dangerously hot journal.

The carrier system has built-in line filters to allow operation on a line without additional line coupling apparatus. The insulation level of the line circuit allows operation on CTC lines with lightning protection in accordance with regular signaling practice.

Compatibility with Standard Signaling Practice

The railway signaling art has developed in the past independently of wire communications and electronics. Certain standard practices have evolved as the result of years of rigorous field experience. Continuity of service and

intainability are important requisites railroad signal equipment.

One important practice is the use of 000-volt insulation in line and power cuits. This insulation level permits e use of lightning arresters with fficiently large gaps to make it unlikely at a discharge will result in a per-anent short circuit. Transistor oper-ed apparatus requires voltage limiting vices in addition to lightning arresters protect them from voltage surges at are tolerated by conventional signal paratus.

Another practice which must be con-lered is the method of wiring apparatus usings. This practice has developed th d-c and power circuits in which re length and arrangement are not portant to circuit performance. Relay usings are generally wired with no. *16* re with very heavy insulation arranged laced cables and connected to rugged terminals. Contrast this wiring with electronic practice with its small-gage wire, small terminals, and often short, carefully dressed leads. Electronic chassis used in signaling must allow the same external wiring practice as other devices such as relays. All external leads must be tolerant of exposure to voltage surges. The impedance of external circuits must be low and pulse widths and rise times must be great enough so that deterioration due to wiring capacitance is not serious.

The apparatus situated along the wayside must withstand vibration and severe humidity and temperature. Railroad specifications require testing over an ambient temperature range of −40 to 160 degrees Fahrenheit. Most installations are unattended and therefore must not require frequent adjustment. The carrier systems previously described will operate with variations in line attenuation of the order of 20 db without adjustment. Adjustments are kept to an absolute minimum. Level and sensitivity controls are provided for carrier equipment. Carrier frequencies, pulse widths, pulse delays and pulse repetition rates, for example, are fixed. Test jacks and indicator lamps are provided where they will help the maintainer. All chassis are provided with plug connectors so that a defective unit may be replaced quickly.

In general, electronic equipment for railway signaling use has been designed to be compatible with long established signal practice and to take its place on the railroad alongside of signal relays and other standard signal devices.

Reference

1. Syncroscan—A High-Speed Control System for Railway Signaling, H. C. Sibley. *Electrical Engineering*, vol. 76, Jan. 1957, pp. 38–43.

Rapid Heating of Dielectric Materials at 915 Mc

G. E. FEIKER
ASSOCIATE MEMBER AIEE

N. C. GITTINGER
NONMEMBER AIEE

THE HEATING of dielectric materials by means of microwave energy was instigated in the General Electric Company a decade ago by members of the esearch Laboratory, who demonstrated e feasibility of preheating plastics and ating foods using a magnetron oscilla-r at a frequency of 1,000 mc (mega-cles). In recent years the *GL-6787* agnetron, operating in the 915-mc dustrial-Scientific-Medical band, has en developed as a source of power these applications. In quantity oduction, this tube will provide eco-mical microwave power for consumer d industrial applications. In order to sign equipment for efficient preheating, is necessary to know the characteristics the materials as a function of tempera-re. This paper presents the results of initial investigation of the effectiveness 915-mc heating on various dielectric materials, and describes means of measuring the characteristics of materials at this frequency.

per 59-30, recommended by the AIEE Electric ating Committee and approved by the AIEE chnical Operations Department for presentation the AIEE Winter General Meeting, New York, Y., February 1–6, 1959. Manuscript submitted vember 3, 1958; made available for printing vember 19, 1958.

E. Feiker and N. C. Gittinger are with the neral Electric Company, Schenectady, N. Y.

Basic Considerations

The power absorbed by a dielectric subjected to an alternating electric field can be calculated from the equation:[1]

$$P = 0.555 f \epsilon'' E^2$$

where

P = the power absorbed, watts/centimeter^3
f = the frequency, mc/second
E = the rms voltage gradient, kilovolts/centimeter
ϵ'' = the loss factor of the material

The rate at which a material can be heated by dielectric heating depends on two factors:

1. The loss factor ϵ'' of the dielectric. This is the property of the material which gives the loss per unit volume for a given voltage gradient.
2. The frequency of operation.

The gradient E is usually limited by the breakdown of air between electrodes and the dielectric.

Since the loss factor is very low for many important dielectrics, the frequency of operation should be made as high as practicable in these applications. Because presently available dielectric heating apparatus operates at frequencies below 100 mc, the application of 915 mc makes it possible to heat some materials which previously could not be heated by this means.

Description of Experimental Equipment

The equipment set up for the tests to be described is shown in Fig. 1. It consists of a power supply and magnetron oscillator, directional couplers, slotted lines, heating cavity, and associated instrumentation. The oscillator employs the *GL-6787* metal and ceramic magnetron, having a rated continuous-wave output of 2.5 kw. The power supply associated with the tube is capable of operating the tube at any power level from 50 watts to the full 2.5 kw. The magnetron output is coupled to a system of $3^1/_8$-inch-diameter coaxial line, which feeds the heating cavity. This cavity consists of a cylinder with re-entrant posts, shown in Fig. 2. The sample to be heated is placed in the air gap between the two re-entrant posts, where it is subjected to an intense electric field when the cavity is resonated. The cavity is tuned by adjustment of the gap between the re-entrant posts and is coupled to the line by means of an adjustable coupling loop in one side of the cavity. By properly ad-

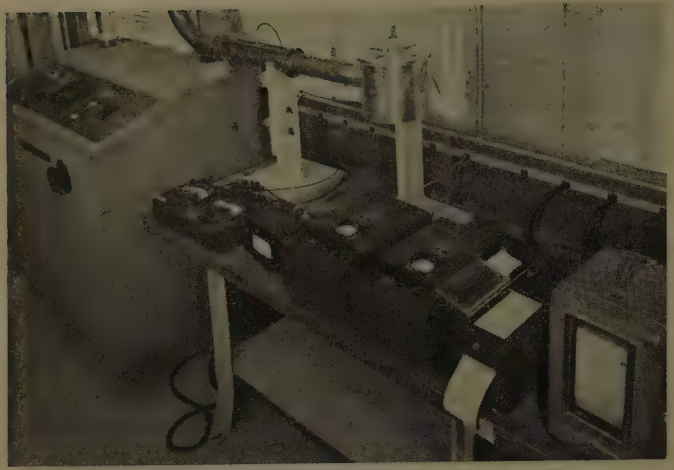

Fig. 1. 915-mc dielectric heating equipment with manually tuned heating cavity

Fig. 2. Interior view of heating cavity showing coaxial thermocouple inserted in sample

justing the coupling loop and the tuning gap, this cavity will match a wide variety of materials to the 50-ohm coaxial transmission line.

Measurement equipment in the coaxial line consists of a dual directional coupler arrangement for continuous measurement of power and VSWR (voltage standing wave radio), and a slotted line section for impedance measurements. Temperature measurement of the dielectric samples in the cavities is accomplished by means of a special thermocouple. The thermocouple element is of coaxial construction, and is enclosed in a stainless steel shielding tube over its entire length, except at the actual junction. The shielding tube prevents thermocouple self-heating caused by the strong electric field within the cavity. The thermocouple is installed from the side of the cavity perpendicular to the electric field, so as to reduce heating of the thermocouple shield as much as possible. The directional couplers and thermocouple are connected to photo-recorders. This arrangement permits measurements of these quantities during rapid heating tests.

Comparative Tests at 915 Mc and 70 Mc

It has been stated previously that the rate of heating of a given material is proportional to frequency. As a consequence, it should be possible to heat some materials at 915 mc which are difficult or impossible to heat in conventional preheaters operating at frequencies below 100 mc. In order to investigate this possibility, comparative tests of heating effectiveness were made at 915 mc and 70 mc, using a 3.5-kw preheater manufactured by W. T. LaRose and Associates, Inc. A variety of materials was obtained for these tests as shown in Table I. Samples were heated in both machines under similar conditions, and from the results, the following conclusions were drawn:

1. If the loss factor of a material exceeded 0.01, the material could be heated at either frequency. The 915-mc equipment could heat it faster for a given voltage gradient, however.

2. If the loss factor of the material was between 0.01 and 0.001, the low-frequency heater heated the material very slowly. The 915-mc equipment could heat these materials at a relatively high rate.

3. If the loss factor of the material was below 0.001, neither equipment could heat it well.

4. In most cases, the limitation of heating in the lower frequency unit occurred because of arcing. At 915 mc, arcing rarely occurred at the powers used in the tests (100–600 watts).

Materials such as Rubber Styrene, Teflon *100X*, Fluorothene, and Styrene Acrylonitrile could not be heated well at the lower frequency, but were heated easily at 915 mc. A special low-loss glass was also heated to the melting point at 915 mc, but could not be heated at the lower frequency. Final temperature of the glass reached 800 C (degrees centigrade) at 915 mc.

Table I. Heating Tests of Various Materials at 70 Mc and 915 Mc

Material	Dielectric Constant	Power Factor	Loss Factor	Heated At 70 Mc	Heated At 915 Mc
Asbestos-filled melamine	5.2	0.035	0.18	Yes	Yes
Bakelite	4.6	0.03	0.14	Yes	Yes
Mineral-filled silicone	4.1	0.0055	0.03	Yes	Yes
Low-loss phenolic	4.3	0.01	0.04	Yes	Yes
Nylon	3.4	0.04	0.136	Yes	Yes
Lucite	3.6	0.025	0.09	Yes	Yes
Polyvinyl chloride	3.4	0.06	0.20	Yes	Yes
Fluorothene	2.3	0.0085	0.02	marginal	Yes
Styrene-acrylonitrile	2.8	0.0083	0.023	marginal	Yes
Rubber styrene	2.5	0.001	0.0025	No	Yes
Mycalex	7.4	0.0018	0.013	No	Yes
Teflon 100X	2.0	0.0005	0.001	No	marginal
Teflon	2.0	0.0001	0.00025	No	No
Polyethylene	2.3	0.0005	0.001	No	No
Polystyrene	2.5	0.0001	0.00025	No	No

Detailed Measurements on Phenolics

A detailed investigation has been made of the feasibility of rapid preheating of a general purpose phenolic compound, General Electric *12900*. As supplied for these tests, the phenolic was in the form of cylindrical preforms, $1\frac{1}{2}$ inches in diameter and 3/4 inch high, weighing 22 grams. The material is exothermic in nature.

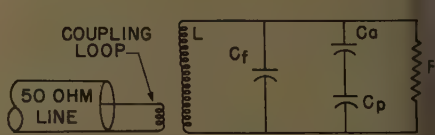

Fig. 3. Equivalent circuit of re-entrant heating cavity

L = cavity inductance
C_f = fringe capacity of electrodes
C_a = capacity of air gap between the preform and the upper electrode
C_p = capacity of preform
R = shunt resistance due to preform losses

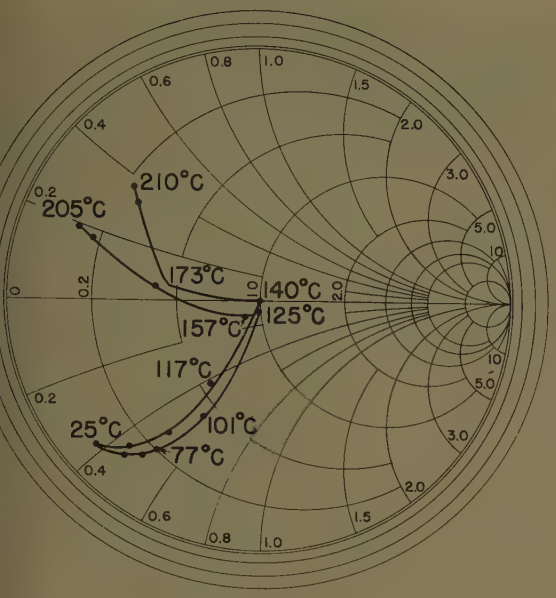

Fig. 4 (left). Smith chart of cavity impedance versus sample temperature

Fig. 5 (right). Smith chart of cavity impedance versus sample temperature

ien heated to about 175 C, the material dergoes a chemical reaction, gets soft l pliable, and produces heat. After ıpletion of the reaction, the material dens into a brittle substance.

Measurements on samples of the enolic at 30 mc showed a dielectric con-ıt of 2.8 and a power factor of 0.06. It s felt necessary to measure these ıntities at 915 mc, however, since racteristics depend on frequency in ny substances. The cavity shown in . 2 was used for this measurement. h a phenolic preform in place between re-entrant electrodes, the cavity has equivalent circuit closely approximated the diagram of Fig. 3. In this circuit, capacitances C_a and C_p could be culated, whereas C_f and L were ob-ıed by measuring samples of known ectric constant, such as Teflon, Poly-rene, and air. By comparing the gap ing required to resonate the cavity ded with phenolic to the settings re-red with the standard samples, and recting for the known fringe capaci-ce, the dielectric constant of the nolic could be measured.

Power factor of the phenolic was ob-ıed by measuring the Q of the loaded ity. This measurement determined value of the shunt resistance R. As unloaded cavity has a very high Q, es in the cavity walls could be neglected, and the equivalent resistance R was assumed to be entirely attributable to the sample losses. By transposing R to a resistance in series with C_p, the power factor of the material was obtained.

Measurements made at 915 mc did not agree with those made at 30 mc. In order to check the 915-mc measurements, tests were made at several other frequencies. The results are shown in Table II.

It may be seen that the power factor and dielectric constant of the phenolic sample change considerably with frequency.

The dielectric constant and power factor of the material also change with temperature. As the phenolic heats up, there is a definite change in impedance presented to the 50-ohm coaxial line by the cavity. The change in cavity impedance with temperature, obtained by point-to-point measurements with the slotted line, is shown on the Smith charts of Figs. 4 and 5. These data were taken under different conditions of cavity tuning. They show that there is a definite problem in matching the cavity to the line, since a VSWR much above 3.0 will cause a large power loss due to reflection.

It has been found that most of the change in the sample as it heats is in the dielectric constant, which tends to detune the cavity. Heating tests have been conducted with the cavity tuned manually by adjusting gap spacing. A plot of gap spacing required for cavity resonance with temperature is shown in Fig. 6. The change in dielectric constant with temperature is found to be from a value of 2.8 at room temperature to 3.6 at 175 C.

The change in dielectric constant causes the power actually absorbed by the sample to change with temperature. Fig. 7 shows a plot of power entering the phenolic versus time for a typical heating test where

e II. Electrical Properties of Phenolic pound GE 12900 at Various Frequencies

uency, Mc	Dielectric Constant	Power Factor	Loss Factor
30	2.8	0.06	0.17
915	2.8	0.03	0.08
050	3.2	0.04	0.13
715	3.0	0.035	0.11

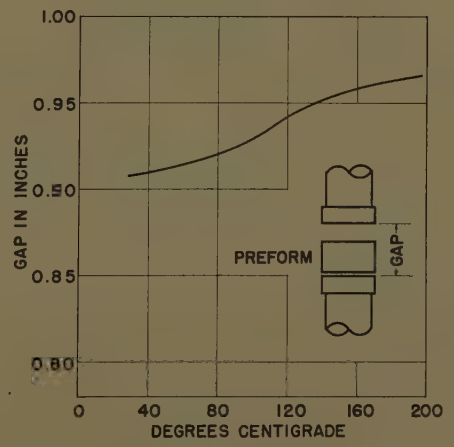

Fig. 6. Gap spacing required for resonance versus temperature, large re-entrant cavity loaded with phenolic preform

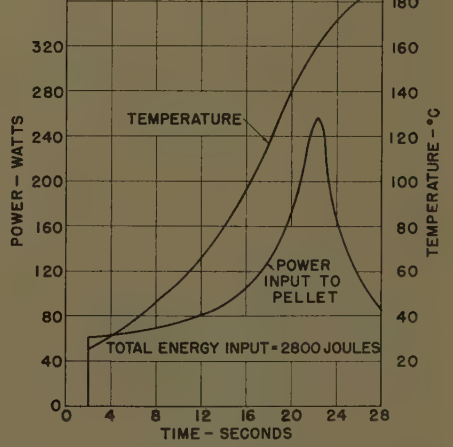

Fig. 7. Temperature rise and power input versus time for typical heating run of sample 22-gram phenolic pellet

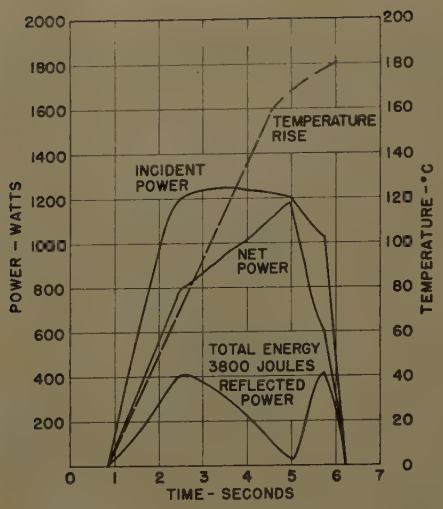

Fig. 8. Temperature rise and power versus time for typical heating run

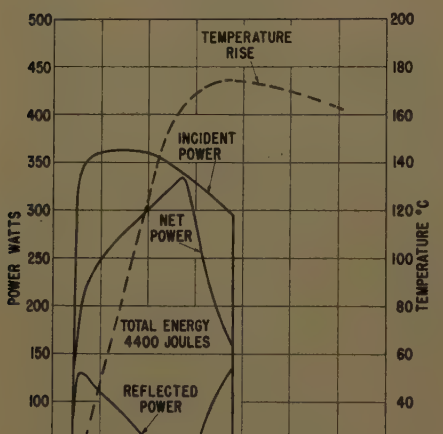

Fig. 9. Temperature rise and power versus time for typical heating run

the cavity gap adjustment was fixed. In this particular test, the power into the sample pellet at the instant of cavity resonance was 256 watts, but the power during half of the heating time was below 100 watts.

The energy required to heat the preform to a temperature of 175 C has been obtained in test runs during which the incident power, reflected power, and preform temperature were simultaneously recorded. Three typical test run plots are shown in Figs. 8, 9, and 10. In these plots, the net power input is the power actually absorbed by the sample, and is equal to the difference between the incident and reflected power curves, which were obtained from the directional coupler readings.

The average energy requirement of the large number of tests made was 4,000 joules. Theoretical calculations have shown an energy requirement of 4,300–5,000 joules, which is considerably larger than the value obtained by measurement. The difference is believed to be the result of the exothermic chemical reaction.

Uneven Heating Effects

During most of the tests, definite unevenness of heating was observed in the phenolic preforms. The interior and top of the preform were well heated, but the sides and bottom were somewhat cooler. This uneven heating was traced to two effects:

1. The uneven heating at the sides of the preform was caused by the lack of a constant field intensity at the edges of the electrodes. By using considerably larger electrodes, the sides of the preform were evenly heated.

2. The uneven heating at the bottom of the preform was caused mainly by the presence of the cold-metal electrode in contact with the preform. By suspending the preform in space between the electrodes by means of a thermocouple lead, the cold area on the bottom of the preform was eliminated. Since this method is not convenient or practical, a feasible alternative is to use internal heaters for heating the electrode to the desired final temperature.

Considerations of Preheater Design

The usual preheater operating in the very-high-frequency band consists of a self-resonant tank circuit in which the sample is placed. The frequency of operation adjusts to changes in capacitance caused by changes in the dielectric constant of the material. Since the magnetron oscillator has its own resonant circuit, the load cavity must be kept resonably well matched in order to obtain rated output from the tube. During the experiments described previously, it was found that the resonant frequency of the cavity changed considerably with sample temperature, but the cavity impedance at resonance changed comparatively little. Heating of most of the sample was successfully accomplished by adjusting the cavity tuning while the sample heated up, with no change in the coupling of the cavity to the line. This fact suggested that a servo system designed to keep the resonant frequency of the cavity constant at all times would considerably alleviate the matching problem. This servo system was built and successfully demonstrated. Its design will now be described.

The tuning servo consists of a phase detector in the coaxial line, an amplifier and a servomotor which tunes the cavity. A diagram of the system is shown in Fig. 11.

The principle of operation of the servo tuning system is based on the change of phase that occurs in the coaxial line as the cavity is tuned through resonance. The cavity will appear to the line as a parallel resonant circuit across the end of the line.

The cavity impedance will appear as a pure resistance only when it is tuned exactly to the operating frequency. When detuned appreciably, it will present an almost pure reactance to the line which is either inductive or capacitance, depending on which side of resonance the cavity is tuned. A large standing wave is therefore present in the line. The minimum position of this standing wave will be found to shift along the line by a half wavelength as the cavity is tuned from one side of resonance to the other side. At resonance, the standing wave minimum will be exactly half way between the positions it occupies when the cavity is detuned each side of resonance. The transition of the minimum is quite sharp as indicated in Fig. 12(A).

This figure shows the change in minimum position which will be obtained in

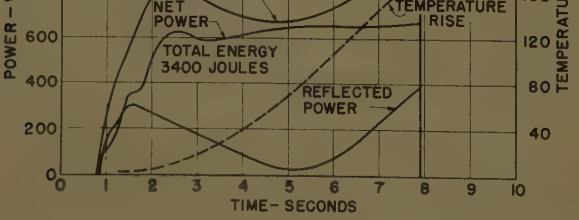

Fig. 10 (left). Temperature rise and power versus time for typical heating run

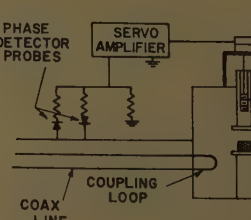

Fig. 11 (right). Schematic diagram of servo-tuned heating cavity

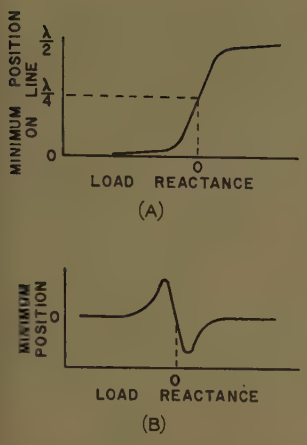

12. Voltage minimum shift versus load reactance

-Cavity resistance greater than characteristic impedance
Cavity resistance less than characteristic impedance

xial line feeding a cavity with losses, he resonant resistance of the cavity is ater than the characteristic impedance he line.

The phase detector employed uses two bes in the coaxial line spaced one-arter wavelength apart.

The probes feed a matched pair of stal detectors with opposite polarities. e outputs of the detectors are added l fed to the servo amplifier. The polar- of the output of the crystal pair de- ds on which crystal is in the stronger d. If the probes straddle a voltage nimum, the output is zero, since both stals are in the same intensity field. the cavity is detuned, however, the nding-wave ratio will shift, and a volt- unbalance will appear at the servo- plifier input, with polarity dependent the direction by which the cavity is uned. The servo amplifier feeds a vo motor which corrects the tuning. t might seem that if the cavity is de- ed sufficiently to appear as a pure re- ance, the probes will straddle a maxi- m and no correction voltage will ap- r. However, the losses always pres- will prevent the cavity from ever ching this condition, no matter how it is detuned. A correction voltage l always be present and will be of the rect polarity.

The foregoing description of the tuning vo is based on the resonant resistance he cavity being greater than the char- eristic impedance Z_0 of the line. If resonant resistance is less than Z_0, the nimum position changes from the *S*- ped curve of Fig. 12(A) to a discrim- tor type of characteristic as shown in . 12(B).

Fig. 13. 915-mc dielectric - heating equipment with servo-tuned heating cavity

Under this condition, the probes are set to straddle a maximum at resonance. Output polarity for a given direction of standing-wave shift is opposite to that in the previous case. However, the slope of the standing-wave shift with load reactance is also reversed, so the net effect is still in the proper direction for correction.

The system just described has been built and tried out with various dielectric loads, using the cavity previously described. The equipment is shown in Fig. 13. The servo amplifier used is a Brown Electronik unit, with a matching Brown servo motor for tuning the cavity. The phase detector consists of two adjustable Hewlett Packard probes, with a Microlab *XM-1000* crystal detector mounted on each probe. The probes are mounted on the slotted line assembly with a quarter-wave spacer between them, so that the positions of both probes can be adjusted simultaneously. Matched crystals of opposite polarity were used, and the sensitivities of the probes were equalized by adjusting probe depth.

Operation of the system was highly satisfactory when heating materials with loss factors of 0.03 or greater. Probe position was found to be somewhat critical, requiring that the probes be set within a range of 2.0 millimeters at 915 mc. Once set, however, the probes required no further adjustment. The cavity would come into resonance as soon as power was applied, from any tuning condition whatever. Tuning was found to track the change in the sample very closely. The match of the cavity to the line was reasonably good, with a maximum VSWR of 2.0 for most samples. The cavity coupling still had to be matched to the sample impedance when changing sample material or sample size, but did not need to be changed during the heating of any particular type of sample.

Operation of the system with low-loss materials (loss factor below 0.03) was more critical and less satisfactory. The system tended to hunt when the probe position straddled the minimum at resonance, and the probes had to be moved slightly along the slotted line before the system would stabilize. This adjustment destroyed the ability of the system to seek correct tuning from all initial tuning conditions, but would hold nearly correct tuning once it was achieved. The trouble appeared to be caused by magnetron frequency jumping rather than any servo system malfunction, since the same unstable characteristics were present when the cavity was manually tuned. This effect has not yet been eliminated and further work is indicated.

Conclusions

An investigation of the characteristics of rapid heating of various dielectric materials at 915 mc shows that at this frequency materials can be heated which cannot be heated at conventional preheating frequencies below 70 mc. A detailed investigation of phenolic preforms shows that it is possible to design a heating cavity which will provide rapid heating with reasonable uniformity. The problem of impedance matching requires special consideration, since the heating cavity is not the primary resonant circuit as in the case of a conventional preheater operating in the very-high-frequency band. A servo-tuned cavity has been devised which serves to keep the cavity reasonably well matched to the magnetron output during the heating cycle. This technique provides a satisfactory solution to the matching problem for materials having a loss factor greater than 0.03. For lower loss materials, an initial tuning adjustment was necessary.

References

1. Dielectric Nomenclature (Letter to Editor), H. H. Race. *Electrical Engineering*, vol. 61, no. 2, 1942, p. 105.

Some Unusual Designs of Electric Resistance Heating

LEE P. HYNES
FELLOW AIEE

LARGE installations of electric heating depend for their success on a correct analysis of the many technical problems involved. Too often these are not given the proper study and unsatisfactory operations result from inadequate engineering design.

Some unusual installations of resistance heating will be described and the technical problems, including heat transfer, will be analyzed. As a refresher, some of the basic inherent advantages of resistance heating and the laws of electric heat transfer, will be briefly discussed.

Resistance Heaters

Resistance heaters have a unity power factor and an efficiency of 100% in the conversion of electric energy into heat. There are no inductive losses and one kilowatt-hour can be counted on to produce 3,415 Btu. Some loss is unavoidable during the transfer of the heat to the work material, but this can be reduced to a minimum by careful design and good thermal insulation.

Nickel-chromium resistors have a low temperature coefficient and will never draw more than about 7% added inrush of current, when starting up cold. Circuits do not need extra large conductors and can be protected by normal fuse ratings, without overload time lag features.

Resistance heaters can be designed to meet all code requirements for use in hazardous atmospheres and for all standard commercial power lines, without special transformers.

Heat Transfer

Too little consideration is usually given to the transfer of heat from the resistors which produce it to the work material. This heat transfer is the key to a successful installation of electric heat, especially when the operating requirements are new and difficult. Heat is primarily transferred from a resistor by conduction and by radiation but can be further distributed by convection.

Conduction passes heat from one part of a material to another, or from one material to another which is in physical contact with it. This transfer does not involve any displacement of the body particles. Different materials vary greatly in their ability to conduct heat.

Convection distributes heat energy within the body of a fluid by thermal currents or by forced circulations that displace body particles and cause thermal mixing. The flow of fluid over a heating surface wipes away film and improves heat transfer. This reduces the ΔT and results in a lower temperature of the heating surface, but with an electric heater this does not change the rate of heat input.

Radiation disperses heat energy in all directions by electromagnetic waves of high velocity. When two bodies of differing temperatures, for example a heater and the work material, are located within an enclosure, there is a continual interchange of radiated energy between them. The hotter body radiates more energy than it absorbs and the cooler body absorbs more energy than it radiates.

Radiant heat rays have differing wave lengths, according to the temperatures of their sources. This gives them differing powers of penetration into various materials, depending upon the absorptivity of each material.

Some materials are transparent to short-wave radiations from high-temperature sources, such as heat lamps, which have filaments running up to 4,000 F (degrees Fahrenheit). Ordinary glass is a good example of a material that cannot be effectually heated by such short-wave radiations, as the heat waves pass straight through it and are not absorbed. Such a material can be satisfactorily heated by longer waves from a source in the 700 F range.

The efficient application of radiant heat requires a full understanding of the absorptive qualities of each material and the wave length that will give the best results. Most common gasses such as air, nitrogen, hydrogen, and oxygen will not absorb radiant heat, but vapors are good absorbers of radiation.

The problems of heat transfer must be carefully considered in designing any large industrial heating project. Too many engineers seem to think only in terms of steam heat transfer, and fa to realize that electric heat operates c radically different basic principle Steam has a fixed temperature, for given pressure. When the work is col the condensation rate is high, but th tapers off as the work temperature rise and the rate of heat input falls because th ΔT is reduced.

Electric heat operates in a differen manner because the rate of heat inpu (wattage) remains constant, for a give voltage, regardless of the work temper ture. As the latter rises, the heat temperature also rises and there is no r duction of the ΔT, because all of the he energy produced by the electric heat must be disposed of, regardless of th temperature required to do so.

This basic characteristic of temper ture change in an electric heater, has a important bearing on every electric hea ing application, because materials vary much in their inherent ability to abso heat, without damage, from contact wi hot surfaces.

This makes it necessary to understan and provide for a proper heat density, watts per square inch of heating surfac for each material. Molasses and sug are good examples of materials extreme sensitive to heat; they readily caramel and burn on hot surfaces at comparative low temperatures.

The heat capacity of each material, i conductivity, and the mass being heate also play a large part in the proper desig of an electric heated process and its aut matic control. Large masses chan temperature slowly, and tanks of oil water, for example, seldom are difficult control. Where materials are passe rapidly through heating zones, especial at variable speeds, the control proble become more complicated.

The many special characteristics electric heat offer the alert designer ma opportunities for producing new desig that will obtain surprising results a that are not possible with other types heat sources. A few examples of uniq installations of resistance heaters will described, and the heat transfer which involved in each will be analyzed. The will show how important heat transfer for securing the desired operating resul A factor of great importance is the corre utilization of radiant heat waves, ev

Paper 59-77, recommended by the AIEE Elect Heating Committee and approved by the AI Technical Operations Department for presen tion at the AIEE Winter General Meeting, N York, N. Y., February 1–6, 1959. Manuscr submitted October 30, 1958; made available printing December 9, 1958.

LEE P. HYNES is a consulting engineer, Hadd field, N. J.

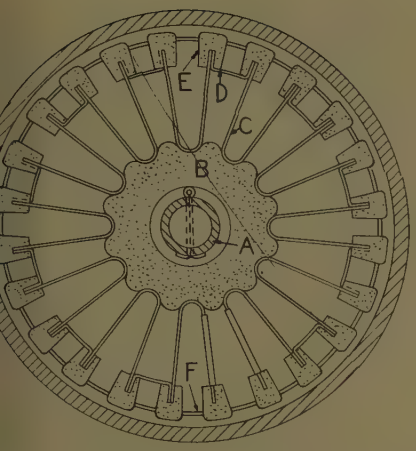

. 1. Cross section of Radi-Fin electric heater for gases

ien the material being heated does not rectly absorb radiation.

eating Hydrogen and Other Gasses

The manufacture of ammonia presented problem requiring the heating of 2,400 unds per hour, of hydrogen, at a essure of 3,000 pounds per square inch. ie required temperature was 1,400 F d the space limitations were very severe. cause of the high pressure, it was essen- l to keep the pressure vessel diameter wn to 6 inches inside diameter. The ated length could be only 14 feet. The quired heat input was 400 kw at 440 lts, single phase. This job posed prob- ns for which little precedent was avail- le as a guide.

The internal wall of the cylinder had a rface area of only 22 sq ft (square feet) d to use that wall as the sole heating rface, with an external electric heater, ould require a heat density on this sur- ce of 125 watts per square inch. Such high rating would require a very high ', in order to force so much heat energy rough the wall of the cylinder and into e gas it contained. It was at once vious that a much greater area of heater surface would be required and that it must be located within the gas stream, where all the heat could be transferred to the gas by conduction, as the gas wiped over the heating surfaces. As previously mentioned, hydrogen does not absorb radiant heat.

The great importance of heat density has been mentioned but in this case the hydrogen would not be harmed by contact with high-temperature surfaces. The problem was to keep down the temperature to a safe value for the wall of the cylinder and for the heating resistors. The life of a metallic resistor is long, up to a certain operating temperature. Then it decreases fast and at an accelerating rate, as the temperature is further increased. As the temperature of an electric resistor rises until it can deliver all of its rated heat output, the abnormal rating of 125 watts per square inch, would have greatly overheated the resistor and reduced its life to a serious degree. Surface density is a factor of surface temperature.

Unfortunately, the suitable heat density rating for different materials, under different operating conditions, has never been sufficiently explored scientifically. Even the manufacturers of resistor materials did not know what would be a safe rating under the severe operating conditions outlined for this job. Some attempts had been made to heat hydrogen with round rods as resistors, but the resistors had lasted but a very short time. Computations clearly showed why they had failed as they had a heat density of over 150 watts per square inch, which is a fantastic figure. This was the only lesson available from practical experience, so a new start had to be made.

It was decided to approach the problem in reverse order, by first determining the maximum area of heating surface that could be designed into the available space, and then see what amount of heat density would result. The obvious location for the heating surface was inside the pressure cylinder, where the gas would wipe directly over it. This was feasible as hydrogen is not a conductor of electricity.

Much thought was given to finding a geometrical shape of heating surface that would have the maximum area and still offer the least resistance to the flow of gas through the vessel. The unique design shown in Figs. 1, 2, and 3, was finally developed. This had over 60% of free area for gas flow and the radial fin construction had a total prime heating surface area of 85 sq ft. This was nearly four times the internal wall surface of the vessel and it resulted in a heat density of only 32 watts per square inch.

It was possible to reduce this still further by utilizing radiant heat. Although hydrogen does not absorb heat radiation waves, the waves are radiated through the gas to the internal wall of the vessel, which they heat. As the gas wiped this wall in passing longitudinally through the cylinder, the wall became a very good secondary heating surface, with an area of 22 sq ft. This brought the actual average heat density down somewhat below the 32 watts, as given in the foregoing for the heating resistor. Several years of continuous service has proved that the rating was a safe and conservative one.

A warning should be given here that there is no standard safe heat density, for even a single material. Heat density depends on several factors, such as the specific heat, the density and flow rate of the gas, and the final temperature to which it is to be heated. For heat absorption, hydrogen has the best combination of favorable factors.

Similar designs have been successfully used for heating air and other gases, but in each case the heat density was computed for the gas and the operating condi-

Fig. 2 (left). Complete assembly of Radi-Fin heater for gases

Fig. 3 (right). Radi-Fin heater being inserted into a high-pressure vessel

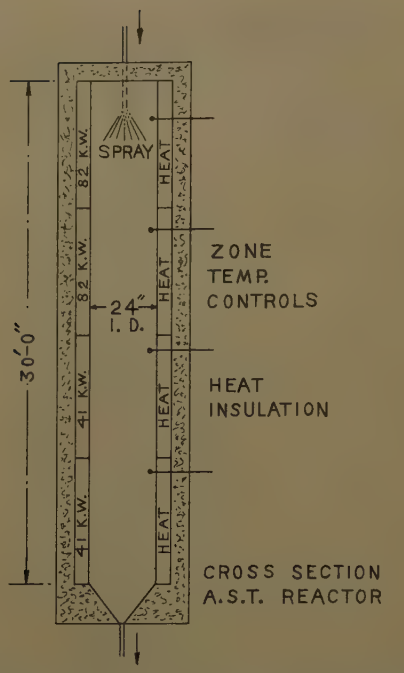

Fig. 4. Cross section of an AST process vessel for treating sewage with electric heat

tions. Although good results have been obtained by careful estimating, and conservative ratings, it is to be hoped that the subject of over-all heat transfer rates for electric heaters, in gases, liquids, and other materials, will eventually be more thoroughly studied scientifically. This would provide better design data for engineers.

Returning to the design details, Fig. 1 is a cross-sectional drawing. The heating fins were installed around a tubular backbone member, *A*. This was not alive electrically; it was supported rigidly by brackets at the terminal end. The other end was guided but was left free to expand and contract freely without putting any strain on the fixed terminal connections. At intervals along the tube *A* are loosely mounted gear-shaped refractory insulators *B*. Each insulator has 12 curved recesses in its perimeter. In these recesses were seated 12 U-shaped resistors *C*, formed of nickel chromium furnace ribbon 3 inches wide.

The 12 U-shaped resistors were electrically connected in series by jumpers *D* for single-phase. For 3-phase, each phase would consist of four resistors in series to an internal Y bus. For single-phase, two conductors are brought out through one end of the vessel, and for 3-phase there are three such conductors. Special high-temperature, high-pressure terminals were developed for this hard service. With the terminals located at one end of the vessel, it is possible to introduce or to remove the complete heating element, by removing one vessel head. This does not disturb the general setup, nor interfere with the thermal insulation which surrounds the vessel walls.

Fig. 1 also shows a series of small refractory insulators *E* which fit the outer edges of the fins of the U-shaped resistors *C*, and form a circle. They are held in place by an external band *F* of nickel chromium that lies in grooves of the insulators *E*. These circles of insulators are located at intervals along the heating element and serve to keep the outer edges of the U-shaped fins, properly spaced from each other and from the wall of the vessel. Fig. 2 shows a complete heating unit and Fig. 3 shows the unit being inserted into the 6-inch pressure tube enclosure. It also shows the 3-phase terminal rod connections.

The entire assembly is very rugged, yet flexible enough to meet all normal stresses of high temperature and high velocity of dense, high-pressure gas flow. There were many mechanical and electrical problems to be solved in the manufacture of this new type of heater unit, but by care and patience they were overcome. The new design has been named "Radi Fin."

Atomized Suspension Technique for Treating Slurries, and Solutions

The heating problem under discussion arose from a research program which had been established to find some way to recover sulphur from paper pulping liquor, which for disposal had heretofore been poured into streams and thus wasted. The lost sulphur was costly and the waters were badly contaminated. Preliminary tests by the research staff indicated that no standard commercial electric heaters would endure under the severe operating conditions demanded, and a design engineer was retained to study the problems involved.

For the new process with which the scientists planned to experiment, an internal temperature of about 1,500 F was specified. To prove their theory of preliminary drying, with a following radiation reaction to destroy the solid particles by combustion, the scientists were willing to accept an electric heating system which might be expected to endure even for a few hours only.

No heating equipment could be installed inside the vessel and the only possible heating surface was the actual wall of the vessel itself. Electric heaters would

Fig. 5 (left). Radiant electric heater section for an AST vessel

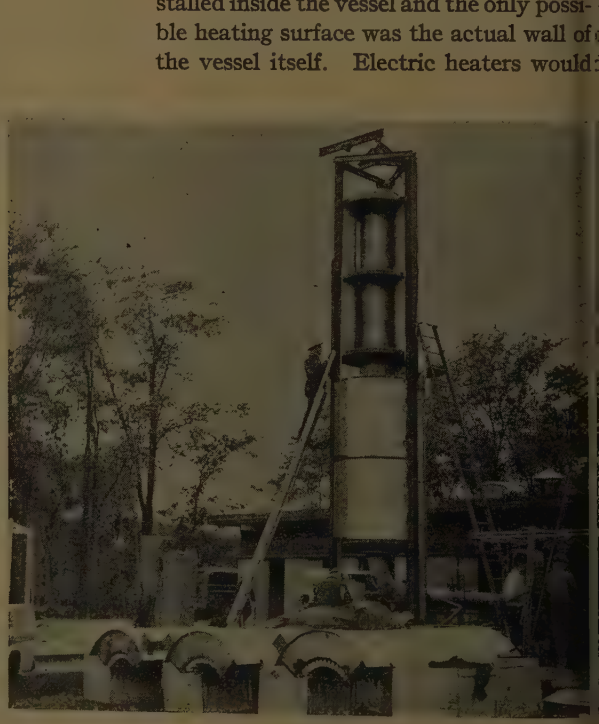

Fig. 6 (right). Field assembly of an AST process vessel

to be mounted outside this wall and ıte heat to it. A design was de- ɔed with four heat zones, in vertical ions, with separate temperature con- for each zone. With this system it possible to recover over 70% of the hur from pulping liquor and the ers were so durable that they survived ıany subsequent experiments on other pounds.

ıe process was found to have wide ication and it has been patented in y countries. Many firms are licensed se it for a number of important in- rial processes in the treatment of ies and other solutions. The "Atom- Suspension Technique," (AST), he process has been named, was ked out by Prof. W. H. Gauvin of Gill University and is owned by the) and Paper Research Institute of ada. The original vessel was only inches in diameter and approxi- ely 8 feet high. Following the suc- of this small unit, several larger have been constructed for further riments.

n unexpected discovery was that tary sludge from raw sewage could be essfully treated and destroyed by ing it through one of these AST proc- units. The first large units for this ice have been designed and installed Canadian city and if the results in al daily use equal the experimental s, a new field for sewage treatment by ric heat may be opened up.

Fig. 4 shows a vertical cross section of one of these sewage-treatment vessels, now being installed. Its inside diameter is 24 inches and it is 30 ft high. The total electric load is 246 kw with four vertical heat zones. The temperature of each zone is independently controlled. The two upper zones are rated at 82 kw each and the two lower at 41 kw each. Each zones has a complete 3-phase 575-volt electric heating unit. Fig. 5 shows one of the three single-phase heating units which comprise each heat zone.

The three heating units for each zone are arranged with one on each phase. These heat sections are removable from the main vessel without disturbance to any other zone. Each section has its own structural frame which carries a series of refractory insulators arranged horizontally in parallel arcs. They support heavy helical resistor coils which are free to expand horizontally, but which cannot sag under high temperature.

Fig. 6 shows the field assembly of one of these sewage-treatment units. The internal work cylinder is shown with the four separate heat zones. Each zone is also divided into three compartments by vertical partitions, one for each of the single-phase heater elements. The inner chamber is free to expand and contract independently of the external structural supports. Heating units as shown in Fig. 5 have been installed in the two lower heat zones. The heaters for the two top zones may be seen on blocks in the foreground, awaiting installation.

The heat sections are mounted to vertical supports in such a way that they may expand freely. Metallic reflector shields surround the heaters and an external layer of suitable thermal insulation conserves the heat energy.

The method of operation is to introduce the fluid material into the top of the vessel as shown in Fig. 4, in the form of a fine spray. As it travels downward it is subjected to a drying process that evaporates most of the moisture. Solid particles float toward the bottom and are further acted upon by radiation, which destroys organic matter and converts it into gases and some fine ash.

At the bottom of the vessel all the treated products are vented through separators and other apparatus. Some of the waste heat can be recovered, and the gases and ash disposed of in a safe and sanitary way.

Engineering Considerations

The brief description of these two processes should serve to point out the opportunities for special designs of resistance heaters, in the solution of industrial problems. There is also need for more comprehensive data on basic electric heating information. Engineers should recognize the importance of bold and imaginative approaches to new and difficult heating problems, in which electric heaters may serve in a unique way.

Anode Breaker Testing with a High-Capacity Rectifier System

L. J. HARRIS
NONMEMBER AIEE

T. J. SCULLY
ASSOCIATE MEMBER AIEE

V. N. STEWART
MEMBER AIEE

ɔpsis: An extensive testing program anode breakers using a high-capacity er-rectifier system of the Aluminum pany of America was an unusual oppor- y for an appraisal of the combined per- ance of the system equipment. The rmation gave an evaluation of the pro- on to the equipment and has provided a er understanding of the influence of the em components on operating service itions. This was done with special rols and comprehensive instrumentation h achieved a uniform testing procedure ding the rectifier-tank characteristics, e control of rectifier-tank firing, and phase transformer saturation control. ough the repetitive consistency of the arc-back currents, a reliable perform- ance was given by the high-speed current-limiting breaker over the range of available power. In addition, these tests with the large aluminum potline rectifier system gave a real measure of the combined performance of the equipment up to the maximum service requirements rather than by individual device tests, the data for comparison and evaluation of other test facilities, and a guide to future applications.

POWER CONVERSION systems for electrochemical processes including aluminum, chlorine, and sodium, railway, mines, and general industrial applications are important loads on the total electric power generation. Not only are these applications using larger concentrated blocks of power but are striving to achieve higher over-all efficiency in the process operations in the electrochemical industry. Likewise, there is a growing use of d-c power for the greater versatility and control which can be attained by d-c devices. The use of d-c motors has increased percentagewise several times that of the a-c motors in sizes suitable to machine-tool applications during the past 10 years.

Paper 58-224, recommended by the AIEE Industrial Power Rectifiers Committee and approved by the AIEE Technical Operations Department for presentation at the AIEE Winter General Meeting, New York, N. Y., November 2–7, 1958. Manuscript submitted November 6, 1957; made available for printing September 12, 1958.

L. J. HARRIS is with the Aluminum Company of America, Rockdale, Tex.; T. J. SCULLY and V. N. STEWART are with the General Electric Company, Philadelphia, Pa.

The authors acknowledge the assistance of A. Schmidt, Jr., and W. G. Abbott of the General Electric Company, and of the engineers of the Aluminum Company of America (Alcoa), Rockdale Works, in carrying out the successful test program.

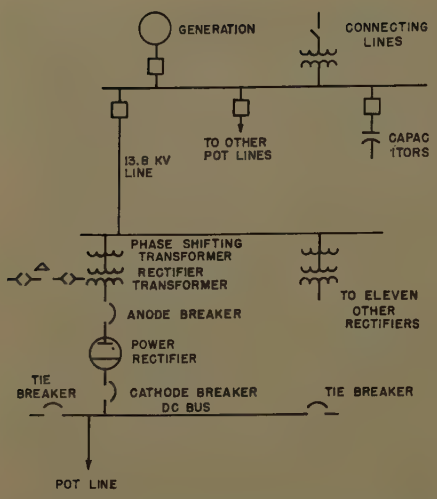

Fig. 1. One-line diagram of Aluminum Company of America mercury-arc-rectifier system

Such systems must be reliable, rugged, dependable, and efficient to maintain an uninterrupted flow of d-c power. Field testing of components such as the anode breaker will assure the reliable performance of the equipment and the adequacy of the application.

The anode breaker plays an important part in the system where power disturbances are caused by arc backs in the power-rectifier tanks. Arc backs are a failure of the rectifier action and result in the flow of current from the cathode to the anode within the rectifier tank. This is equivalent to a short circuit on the secondary terminals of the rectifier transformer, and the magnitude of the current contributed through the rectifier transformer, and the magnitude of the current contributed through the rectifier is determined by the impedance of the a-c system. In addition, on these high-capacity systems, there will be a d-c bus feedback of an exponentially increasing current due to the associated rectifiers, generators, and the loads. The magnitude of this current and the ability of this breaker to open the fault with minimum loss of forward power are important factors in achieving a dependable system.

This tank which is conducting current in the reverse direction will have an initial peak current after a time of 0.009 second.[1,2] For high-speed breakers, this first-crest arc-back current is the point of interest, as it represents the maximum duty during interruption. Further, the high-speed operation of the anode breaker gives current-limiting action to minimize this peak current and reduces the stresses from the short-circuit duty on the associated equipment.

Power Rectifier System

The system used in this test program is represented in the 1-line diagram, Fig. 1, which shows the normal components of generation, transmission, and transformation feeding an aluminum potline through 12 double-Y-connected mercury-arc rectifiers. The major source of power is 300,000 kva of generation and it is supplemented by three tie lines connecting with the local power utilities.

The normal operating duty and arc-back conditions handled by the breakers and other components are related to the capacity of 12 double-Y-connected mercury-arc rectifiers which are associated with one potline. However, the system arrangement provides bus ties with adjacent potlines for emergency operation. The tie breakers could be closed and during this abnormal connection greater arc-back currents woud be obtained.

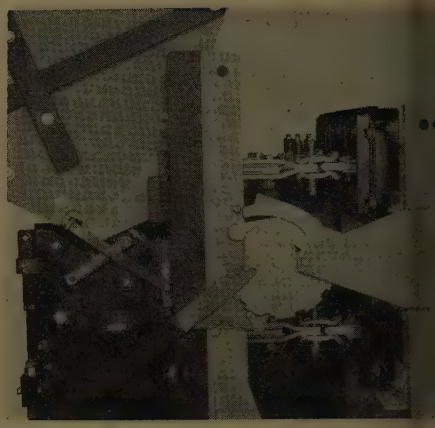

Fig. 3. Detail of test drawout mechanism for anode breaker

Test Arrangements and Facilities

The rectifier unit selected for this program was located at the end of a line-up of 12 identical units with an equivalent line of high-capacity rectifiers extending in the opposite direction from the test location. Tie breakers permitted the combined operation of these and other potline busses.

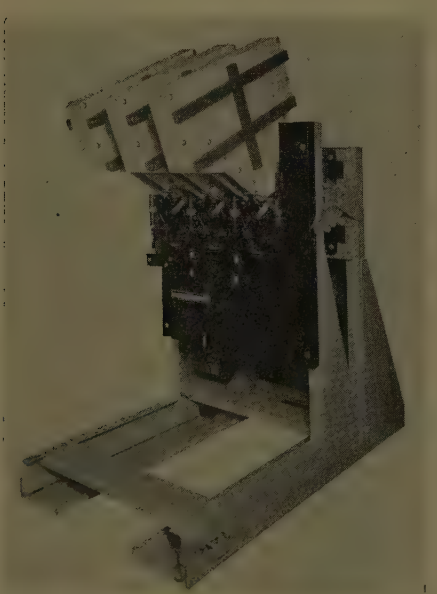

Fig. 2. Three-pole type AG-3 drawout anode breaker and frame used for arcback tests

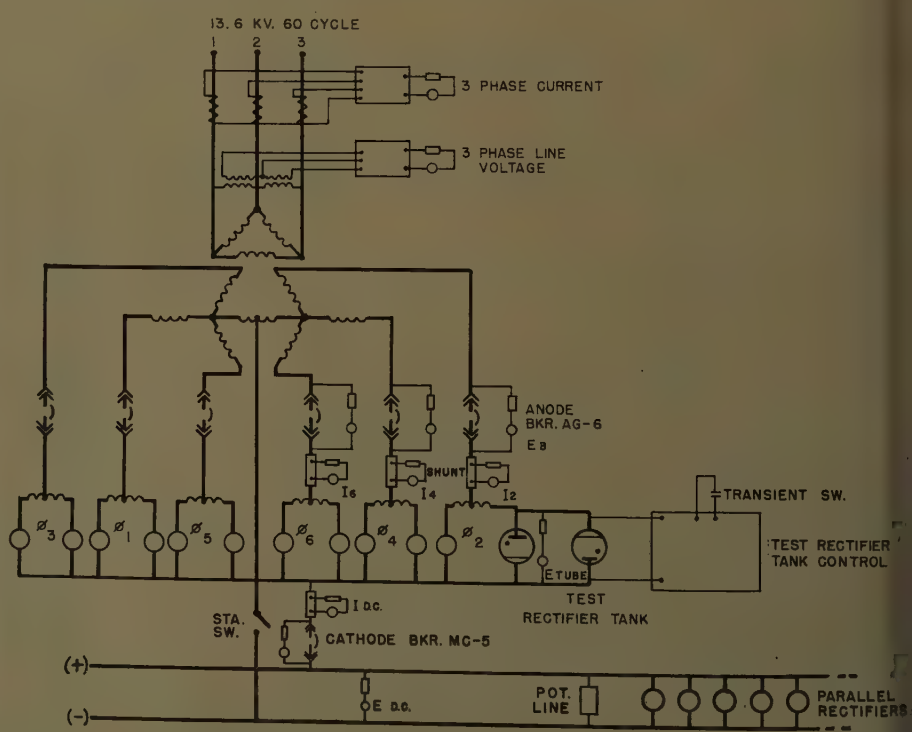

Fig. 4. Test connections on mercury-arc power rectifier

Fig. 5. View of instrumentation and control in test area

Two test anode breakers, Fig. 2, for ole operation, were inserted in the sys- in place of the normal station equip- nt and controls were provided for gle-pole operation. This type of op- tion kept the rectifier supplying the ver load and the phase or phases opened arc backs could immediately be re- red to service. The drawout features d on these anode breakers, Fig. 3, de them easily removable from the tem during the testing program for id inspection and such changes as were essary to vary the time of tripping ring system measurements.

A pumpless rectifier tank, 16 inches in meter, was connected in parallel with hase-2 rectifier tank as shown in Fig. 4. is test-rectifier tank with throw-over ilities could be operated to carry d or to give arc-back current. By this ans normal arc-back characteristics of tank were present in the circuit for equipment tests.

A full-phasing control unit operated in conjunction with a selsyn and provided the necessary synchronous timing for the firing pulse of the ignitor. The single-short feature is obtained in the control by limiting the ignitor pulse to the energy stored in a capacitor. Blocking of further firing pulses is obtained by the initiating relay which prevents renewal of the charge on the capacitor until a reset sequence had been completed. The phasing-control circuit in turn received initiation from the magnetic oscillographs. These oscillographs and the other test equipment are shown in Fig. 5. Experience confirmed the highly accurate and consistent timing of the rectifier-tank firing during the entire testing program. The majority of the tests were made to give commutation arc backs which subjected the anode breaker to the maximum service condition.

The measurements of recovery voltages were recorded with three types of instrumentation including the cathode ray, surge-crest voltmeters, and the magnetic oscillograph. This permitted full observation for all possible peak voltages that existed in the test program. An agreement was found between all methods used.

Interphase Transformer Saturation Control

During the planning stages for the test, it was recognized that a wide variation could occur in the arc-back current due to the recent past magnetic history of the interphase transformer. It could be reasoned that the volt-seconds of the interphase transformers have varied in previous test programs so that an equal comparison between even sequential tests was difficult. A rectifier subjected to the varying conditions of the test program could readily produce an unbalance through such conditions as a rectifier-tank misfire. Therefore, a means was provided to saturate the core of the interphase transformer in a predetermined direction by the deliberate removal of the current in one phase which simulated misfire operation. The resulting unbalanced magnetization of the interphase transformer was sufficient to carry the core iron into a maximum saturated condition. Immediately before the initiation of the arc back, the circuit was allowed to operate normally as shown by the return of the load-current loop of phase 6 in Fig. 6(A). In addition to the direction saturation of the interphase transformer, this allowed phase 6 to contribute to the arc-back current in a normal manner.

The location of the ignitor-blocking means on a rectifier tank in the same Y as the arc back, or in the other Y, determined whether the interphase transformer core was conditioned to give maximum or minimum arc-back current. To demonstrate the opposite effect of the interphase saturation, the ignitor-blocking means was shifted to phase 5. This

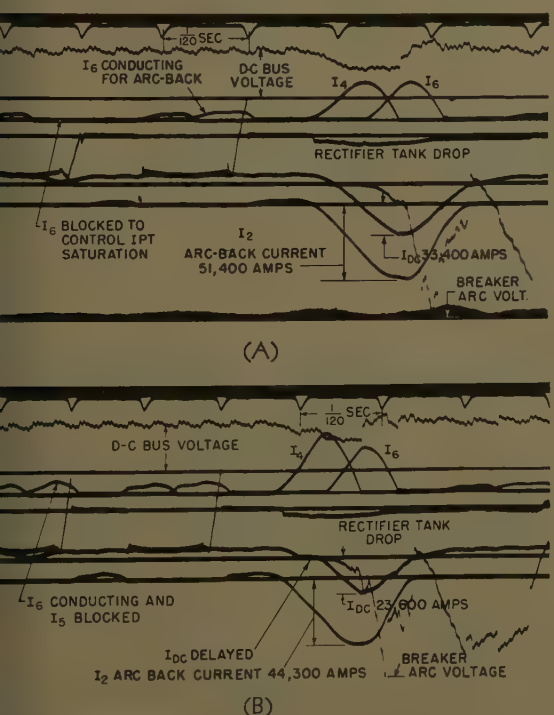

Fig. 6 (left). Oscillogram of arc-back current on normal system with interphase transformer saturation controlled to give delays in d-c contribution

A—Minimum delay: circuit condition B

B—Maximum delay

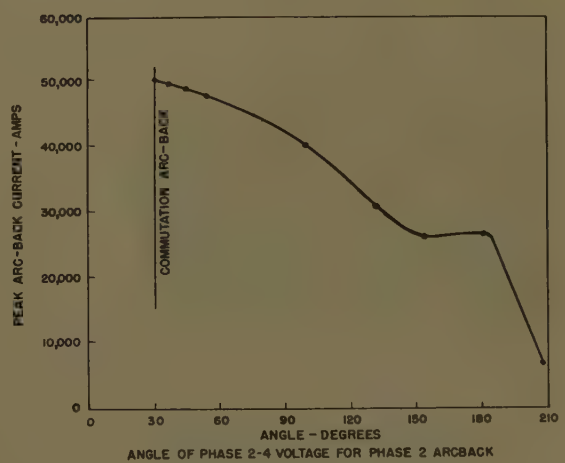

Fig. 7 (right). Variation of peak arc-back current with initiating angle

Table I. Arc-Back Tests with Interphase Transformer Saturation Control

Test No.	Oscillogram, Fig. No.	Circuit Condition	Breaker Operating Speed	Saturation Direction	Rate-of-Rise, Amperes Per Second	Peak Arc-Back Current, Amperes	Time to Peak, Milliseconds	Peak Current From D-C Bus, Ampere
4	5	B*	High Speed	For maximum rate-of-rise of arc-back current	8.5×10^6	51,400	8.4	33,400
2	6	B	High Speed	Reversed	7×10^6	44,300	7.9	23,600
130	7	B	Delayed	For maximum rate-of-rise of arc-back current	8.0×10^6	56,300	9.2	33,400
123	8	B	Delayed	Reversed	6.75×10^6	47,300	9.0	22,300
159	12	D	Delayed	For maximum rate-of-rise of arc-back current	8.9×10^6	63,500	9.0	36,100

* Condition B is normal.

created a condition giving maximum flux change to oppose d-c fault current through the interphase, and the reverse bus current was delayed, as shown in Fig. 6(B), which resulted in a lower peak magnitude.

Table I gives measured values of the effect of the magnetic conditions of the interphase transformer associated with rectifier-tank misfire performance. With normal system condition and using a delayed breaker, the saturation control varied the peak arc-back currents 19% and the rate-of-rise 17%. The difference in the peak current reached by the reverse feed from the d-c bus was 11,000 amperes and represents a 50% variation. These variations without control would cause considerable error in the appraisal of the breaker's current-limiting ability. Arc-back tests were repeated many times with the interphase magnetization controlled to produce maximum arc-back current for each power level. This procedure with phasing control did remove variations and gave reproducible results in all tests.

Arc Backs at Various Initiating Angles

While the commutation arc back produces the largest current and has been recognized as the most severe duty for breakers, arc backs do occur at other conditions. However, to assure a complete investigation, tests were made with a complete range of initiating angles. The selsyn phase control on the firing of the test rectifier tank provided the means for varying the arc back. The peak values of arc back current are shown in Fig. 7 with reference to the phase-2-4 voltage. The delay in arc-back initiation was increased until the arc back current was of such a small value that it tripped the anode breaker without a visible flash and very little noise. Hence it is possible to have a "silent arc back" and to open the anode-breaker pole. A picture of the interruption of a normal commutation arc back is shown in Fig. 8.

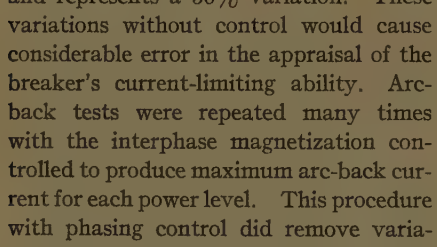

Fig. 8. Still photograph of anode breaker interrupter with normal system conditions

Measurement and Control of the Available Arc-Back Current

The available power could be set at four levels for the test program. This gave a range which included a value less than normal and two values greater than normal operating duty. The first step above normal level of operation was obtained by connecting two potline busses in parallel. The second level above normal was obtained by a short circuit around the rectifier transformer reactor in addition to connecting two potlines in parallel. For the level less than normal, a special air-core reactor was used in place of the normal anode-dividing reactor. These circuit conditions are shown in Table II with code for easy use with other references.

Establishment of the available first crest in the arc-back current was determined by test for the normal and maximum conditions. For this test the magnetic trip circuit of the anode breaker was modified to delay the opening of the anode breaker pole. The arc-back current under maximum system conditions

Table II. Circuit Conditions for Control of Available Power

Circuit Conditions	Potlines No.	Special Air-Core* Reactor	Rectifier Transformer Reactor	Measured Available Peak Arc Back, Amperes
A	3	In	In	
B	3	Out	In	55,000
C	2 & 3	Out	In	
D	2 & 3	Out	Out	63,500

* Used in place of anode-dividing reactor.

reached a first-crest value of 63,50 amperes which is a lower current tha determined by many of the past metho of calculation. This value using rigorous solution has been checked by method given in two companion papers.[1] The oscillogram for the maximum te level is shown in Fig. 9.

Anode-Breaker Field-Test Performance

The entire test program resulted i more than 200 controlled arc backs on th potline. This program was associate with a single rectifier unit and the anod breakers under test were located direct in the circuit to provide normal pow to the load. Except for a few speci tests, interrupting duty was limited to single phase of the system. In compari son with normal system operations suc a series of tests represents 50 years of ar back duty and gives a good record fo design of the whole power-conversio system.

Representative of the anode-breake performance in all these tests is the fiel record of one breaker shown in Table II In this series, a measure was give of the current-limiting ability, minimu interrupting time, and consistency operation over the minimum-to-maximu range of current. All tests were accom plished without system disturbance an permitted immediate reclosing of th open phase for continuous output fro the unit. A typical film is selected fo

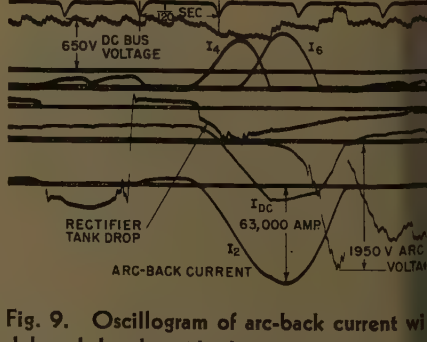

Fig. 9. Oscillogram of arc-back current wi delayed breaker tripping to measure pe available under maximum circuit condition

Table III. Field Test Performance for a High-Speed Anode Breaker

	Circuit Condition	Measured First-Crest Available Current, Amperes	Peak Arc Backs, Amperes	Total Clearing Time, Milliseconds	Peak Arc Voltage	Rate-of-Rise, Amperes Per Second
*	B	55,000	50,000	13.9	1,480	8,270,000
*	B		44,300	13.0	1,830	6,780,000
*	B		44,300	13.1	1,630	7,000,000
*	B		51,400	13.2	2,100	8,480,000
*	B		51,400	12.8	2,030	8,500,000
*	A		45,700	12.0	1,780	6,890,000
*	A		45,000	12.2	2,000	7,220,000
	A		44,300	12.2	2,100	6,480,000
	A		44,300	12.4	1,833	6,180,000
	A		44,300	11.9	1,933	7,230,000
	B	55,000	51,400	11.9	2,200	7,500,000
	B		51,400	11.8	2,200	8,240,000
	B		51,400	12.3	2,100	8,330,000
	B		51,400	12.1	2,200	8,460,000
	B		50,400	12.2	2,100	8,140,000
	C†		50,700	12.1	2,270	8,190,000
	C†		51,500	12.2	2,200	8,440,000
	C†		51,500	12.4	2,270	8,480,000
	C†		51,500	11.9	2,270	8,260,000
	C†		51,500	11.9	2,130	8,320,000
	C†		58,600	12.2	2,270	9,930,000
	C†		55,800	11.5	2,230	9,470,000
	C†		57,300	12.2	2,230	9,490,000
	C		52,900	12.9	2,465	8,720,000
	C		52,900	11.8	2,430	8,640,000
	C		52,900	11.4	2,465	9,000,000
	C		52,900	11.5	2,100	9,240,000
	C		52,200	11.5	2,300	8,990,000
	D	63,500	57,250	11.5	2,065	10,100,000
	D		56,500	11.6	2,300	9,230,000
	D		57,250	11.5	2,165	9,790,000
	D		58,600	11.6	2,230	9,810,000
	D		55,700	11.6	2,400	9,370,000

reliminary tests to explore saturation control.
arallel potlines 3 and 4 instead of 2 and 3.

Table IV. First-Crest Arc-Back Currents with Various System Conditions

t No.	No. of Generators	No. of Connecting Lines	Potline No.	No. of Capacitors (7,500 Reactive Kva)	Transformer Reactor	Peak Arc-Back Current	Time to Peak Current, Milliseconds
47	3	2*	3	4	in	55,000	8.9
52	3	2*	3	0	out	61,800	8.7
53	3	0	3	0	out	61,500	8.6
55	3	0	3	7	out	63,000	9.2
57	3	2*	3	7	out	61,500	9.2
59	3	2*	2 & 3	7	out	63,000	9.6
61	3	2*	2 & 3	0	out	63,000	9.1

ower out.

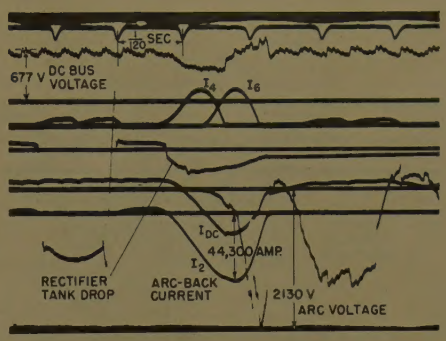

Fig. 10. Oscillogram of arc-back current with special anode reactor for less than normal available current (circuit condition A)

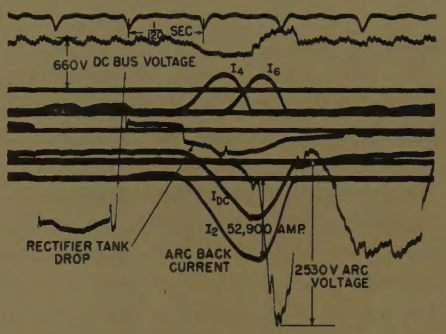

Fig. 11. Oscillogram of arc-back current with parallel d-c busses for greater-than-normal available current (circuit condition C)

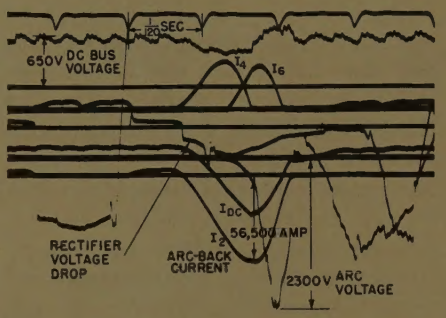

Fig. 12. Oscillogram of arc-back current with parallel d-c busses and rectifier transformer reactor omitted for maximum available current (circuit condition D)

h level of available current, Figs. 6, 10, and 12, and includes the record of all ase currents in the Y under test, the d-c dback, arc voltage of breaker, voltage the rectifier tube under arc back, and bus voltage. These oscillograms w the controlled misfire of phase 6 to ure maximum arc-back currents for h level tested. The consistency of de-breaker performance over all levels epresented by a 3% variation in let-ough peak arc-back current and a 14% iation in total clearing time. The ence of any restrikes at any level of rations makes possible the consistent ues of total clearing time.

stem Measurements

The test program had a dual purpose, both objectives are significant in establishing adequate knowledge and performance of mercury-arc-rectifier systems. In addition to anode-breaker performance, system measurements were made to determine actual service condition and the influence of each component.

To obtain the desired information, the anode breaker was modified to delay the opening of the contacts until the first crest of arc-back current was reached. This delay was used for combined system measurements as well as those special tests conducted to establish the independent contribution of the d-c bus, single-Y and double-Y connections. Oscillograms, Figs. 13 and 9, are given for the normal and maximum levels with corresponding crest arc-back currents of 55,000 and 63,500 amperes using circuit conditions shown in Table II. This is appreciably less than a calculated value of over 75,000 amperes for these systems using previous methods and gives a better basis for establishment of the system requirements.

In addition to the control of the immediate circuit with reactors, the system conditions were varied and the first-crest arc-back currents measured. The results indicated in Table IV are based on repeated tests in all cases with identical results. Further, it is evident that the influence of adjacent potlines through bus ties, connecting transmission lines, and capacities banks are small or negligible compared with the impedance changes in the individual rectifier-tank circuits and transformers.

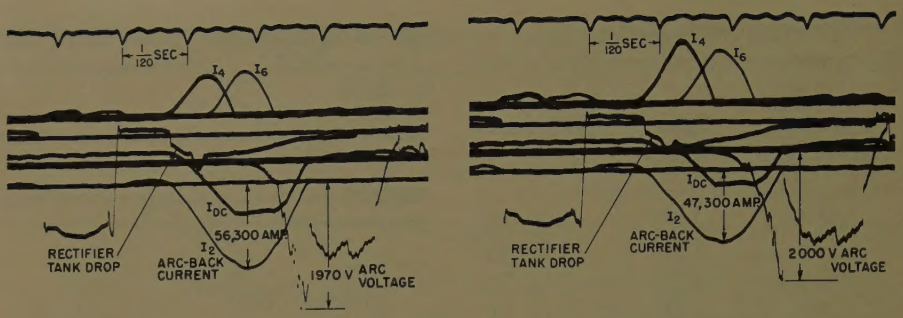

A—Minimum delay in d-c contribution

B—Maximum delay in d-c contribution

Fig. 13. Oscillogram of arc-back current with delayed breaker tripping to measure peak available current on normal system with inter-phase transformer saturation controlled to give delays

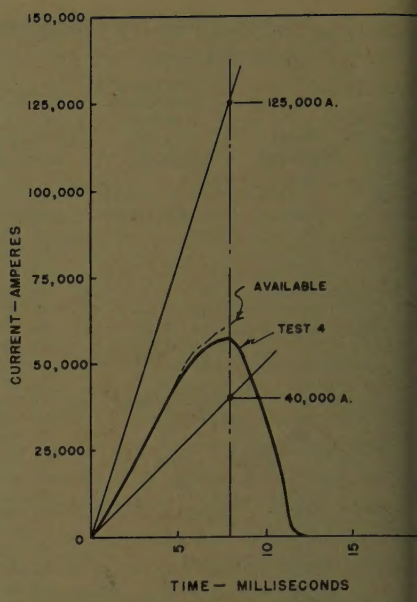

Fig. 14. Interrupting performance of breal compared with National Electrical Manuf turers standard for high-speed breaker appli tions

Breaker Standards

Present-day standards[3] for high-speed breakers present two forms of interrupting rating based on the application. For the anode breaker, it is stated as a maximum of 75,000 amperes during the first cycle at rated voltage based on supply frequency of 60 cycles per second. On the d-c air circuit breaker, the available current at 0.008 second should be between 40,000 and 125,000 amperes at rated voltage and the breaker speed sufficiently fast to limit the crest current by a time of 0.010 second.

These field tests do not represent the maximum requirements in either case but they do demonstrate the performance within these limits. Early estimates of the system available indicated higher than the 75,000 amperes but the actual measurement was only 63,500 amperes. This emphasizes the need of a correlation with the similated tests to demonstrate satisfactory performance of the breakers for systems where such extensive tests cannot be conducted.

In the field tests against high-speed d-c air circuit breaker requirements, Fig. 14, the inherently fast anode breaker readily demonstrates its ability for this function even though the rate-of-rise is varying with the a-c system. The high speed makes it a current-limiting device and limits the peak well in advance of the first crest of the system and within the 0.010-second time of the standard.

Conclusions

The extensive testing program conducted on the high-capacity mercury-arc rectifier system of the Aluminum Company of America provided considerable information about the system and anode breaker performance. These conclusions were reached:

1. Testing means, which gave conditions comparable to the service conditions, could control and repeat the arc-back current through the anode breaker with extremely good consistency as indicated by very small variations of 6% in peak current observed in the anode breaker tests. Uncontrolled, the nonlinear impedance of the interphase transformer could cause variations of 50% in the d-c contribution, and this alone amounted to a variation of 19% in the total arc-back current.

2. Consistent high-speed current-limiting action of the breaker was demonstrated. This program included a range of duty and as many as 60 operations on a single-pole unit were performed. The current through the breaker was only 90% of the maximum available first-crest current.

3. Measurement of the available first-crest arc-back current levels were made with delayed breakers and the results were in full agreement with new calculations. The 63,500 amperes measured for the system is under the 75,000 amperes maximum for the anode-breaker standard.

4. The contribution of the d-c bus to t first-crest arc-back current is approximat 65% for normal system operation with transformer reactor, and 45% of the to when the reactor is omitted.

5. Variations due to the random magne conditions in the interphase transform were eliminated and precise control gave maximum arc back during all performan tests.

6. Factors influencing the magnitude arc-back current have been measured. T greatest changes are associated with t rectifier tank circuit and transformer i pedance. This information can be used advantage in planning future designs a applications.

References

1. Mathematical Model and Procedure f Arc-Back Current Calculations for Pow Rectifiers, **H. P. Fullerton, J. Teno.** *AI Transactions*, vol. 77, pt. II, Nov. 1958, pp. 4 64.

2. Comparison of Calculated and Measur Arc-Back Currents in Large Power Rectif System, **J. Teno, C. H. Titus, R. N. Wagn** *Ibid.*, 1958 (Jan. 1959 section), pp. 585–89.

3. Large Air Circuit Breakers. *NEM Standard SG3-1955*, National Electrical Manuf turers Association, New York, N. Y., 1955.

Power Apparatus and Systems—February 1959

58-41	Current-Carrying Capacity of ACSR	House, Tuttle	1169
58-360	The Magnetic Properties of ACSR Core Wire	Matsch, Lewis	1178
58-1029	The Resistance and Reactance of ACSR	Lewis, Tuttle	1189
58-769	Performance of Generator Thrust Bearings	Looper	1216
58-1023	Nodal Representation of Complex-Element Networks	Siegel, Bills	1226
58-1089	Using a Computer in the Design of Generators	Harrington, Larney	1230
58-1085	IBM 650 as Tool for Analysis of System Problems	Adams, Gerngross	1236
58-1088	Computer Applied to Distribution System Planning	Strausser	1244
58-1093	Solution of Distributed Parameter Problems	Bewley, Harvey	1252
58-1090	Design of Armature Coils for Large A-C Motors	Sexton, Balik	1257
58-1095	Transformer Design and Cost Program with an IBM 650	MacKinnon	1262
58-1097	Overhead-Transmission-Line Constants	Coleman, Watts, Shipley	1266
58-1098	Calculation of Transmission-Line Impedances	Thomas	1270
58-1100	Computation of Load-Flow Studies Using Computers	St. Clair, Stagg	1275
58-1094	Complete Transformer Design with Computer	Williams, Abetti, Mason	1282
58-1101	Transient Stability Studies—II	Lane, Long, Powers	1291
58-1099	Calculation of Power Networks	Byerly, Long, Baldwin, Jr., King	1296
58-1096	Sag-Tension Calculation Program for Digital Computer	Pickens	1308
58-1091	Digital Computation of Generator Pullout	Cawson, Brown	1315
58-1084	Compiler Programs and Power Problems	Carleton, Baldwin, Jr.	1319
58-1107	Auxiliary Power for Eddystone Station	Adams	1324
58-1110	PBR-Steam-Power Plant of 125 Electrical Mw	Benenati	1329
58-1108	Large Steam Turbine Generators	Barton, Massingill, Taylor	1335
58-1109	Large Steam-Turbine-Generator Design Practice	Fleischmann, Staats	1348
58-1115	Automatic Tripping	Beattie, Bauman, Driscoll, Onderdonk, Webb	1353
58-1106	Relay Protection in Steam Power Stations	Barnes, Murray, Verrall	1360
58-1111	Dresden Nuclear Power Station	Elliott, Maxson, Nixon, Merryman	1367
58-1151	Protecting Turbine from Thrust-Bearing Failure	Bruce, Roberts, Byram	1383
58-943	Effect of Linkage Flexibility on Dynamics of Breakers	Barkan, Tuohy	1386
58-258	Higher Secondary Voltage for Residences	Anderson, Hutchinson, Pearson	1394
58-1165	Survey of Published Data on Surge Performance	Abetti	1403
58-403	Lightning Current in Towers and Ground Wires	Johnson, Price, Schultz	1414
58-1178	Magnification of Switching Surges	Schultz, Johnson, Schultz	1418
58-1170	Lightning Protective Requirements of Generators	Dillard, Hileman	1426
58-1171	A Primer on Loss Formulas	Harker	1434
58-1180	A General Method for Slot Constant Calculation	Waldschmidt	1437
58-1153	Electrical Insulation Research in a Power Utility	Cameron	1441
58-1156	More Angles of Phase Shift Added to Ice-Melting Methods	Ekstrom	1449
58-1184	Survey on Connection of Shunt Capacitor Banks	Committee Report	1452
58-1280	Results of Motorette Evaluation of Insulation Systems	Boettcher	1459
58-1167	New Inorganic Insulation for 500 C Electric Equipment	Vondracek, Croop	1463
58-1296	Supervisory Control for Air Force Missile Test Center	Cadwell	1467
58-1203	Lightning-Arrester Testing: Proposal for Revision in Standards	Beck	1472
58-1295	Rural Distribution Planning	Breckenfelder, Stanley	1481
58-1199	Atomic Power Station Features	Frus, Thompson, Van Wassen, Woolever	1487
58-1185	Overvoltages Following Secondary Switching	Barthold, Johnson, Schultz	1492
58-1179	Noise Rating of Large Electric Rotating Machines	Talaat	1501
58-1155	Mathematical Analysis of A-C Arc Extinction in Breakers	Browne, Jr.	1508
58-1255	Bibliography on Extra-High-Voltage Systems	Abetti	1517
58-1214	Unbalanced Loading of 3-Phase Transformer Banks	Anderson	1536
58-1160	Surge Transfer Through 3-Phase Transformers	Hileman	1543
58-1201	Time-Error Control for Interconnected Synchronous Systems	Broadbent	1554
58-1173	Testing Magnetic Air Breakers for 5-Cycle Performance	Wood, Carter	1560
58-1187	Computer Technique for Development of Maintenance Cost	Light	1562
58-1172	Motor-Starting Lamp Flicker on Transformer Banks	Neupauer, Smith	1568
58-1189	Loss Minimization in Utility Systems	Sze, Garnett, Calvert	1577
58-1224	Operation of Protective Relaying at Reduced Frequencies	Committee Report	1585
58-1195	Water Routings on U. S. Columbia River Hydro System	McIntyre, Sachs	1588
58-1216	Transmission Line Switching Surges	Shankle, Taylor, Jr.	1596
58-1186	Voids in Insulation Under Internal Discharge	Reynolds	1604
58-1226	Arresters for Lightning Protection of Substations	Clayton, Powell	1608
58-1218	Noise Measurements on Rotating Machinery	Committee Report	1615
58-1262	Economic Selection of Generating Capacity Additions	Cohen, Jensen	1628
58-1220	Dynamic Response of Arcs in Various Gases	Yoon, Spindle	1634
58-1221	Influence of Higher Operating Temperatures on Motor Design	Woll	1642
58-1253	Magnetic Fields Around a Transmission Line Tower	Anderson, Hagenguth	1644
58-1228	Experiences with Broad-Band Carrier Coupling	Dobson	1650
58-1239	Electrical Breakdown of Gases and Vapors	Works, Lindsay	1659
58-1279	Iron-Loss Calculations on Induction Motors	Trickey	1663
58-1313	A New Isolated-Phase Bus Design	Rugg, Westermeyer	1669
58-1320	Torque and Speed Control of Induction Motors	Szablya	1676
58-1225	Field Testing of a 69-Kv Oil Circuit Breaker	Edwards, Nelson	1682
58-1304	Measuring Amplitude and Harmonic Content of Surge Voltages	Scheda	1694
58-1307	Frame-Mounted Outdoor Oil Circuit Breakers	Briggs, Hambrick	1698
58-1306	Temperature-Rise Tests on Transformers	Beavers, Whitman	1707
	Addendum		1719
	Index		1720

Conference Papers Open for Discussion

Conference papers listed below have been accepted for AIEE Transactions and are now open for written discussion until May 27. Duplicate double-spaced typewritten copies of each discussion should be sent to Edward C. Day, Assistant Secretary for Technical Papers, American Institute of Electrical Engineers, 33 West 39th Street, New York 18, N. Y., on or before May 27.

Preprints may be purchased at 40¢ each to members; 80¢ each to nonmembers if accompanied by remittance or coupons. Please order by number and send remittance to:

AIEE Order Department
33 West 39th Street
New York 18, N. Y.

58-210 A Recommended Program for Resistance Welding Instrumentation.....Dixon
58-1057 Electrical Features of the Four Corners Pipe Line..Sonnier, Siler
59-247 Improved D-C High-Potential Testing of Insulation Systems in Low- and Medium-Voltage D-C Equipment..Odok, Soelaiman

AIEE PUBLICATIONS

	Member Prices	Nonmemb Prices

Electrical Engineering

Official monthly publication containing articles of broad interest, technical papers, and three news sections: Institute Activities, Current Interest, and Electrical Engineering Education. Automatically sent to all members and enrolled students in consideration of payment of dues.

		annually $12* per year
		Single copies $1.50

* Subscription price and $1.00 extra for foreign postage both payable in advance in New York exchange.

Bimonthly Publications

Containing all officially approved technical papers collated with discussion (if any) in three broad fields of subject matter as follows:

	annually	annually
Communication and Electronics	$5.00†	$8.00‡
Applications and Industry	$5.00†	$8.00‡
Power Apparatus and Systems	$5.00†	$8.00‡

† Members may receive one subscription to any one of the bimonthlies for $2.50. The balance of the $5.00 subscription price shown above will be paid by application of one's annual dues for the year of the subscription. (Members may not reduce the amount of their dues payment by reason of nonsubscription.) Additional subscriptions will be at the $5.00 rate shown above.

‡ Subscription price and 50 cents extra for foreign postage both payable in advance in New York exchange.

Single copies may be obtained when available.	$1.50 each	$1.50 each

AIEE Transactions

An annual volume in three parts containing all officially approved technical papers with discussions corresponding to six issues of the bimonthly publication of the same name bound in cloth with a stiff cover.

		annually	annually
Part I	Communication and Electronics	$4.00	$ 8.00**
Part II	Applications and Industry	$4.00	$ 8.00**
Part III	Power Apparatus and Systems	$4.00	$ 8.00**
Annual combination subscription to all three parts (beginning with vol. 77 for 1958).		$10.00	$15.00***
Annual combination subscription to any two parts.			$12.00***

** Subscription price and 75 cents for foreign postage both payable in advance in New York exchange.

*** Subscription price and $1.00 extra for foreign postage both payable in advance in New York exchange.

Electrical Engineering and Transactions

An annual combination subscription to both publications (effective August 1, 1958). $24.00§

§ Subscription price and $2.00 extra for foreign postage both payable in advance in New York exchange.

AIEE Standards

Listing of Standards, test codes, and reports with prices furnished on request.

Special Publications

Committee reports on special subjects, bibliographies, surveys, and papers and discussions of some specialized technical conferences, as announced in ELECTRICAL ENGINEERING.

Discount 25% of above nonmember prices to college and public libraries. Publishers and subscription agencies 15% of above nonmember prices. For available discounts on Standards and special publications, obtain price lists from Order Department at Headquarters. Send all orders to:

Order Department
American Institute of Electrical Engineers
33 West 39th Street, New York 18, N. Y.